

MODELING OF GROUND-BORNE VIBRATION
FROM UNDERGROUND RAILWAY SYSTEMS

A THESIS SUBMITTED TO
THE GRADUATE SCHOOL OF NATURAL AND APPLIED SCIENCES
OF
MIDDLE EAST TECHNICAL UNIVERSITY

BY

MELİH SARIGÖL

IN PARTIAL FULFILLMENT OF THE REQUIREMENTS
FOR
THE DEGREE OF MASTER OF SCIENCE IN
MECHANICAL ENGINEERING

AUGUST 2007

Approval of the thesis:

**MODELING OF GROUND-BORNE VIBRATION FROM UNDERGROUND
RAILWAY SYSTEMS**

submitted by **MELİH SARIGÖL** in partial fulfillment of the requirements for
the degree of **Master of Science in Mechanical Engineering**
Department, Middle East Technical University by,

Prof. Dr. Canan Özgen _____
Dean, Graduate School of **Natural and Applied Sciences**

Prof. Dr. Kemal İder _____
Head of Department, **Mechanical Engineering**

Prof. Dr. Mehmet Çalışkan _____
Supervisor, **Mechanical Engineering Dept., METU**

Examining Committee Members:

Prof. Dr. Samim Ünlüsoy _____
Mechanical Engineering Dept., METU

Prof. Dr. Mehmet Çalışkan _____
Mechanical Engineering Dept., METU

Prof. Dr. Nevzat Özgüven _____
Mechanical Engineering Dept., METU

Prof. Dr. Yener Özkan _____
Civil Engineering Dept., METU

Asst. Prof. Dr. Ergin Tönük _____
Mechanical Engineering Dept., METU

Date:
23/08/2007

I hereby declare that all information in this document has been obtained and presented in accordance with academic rules and ethical conduct. I also declare that, as required by these rules and conduct, I have fully cited and referenced all material and results that are not original to this work.

Name, Last name :

Signature :

ABSTRACT

MODELING OF GROUND-BORNE VIBRATION FROM UNDERGROUND RAILWAY SYSTEMS

Sarıgöl, Melih

M.Sc., Department of Mechanical Engineering

Supervisor : Prof. Dr. Mehmet Çalışkan

August 2007, 97 pages

Ground-borne vibration from underground rail vehicles is studied analytically. A previously developed model by J.A.Forrest and H.E.M.Hunt[24,25] is modified to account for different track and vehicle models. The tunnel is modeled as infinite cylindrical shell surrounded by viscoelastic soil. The track is coupled to the tunnel with supports of complex stiffness. The rails, which are modeled as infinite Euler beams, are supported by discrete sleepers with regular spacing, and railpads with complex stiffness. A modified hysteretic damping model for moving loads is applied to soil. Linearized Hertzian contact spring is included between the wheel and the rail. The solution is obtained in frequency domain using random process theory. Effects of improvements in the model are graphically presented to enable comparison with the previously developed model and measurements from literature.

Keywords: ground-borne vibration, underground rail vehicles, random process theory

ÖZ

YER ALTI RAYLI SİSTEMLERİNİN TİTREŞİM
MODELLENMESİ

Sarıgöl, Melih

Yüksek Lisans, Makine Mühendisliği Bölümü

Tez Yöneticisi : Prof. Dr. Mehmet Çalışkan

Ağustos 2007, 97 sayfa

Bu çalışma çerçevesinde yer altı raylı sistemlerinden yayılan ve toprak yoluyla taşınan titreşim analitik olarak modellenmiştir. Daha önce Forrest ve Hunt tarafından geliştirilen model, farklı hat ve araç modellerine uygun olacak biçimde geliştirilmiştir. Tünel, visko-elastik toprak ortamı ile çevrilmiş sonsuz silindirik kabuk şeklinde modellenmiştir. Hat tünele kompleks esneklik katsayısına sahip yatak ile bağlanmıştır. Sonsuz Euler kirişleri şeklinde modellenen raylar, düzenli aralıklarla yerleştirilmiş traversler ve pedler sayesinde desteklenmiştir. Toprak modeline hareketli yükler için geliştirilmiş olan yapısal sönümlenme modeli uygulanmıştır. Ayrıca modele yük ile hat arasında doğrusal Hertz yayı da eklenmiştir. Çözümüne frekans alanında rasgele proses teorisi uygulanarak ulaşılmıştır. Modelde yapılan bütün değişiklikler, değişikliklerin etkilerinin izlenmesi amacıyla grafik yoluyla ayrı ayrı verilmiştir.

Anahtar Kelimeler: toprak yoluyla taşınan titreşim, yer altı raylı sistemleri, rasgele proses teorisi

To My Parents

ACKNOWLEDGMENTS

The author wishes to thank deeply to his supervisor Prof.Dr. Mehmet Çalışkan for his guidance and open-minded approach on the subject, which were inspiring throughout the thesis process.

The author also owes many thanks for technical assistance of Mr Egemen Varlı for his guidance in development of MathLab code and RAYTEK LTD.ŞTİ for their support during the studies associated with the thesis.

TABLE OF CONTENTS

PLAGIARISM.....	iii
ABSTRACT.....	iv
ÖZ.....	v
DEDICATION.....	vi
ACKNOWLEDGMENTS.....	vii
TABLE OF CONTENTS.....	viii
LIST OF TABLES.....	x
LIST OF FIGURES.....	xi
NOMENCLATURE.....	xiii
CHAPTERS	
1. INTRODUCTION.....	1
2. LITERATURE REVIEW.....	3
2.1. Problem Areas.....	3
2.2. Modeling.....	5
2.3. Vehicle Models.....	6
2.3.1. Wheelset Models	10
2.3.1.1. Multibody Models	10
2.3.1.2. Continuum Models.....	11
2.3.1.3. Finite Element Models.	11
2.3.2. Models of Car Body and Bogie.	11
2.4. Dynamic Track Models.....	12
2.4.1. Track Structures and Components.	12
2.4.2. Rails.....	13
2.5. Rail Fastening System.....	16
2.6. Sleeper models.....	18
2.7. Ballast and substrate.....	19
2.8. Floating slab.....	22
2.9. The complete track model.....	24
2.10. Tunnel.....	25
2.11 Contact modeling.....	28
2.12 Excitation modeling.....	32
2.12.1 Vehicle Disturbances.....	32

2.12.2 Wheel and rail discontinuities.....	32
2.12.3 Track irregularities.....	34
3. ORIGINAL MODEL	36
3.1. Cylindrical Shell Equations.....	36
3.2. Elastic Continuum Equations.....	39
3.3. Applied load.....	45
3.4. Modeling a thin-walled cylinder with the elastic continuum theory.....	46
3.5. Modeling a tunnel buried in soil.....	47
3.6. Adding the slab beam to the track model.....	49
3.7. Adding the rail beam.....	53
3.8. Adding the axle masses to the complete track model.....	54
3.9. Random process theory applied to the full-track model.....	56
4. MODIFIED MODEL	60
4.1. Track Model.....	61
4.2. Modified hysteretic damping model.....	63
4.2.1. Modified hysteretic damping.....	64
4.3 Vehicle model and Hertz contact.....	65
5. RESULTS AND DISCUSSION.....	68
5.1 Parametric Study.....	68
5.1.1 Track model.....	72
5.1.2 Modified damping model.....	72
5.1.3. Modified vehicle model and Hertz contact.....	73
5.1.4. The complete modified model.....	74
5.2 Discussion.....	77
6. CONCLUSIONS.....	82
REFERENCES.....	84
APPENDICES	
A. SHELL AND CONTINUUM COEFFICIENTS.....	94

LIST OF TABLES

Table 1. Problem areas.....	4
Table 2. Degree-of-freedoms of wagon components used in Sun's work.....	10
Table 3. Effect of subway structure type on tunnel vibration levels.....	25
Table 4. Harmonic excitation sources.....	33
Table 5. Impulse excitation sources.....	33
Table 6. Values of the unevenness a and waviness b of vertical railway track irregularity for three different conditions.....	35
Table 7. Differences between the models.....	60
Table 8. Parameters to model the tunnel surrounded by soil.....	68
Table 9. Parameters for rails, slab beam and sleepers.....	69
Table 10 Parameters for the vehicle model.....	69

LIST OF FIGURES

Figure 1. The sub-systems contained in the complete model.....	5
Figure 2. Rail vehicle.....	7
Figure 3. 10 degree-of-freedom vehicle model.....	9
Figure 4. Different track types: ballasted track (left) and rigid track (right).....	12
Figure 5. A differential beam element.....	14
Figure 6. An infinite beam on viscoelastic foundation.....	15
Figure 7. Wave propagation modes of a UIC 60 rail.....	16
Figure 8. Rail fastening systems.....	17
Figure 9. Ballast and substrate models.....	23
Figure 10. The first tunnel model developed by Degrande and the first in-plane and out-of-plane modes of the reference cell of the Bakerloo line tunnel.....	27
Figure 11. The second tunnel model developed by Degrande and the first in-plane and out-of-plane modes of the reference cell of the RER B tunnel.....	28
Figure 12. The moving irregularity wheel/rail interaction model.....	30
Figure 13. Coordinate system used for the thin-walled cylindrical-shell theory.....	37
Figure 14. In plane ring modes varying according to n , the number of waves developed around the circumference.....	39
Figure 15. Coordinate system used for the theory of an elastic continuum with cylindrical geometry.....	40
Figure 16. Joining an infinitely long slab beam to the tunnel and the interaction forces.....	50
Figure 17. General force distribution per unit length $Q(x)$ acting along the line of joining.....	50
Figure 18. The complete track model and the masses added in regular spacing.....	54
Figure 19. The power spectrum of irregularity.....	59
Figure 20. New track model including rigid sleepers, rails, railpads and bearings represented as complex stiffness elements.....	61
Figure 21. Three degree-of-freedom vehicle model with one contact point.....	66
Figure 22. The MATLAB code algorithm and the lines where modifications are made.....	71
Figure 23. Result of sleeper modification	72
Figure 24. Effect of modified hysteretic damping for moving load	73

Figure 25. Effect of 3 degree-of-freedom vehicle model and Hertz contact to the model	74
Figure 26. Comparison between two models on displacement vibration spectra at $\theta=0$, $r=20\text{m}$	75
Figure 27. Vertical soil displacement spectrum for the modified model for different angles θ	75
Figure 28. Change in vertical soil displacement spectrum at $r=20$ m and $\theta=0$ for different vehicle speeds.....	76
Figure 29. Root mean square value of vibration velocity compared with limit values specified in TSE 2613-2.....	76
Figure 30 One-third octave band vibration levels measured on the tunnel walls for different vehicle speeds and results computed by the modified model	79

NOMENCLATURE

u , displacement components in x direction

v , displacement components in y direction

w , displacement components in z direction

ω , angular frequency

ζ , angular wavenumber

n , number of waves developed around the circumference

a , radius of the shell

h , thickness of the shell

E , Young's modulus

ν , Poisson's ratio

ρ , density of the medium

G , shear modulus

c_1 , speed of pressure wave

c_2 , speed of shear wave

λ, μ , Lamé's elastic constants

τ_{jk} , components of stress

e_{jk} , components of strain

m , beam's mass per unit length

k_r , stiffness per unit length of the resilient layer between the rail and slab beams.

η_r , loss factor for hysterical damping of the resilient layer between the rail and slab beams

k_s , stiffness per unit length of the resilient layer between slab beams and the tunnel invert

η_s , loss factor for hysterical damping of the resilient layer between slab beams and the tunnel invert

L , axle spacing

V , vehicle speed

N , number of axle masses

m_c , mass of 1/8 vagon

m_b , mass of bogie

m_w , mass of wheelset

k_1 , primary vertical stiffness

k_2 , secondary vertical stiffness

c_1 , primary vertical damping

c_2 , secondary vertical damping

\tilde{Y}_1 , displacement along the beam due to a unit point load acting on the slab at $x = 0$.

\tilde{Y}_2 , displacement along the invert due to a unit point load acting on the slab at $x = 0$.

\tilde{Y}_3 , displacement in soil due to a unit point load acting on the slab at $x = 0$.

\tilde{H}_{11} , frequency response function for the response of the free beam due to a point load at $x = 0$

\tilde{H}_{22} , frequency response function for the response of the uncoupled tunnel invert due to a point load at $x = 0$

\tilde{H}_{32} , frequency response function of a particular soil displacement component due to a point force acting on the uncoupled tunnel invert at $x = 0$.

\tilde{H}_{00a} , frequency response function for the unjoined rail beam

\tilde{H}_{11a} , frequency response function of the slab beam to the load on the slab before the rail is added

\tilde{H}_{21a} , frequency response function and tunnel invert due to to a load on the pre-rail-beam slab

\tilde{H}_{31a} , frequency response function of the soil to a load on the pre-rail-beam slab

$S_y(\omega)$, power spectral density function

$S_0(\omega)$, power spectral density function for the rail roughness

$S_{x_p x_q}(\omega)$, cross-spectral density function

CHAPTER 1

INTRODUCTION

With growing demand for public transportation in modern urban cities, more urban railways and metros have been, and continue to be, built. These railway lines are usually constructed underground in tunnels in central areas of cities, due to demand for space for living. Railways, which are built underground to save space at the surface for living and environment will still generate vibrations, and these vibrations can annoy people near the track. Vibrations generated by the trains running in tunnels can propagate through the track and tunnel structure, to the surrounding strata and into the structure of any buildings close to the tunnels. The vibration of the building structure can then be radiated as noise into the building interior. The transportation-induced vibrations add to the static and other types of loads, and their specific spectral features are well distinguished and perceived as nuisance to people.

With the increasing number of new tunnels built in urban cities and towns, the environmental impact of this specific low frequency rumbling noise has become an important issue that needs to be investigated.

When considering the effects of ground-borne vibrations from underground rail transportation three main groups are distinguished due to their different sensitivity to vibrations; namely people, machines and structures. There are regulations in European countries and in Turkey about the maximum level of vibration exposure on the basis of human health. Wolf [118] researches experimentally the effects of these ground-borne vibrations when they are transmitted to sensitive laboratory equipment. Underground trains generate vibrations, which are transmitted

through the soil and interact with the foundations of adjacent buildings, resulting in disturbance from vibrations (1–80 Hz) and re-radiated noise (1–200 Hz). [20] These vibrations are caused by quasi-static and dynamic loading from the vehicle to the track structure and are transmitted through ground to the surrounding. Dynamic axle loads are mainly caused by wheel and rail roughness; impact excitation due to discontinuities of the wheels and the rails; and parametric excitation due to the periodic support of the rails on sleepers. Every excitation has its characteristic frequency range determined mainly by theoretical investigation and experimentation. For example the spectra of vibration caused by wheel and rail discontinuities lie in the frequency range from 50 Hz up to 1500 Hz. The main causes of wheel and rail irregularities are corrugation, deterioration of ballast or unround wheels.

State-of-the-art modeling of vibrations due to trains in tunnels assumes that the tunnel invert and the surrounding soil are relatively stiff with respect to the track, resulting in a two-step approach where the dynamic axle forces on the rails are derived from an uncoupled track model and subsequently applied on a track–tunnel–soil model to compute the radiation of waves from the tunnel into the soil. The disturbing effect caused by these solid borne vibrations can be significantly mitigated by soil replacement of the material under the rails.

The scope of this thesis is to model ground-borne vibrations from underground rail vehicles analytically by modifying the model by Forrest and Hunt [24,25] for different track and vehicle models. It is aimed to obtain results reflecting all the components of vibration spectrum within the frequency range of interest properly. Through the modified model, the frequency composition of vibration from underground railway sources is obtained to form a basis for the planning of underground railway tracks in critical urban areas. Also the current model can be used for mapping of vibration from those sources in urban areas.

This work consists of literature survey, presentation of Forrest and Hunt's model and the chapter for individual modifications made on the model; followed by parametric study, results and discussion chapters.

CHAPTER 2

LITERATURE REVIEW

2.1. Problem areas

Modeling of vibrations from rail vehicles has to be done in the appropriate frequency range according to the area of concern. The limit of the highest frequency associated with wheel/rail noise is taken as the limit of human hearing at about 5kHz. Problems with the running surfaces of wheel and rail and with track components are caused primarily by vertical forces, which are most significant up to about 1500Hz: Higher frequency loads, which arise from relatively short wavelength irregularities, are severely attenuated by the finite size of the contact patch between wheel and rail, whose diameter is typically about 15mm. Forces transmitted on the one hand through the Wheel inertia into the axle, bogie and vehicle, and on the other through the track into the ground and structure, are most significant up to frequencies of about 500Hz. Problems of vehicle dynamics occur largely at frequencies of less than 20Hz.

Dynamic behavior with regard to stability, steering and passenger comfort is most significant at frequencies of only a few Hertz. At frequencies of more than a few Hertz the vehicle's primary and secondary suspension isolate the bogie and body from the wheelset. Consequently the vehicle's "unsprung mass" (comprising essentially the wheelset, bearings and any axle-hung traction motor and gearing) is the only component which significantly affects vertical dynamic loads between wheelset and track, and accordingly through the track itself, at high frequencies. The unsprung mass is indeed represented satisfactorily for vertical excitations as a rigid body.

Table 1. Problem areas [57]

PROBLEMS OF VEHICLE/TRACK INTERACTION		
	Area of concern	Frequency range [Hz]
1	Vehicles	0-20
2	Bogie and unsprung mass a) wheel bearings b) fatigue of axles, brake gear etc.	0-500
3	Irregular running surfaces of wheel and rail a) wheel flats b) out-of-round wheels c) wheel corrugation d) "long wavelength" rail corrugation e) "short wavelength" rail corrugation f) dipped welds and joints g) pitting, shelling	0-1500
4	Track components a) fatigue of rail in bending b) railpads c) concrete sleepers d) ballast and track geometry	0-1500
5	Wheel/rail noise a) rolling noise b) impact noise c) squeal	0-5000
6	Structure-borne noise and vibration a) ground borne vibration b) viaducts	0-500

In order to examine the lateral vibration of the wheel, which is excited by forces in the plane of wheel/rail contact and normal to that plane, a significantly more complicated model is required because of the wheelset's lateral flexibility. A satisfactory model must include the wheelset's resonant behaviour in order to represent phenomena such as noise.

2.2. Modeling

In modeling the dynamic behavior of track and of interaction between the vehicle and track, it is convenient to consider six sub-systems

1. the vehicle including the car body, bogie and wheelset;
2. Wheel/rail contact and representation of excitation;
3. the rail;
4. the fastening system, including the rail fastening itself and the rail pad;
5. the sleeper;
6. the sleeper support, including the ballast and substrate.

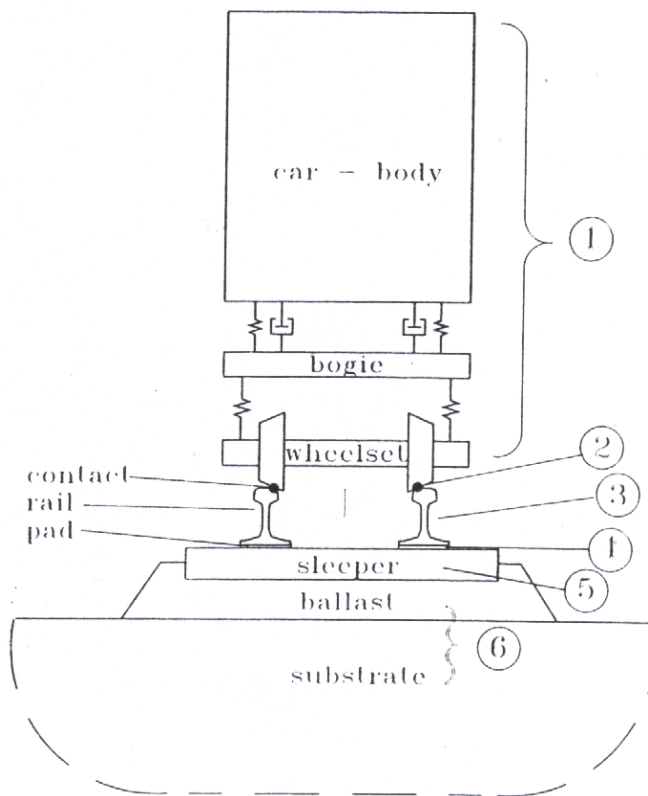


Figure 1. The sub-systems contained in the complete model [57]

Models should be as simple as possible and as accurate as necessary according to the aim of modeling. The first demand of model simplicity is important with respect to computational efficiency. This demand is fulfilled by assuming that all the displacements and strains are small in amplitude. Thus a linear model can be applied, which is accompanied by fast solution methods, which mostly work in the frequency domain. However, refined models often have to account for non-linear effects, so that Fourier transform techniques cannot be applied and, thus, a more time-consuming analysis has to be carried out in time domain.

The second demand of sufficient accuracy of the model is important with respect to modeling errors. Such errors can be caused by neglecting important effects, making wrong assumptions about the loading or the disturbances or by applying wrong system parameters. To avoid these errors, identification methods have to be applied and a model validation has to be performed. This requires experimental investigations in any case.

2.3. Vehicle Models

For a classical rail vehicle, the car body rests on two bogies each containing two wheelsets. The spring and damping elements connecting the wheelset bearings and the bogie frame are called the primary suspension. The secondary suspension connects the bogie frame and the car body.

Usually, the wheelsets of high-speed vehicles have two up to four brake discs mounted on the axle between the wheels. The mass of such wheelsets is high. In most of the designs, the longitudinal and lateral stiffness of the primary suspension are high. This is necessary for a stable running of the wheelsets. In comparison, the secondary suspension is much softer. Since additionally the mass of the car body is high, about 30 tons, car body and bogies are decoupled by a frequency ratio of about 1:10.

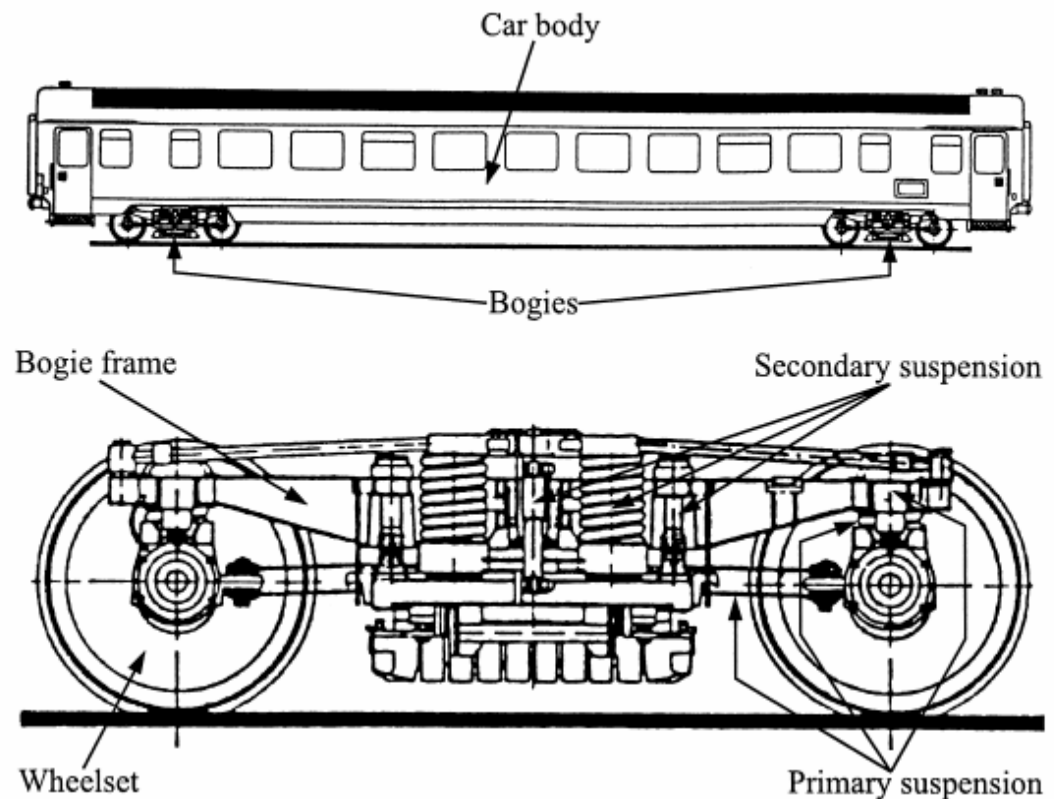


Figure 2. Rail vehicle [88]

The dynamic behavior of the vehicle itself is important with regard to curving, stability and, if it is a passenger vehicle passenger comfort. Vehicle suspensions are commonly designed to ensure that rigid body modes of a vehicle's body occur below about 10 Hz in order on the one hand to ensure adequate isolation of passengers from vibration and on the other hand to reduce the effective unsprung mass, thereby reducing dynamic loads at the wheel/rail interface. At these frequencies the track behaves essentially as a relatively stiff spring. However at frequencies about 20 Hz, the track's inertia becomes increasingly important while the vehicle's suspension isolates all but the unsprung mass (essentially the wheelset, bearings and any axle-hung traction motor and gearing) from the remainder of the vehicle.

At low speeds the response is quasi-static so that the track response due to train axle loads appears mostly downward at the point of

their action. On the other hand, at high speeds the train-induced response becomes dynamic due to the inertia generated in the track–ground system, so that the track vibrations appear evenly in both upward and downward directions. [106]

The vehicle can be modeled mathematically according to the frequency range of interest. The rigid multibody models are appropriate in the low frequency range of about 0 Hz-50 Hz. The most important component is a single free wheelset. Most authors use the assumption of a ‘quasi-stationary’ load, where it is assumed that the effect of vehicle convention is not important for the calculation of vibration propagation. So the knowledge about the wheel loads is necessary. In practice, wheel loads vary over a wide range; an unloaded bogie container wagon for example has a wheel load of about 25 kN, unloaded light rail and metro passenger vehicles are typically 35–40 kN, mainline passenger vehicles range from about 40 to 60 kN, while loaded freight vehicles have wheel loads in excess of 100 kN. [120]

Krylov challenged this assumption by suggesting that trans-sonic effects can be expected when existing high speed trains travel on soft ground.[60] Train loading is basically a problem of a stationary loading when the speed of motion is assumed to be constant. The train geometry determines the periodic vibration frequencies, while other frequencies originating from the sleeper spacing are also essential. Hence, Krylov [59,60] formulated these frequencies in a unified form. Takemiya et al. [106] replaced the sleeper frequencies by driving frequencies for the moving loads. Picoux and Le’Houdec separate this constant wheel load for an engine and carriage unit.[87] L’Mesgoues investigated the transmission of vibrations over the surface of the ground, due to high-speed moving, vertical harmonic rectangular loads theoretically by considering constant rectangular load. The authors have discussed a modified hysteretic damping model defined in the Fourier wavenumber domain and adapted for the problem of moving loads [67].

The elastic multibody models are appropriate in the mid- and high-frequency range of about 50 Hz-5 kHz. The existing component models

have mainly been developed to solve acoustic problems. Of particular importance are elastic wheel models that can easily be extended to models of a wheelset.

Young [123] uses a 9 degree-of-freedom vehicle model, where Zhai [124], and Lei [68] perform their models of vibration prediction based on the same 10 degree-of-freedom vehicle model.

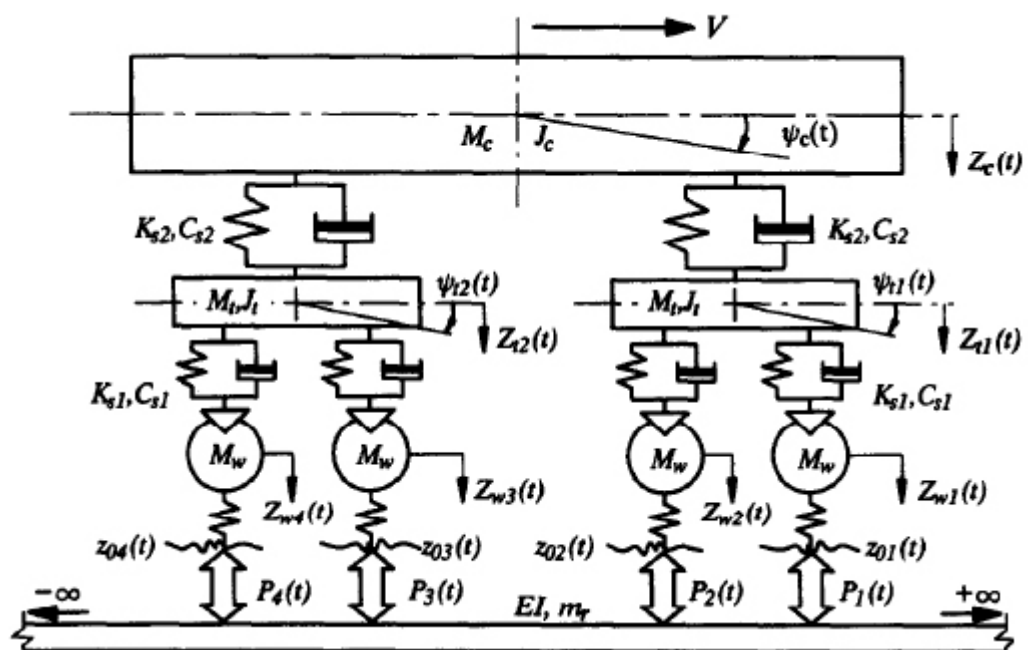


Figure 3.10 degree-of-freedom vehicle model [124]

Lei [68,69] divides the vehicle and track coupling system into two parts; lower structure and upper structure. The vehicle as the upper structure in the coupling system is a whole locomotive or rolling stock with two layers of spring and damping system in which vertical and rolling motion for vehicle and bogie are involved.

Hou [39] employs a two level suspension vehicle model, where the wheelset and the bogie are connected by the primary suspension while the

car body is supported on the bogie through the secondary suspension. He represents a more realistic vehicle model incorporating two wheelsets, two bogie side frames, and half a car body as a 10 degree-of-freedom model. Sheng [97] gives different vehicle models with their stiffness and mass matrices for passenger and freight trains consisting of different degree-of-freedom in his work. Ren [91] and Sun[103] use 33 degree-of-freedoms in a passenger car model and 37 degree-of-freedoms in a three-piece freight car model. Sun uses in his work [104] a wagon model with 37 degree-of-freedoms, which are given in Table 2.

Table 2. Degree-of-freedoms of wagon components used in Sun's work [104]

Components	DOF							Number of items	Number of DOF
	u	v	w	ϕ_x	ϕ_y	ϕ_z	ϕ_{Pa}		
Wagon carbody		X	X	X	X	X		1	5
Bogie frame						X	X	2	4
Sideframe		X	X	X	X			4	16
Wheelset		X	X			X		4	12
Total DOF									37

2.3.1. Wheelset Models

The wheelset can be modeled according to the complexity of the problem as multibody, continuum or finite element models.

2.3.1.1. Multibody Models

The simplest one is to split the wheelset in a certain number of rigid bodies linked together by springs and dampers. The advantage of such a technique is the small number of degrees of freedom. Zheng [125] models each axle as a mass-spring-damper vibration unit in his work to present the derivation of the governing equations for the stability of vibration of an integrated system comprising a moving train and the railway track.

2.3.1.2. Continuum Models

A continuum model is achieved by distributing the mass and inertia along the wheelset axis with consideration of the location of the brake discs. With this model, the three-dimensional deformations of the axle including bending and twisting can be considered. More detailed models should also take into account the shear deformations and the elongation of the axle, out-of plane deformations of the wheels including flexural and umbrella modes and in the high-frequency range also in-plane motions and shear bending. Szolc [105] models the axle as a rotating elastic beam, which can also be deformed torsionally. The wheels and the brake discs are rigid bodies, which are connected to the axle with massless membranes. He shows that the gyroscopic effects lead to a split of the natural frequencies and a quite strong coupling between bending motions in the vertical and lateral plane.

2.3.1.3. Finite Element Models

The Finite Element Method (FEM) enables a nearly unbounded accuracy of the model. Therefore, most FEM models of the wheelset are also applicable in the high frequency range. The corresponding models found in literature show strong deviations in their number of degrees of freedom. One can distinguish between full three-dimensional structures [76], two-dimensional structures [110], where the rotational symmetry is taken into account, and one dimensional structures.

2.3.2. Models of Car Body and Bogie

In the mid- and high-frequency range the dynamic behavior of the car body and the bogies is decoupled by the soft secondary suspension. Thus, very simple models of the car body are sufficient. Frequently it is even replaced by its constant weight and a kinematical constraint. An interesting model is developed by Young [123], where the car body is modeled as a Timoshenko beam with finite length and is supported at each side by a double-axle bogie through the secondary suspension. He treated each bogie as a two degree-of-freedom rigid body and is linked through the primary suspension with two wheelsets, which are characterized as unsprung masses.

In following chapters the spectrum of applied load will be obtained for different models by deriving the appropriate transfer functions.

2.4. Dynamic Track Models

2.4.1. Track Structures and Components

Different track systems are used to meet the requirements of trams, underground systems and high-speed transportation and, of course, other types of design are used on bridges, in urban areas and in tunnels. Different damping or decoupling elements like ballast mats or highly elastic rail supports are added to reduce vibrations and noise radiation.

For typical track types the rails are fixed on concrete or wooden sleepers with different fastening systems. Between sleeper and rail, rail pads are located which are typically made of rubber, plastic or a composite material. Further components of the ballasted track are the ballast layer, the subgrade and the subsoil. In the case of a rigid track the ballast is substituted by a concrete strip. The connection between the one-block or two-block sleepers and this strip is established by different techniques. Often an elastic layer is added to increase the compliance of this structure. Below the concrete the rigid track consists of a hydraulically compacted layer and a frost protection layer. For both depicted track types the subsoil properties can disperse significantly. Its stiffness is quite low for wet, sandy soils and high for rocky ground.

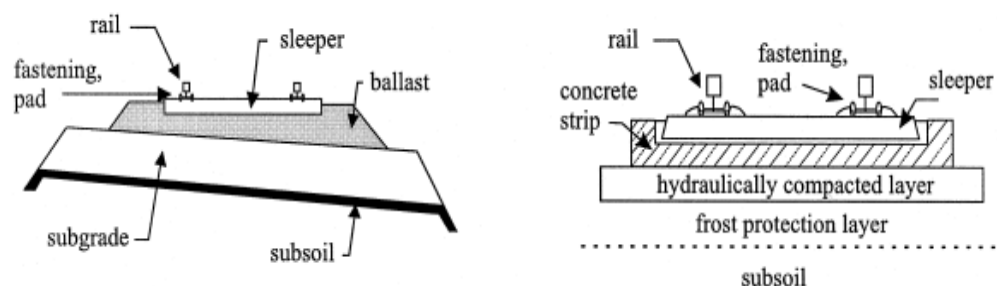


Figure 4. Track types: ballasted track (left) and rigid track (right) [88]

2.4.2. Rails

For static and stability analyses which were undertaken before about 1960 the rail was considered to be a Bernoulli-beam and it does indeed appear that this model is adequate for representation of the rail's response to vertical dynamic excitation for frequencies of less than about 500Hz. [110] Researchers working in this frequency range used the Euler-Bernoulli beam as the rails in their models [24,25,27,38,43,45,51,53,59, 60,65,78,85-91,94-99,106,124,125].

However such a model is no longer adequate for the response to vertical forces at higher frequencies as shear deformation of the rail becomes increasingly important.

The equation of motion for the bending displacement $y(x, t)$ of an Euler beam loaded by a force distribution per unit length $f(x, t)$ is given as,

$$m \frac{\partial^2 y}{\partial t^2} + EI \frac{\partial^4 y}{\partial x^4} = f(x, t) \quad (2.1)$$

It is straightforward to show that the displacement frequency response $Y(x, \omega)$ of such a beam excited by a unit point harmonic force at $x = 0$ is given by,

$$Y(x, \omega) = \frac{1}{4\alpha^3 EI} (e^{\alpha|x|} + ie^{i\alpha|x|}) \quad \text{with} \quad \alpha^4 = \frac{m\omega^2}{EI} \quad (2.2)$$

where, m is the mass per unit length of the beam and EI is its bending stiffness.

An improved beam model, taking into account the shear deformations and the rotatory inertia, is the Timoshenko beam model. Figure 5 represents the model by taking a differential beam element.

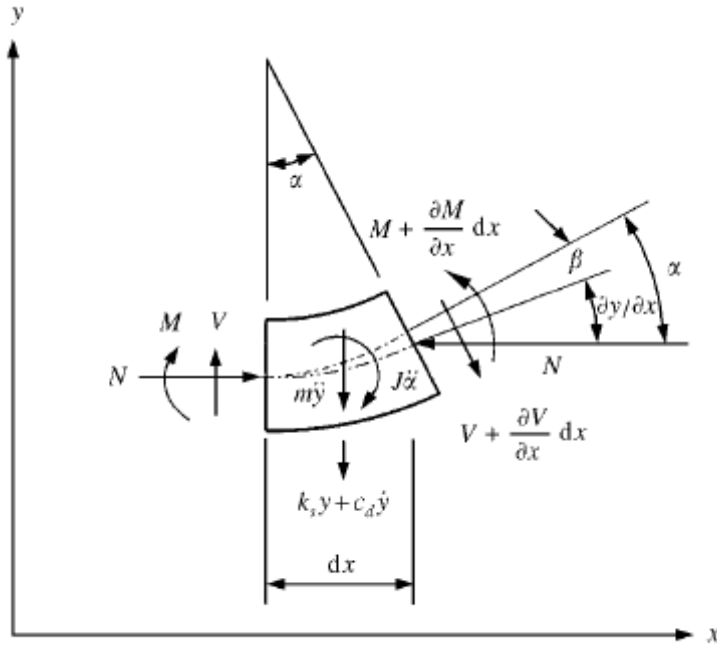


Figure 5. A differential beam element [15]

The equation of motion of such a beam element is given as,

$$m \frac{d^2 y}{dt^2} + c_d \frac{dy}{dt} + k_s y - k' A G \left[\left(1 - \frac{N}{k' A G} \right) \frac{\partial^2 y}{\partial x^2} - \frac{\partial \alpha}{\partial x} \right] = 0 \quad (2.3)$$

$$EI \frac{\partial^2 \alpha}{\partial x^2} + k' A G \left(\frac{\partial y}{\partial x} - \alpha \right) - J \frac{d^2 \alpha}{dt^2} = 0 \quad (2.4)$$

where, y is the deflection of the beam, b is the shear distortion of the beam, a is the bending rotation of the beam, m is the mass per unit length of the beam, J is the rotary inertia of the mass per unit length of the beam, $k' A$ is the effective shear area and I is the second moment of area of the beam.

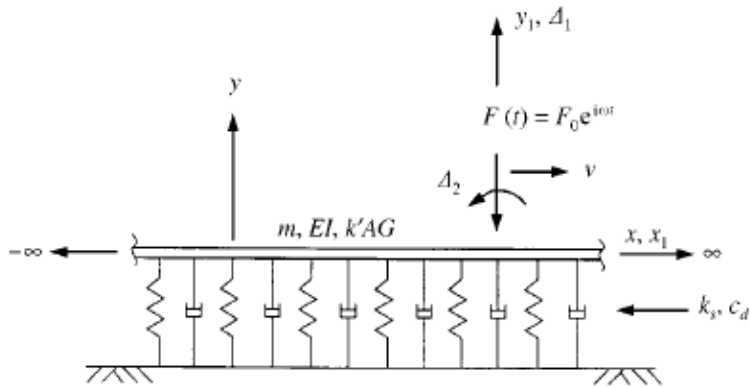


Figure 6. An infinite beam on viscoelastic foundation [15]

The Timoshenko beam model can also be modified according to the frequency range of interest. According to Knothe and Grassie [57] for the case when only the longitudinal vibrations are of interest, the rail can be modeled as a single Timoshenko beam up to 2.5 kHz and for wavelengths greater than 0.4 m. If lateral and torsional modes are to be included in the model, the railhead and foot have to be modeled at least as independent Timoshenko beams interconnected by continuous rotational springs. Many researchers adapted Timoshenko beam model to their models. [7,15,17,27,39,74,103,104,117,119,123] Attempts have been to establish the frequency ranges in which different models adequately represent the rail's behavior. [57] For the frequency and wavelength ranges of interest, five different wave propagation modes occur for a UIC 60 rail, four of which are shown in Figure 7: A lateral bending, B vertical bending, C and D two torsional modes.

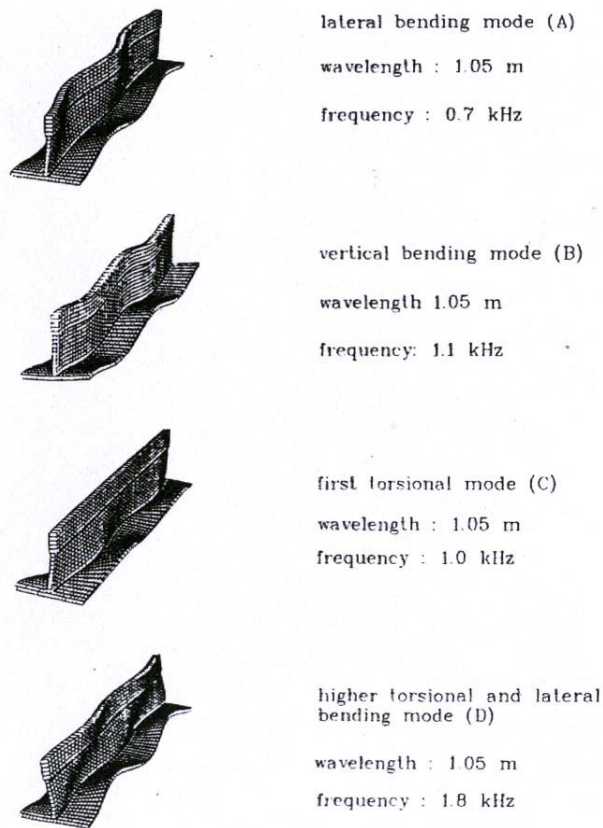


Figure 7. Wave propagation modes of a UIC 60 rail, (A,C,D) lateral-torsional (B) vertical [57]

2.5. Rail Fastening System

In many track systems with concrete sleepers, the rail fastening system is composed of a resilient spring fastening, where it is commonly designed in parallel with a much stiffer railpad (Figure 8a). Typically the rail pad is made of rubber, plastic or a composite material such as rubber-bonded cork. The load/deflection behavior of the fastening system is non-linear, but since its behavior when a loaded wheel is near the sleeper is of greatest interest, some linearization of the load/deflection behavior is justified. [57]

When vertical vibration is of concern, the pad is usually modeled as a spring and viscous dashpot in parallel (Figure 8b). The damping shows a structural behavior with a constant loss factor, which is more consistent

with the known behavior of materials such as rubber. [52] The pad is represented similarly in models of the lateral dynamic behavior of track. For three-dimensional rail and track models it is convenient to represent the pad as a viscoelastic layer distributed across the railfoot (Figure 8c). In two-dimensional models it can be represented as acting at a point on the railfoot. Design of a railpad with prescribed stiffness and damping can not be found in literature due to the difficulty in practice to find appropriate values for the railpad parameters. The required values are obtained in field with impulse testing methods with an impulse hammer or electromagnetic exciter by applying appropriate transfer functions for the track structure.

Sato [92] has proposed in his work that the increase in pad stiffness with frequency should be taken into account by representing the high polymer rubber by three parameters rather than the conventional two.

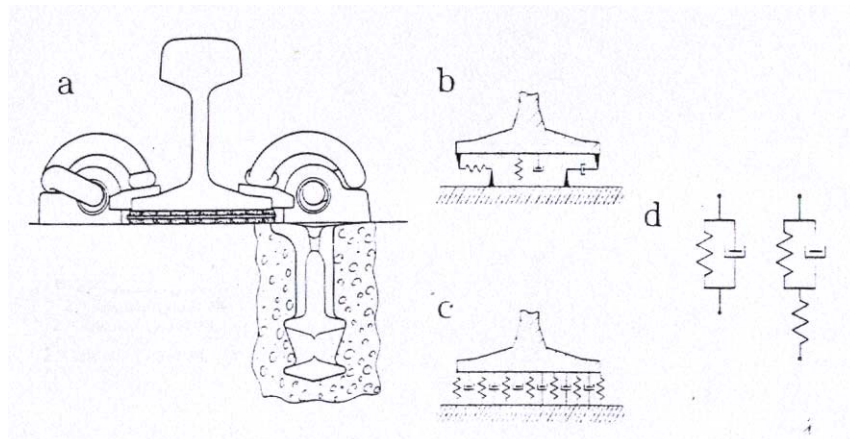


Figure 8. a) Technical drawing of rail fastening systems and b) c) d) different schematic representations[57]

Using the rail fastening system with the appropriate representation, a discrete [39,38,51,65,74,85,91,103,104,119,123] or a continuous [7,45,48,68,69,86,95-99,119] model is obtained according to the requirements of the complete track model.

2.6. Sleeper models

A ballasted railway track is commonly constructed with monoblock or twin-block concrete sleepers. In most of the designs monoblock sleepers are preferred. It is observed that in most cases the damage occurs from the sleepers' resonant behaviour.

Grassie [31] has shown that by modeling the dynamic behavior of a typical concrete railway sleeper, shear deformation and rotatory inertia should be included. Thus the most complete sleeper model is a Timoshenko beam of variable thickness. He proposes that a typical non-uniform monoblock concrete sleeper can be modeled with sufficient accuracy for most practical purposes as an equivalent uniform beam with the effective flexural rigidity, cross-sectional area and the radius of gyration given as

$$EI = \sqrt{(EI_r)(EI_c)} \quad (2.5)$$

$$A = M / \rho L \quad (2.6)$$

$$r_g = (I / A)^{1/2} \quad (2.7)$$

where the subscripts r and c denote the values at the railseat and sleeper center respectively.[31] Young [123] also adapted a Timoshenko beam in his model as the sleeper model.

Another sleeper model is obtained by representing the sleeper as a uniform beam. [17,30,85,91,103,104] With this model, considerable success is obtained by correlating the response of rail and sleepers in track to that measured at frequencies about 700 Hz. Ren [91] modeled the uniform beam with uniformly distributed damping. Hou [39] modeled the sleeper as an Euler-Bernoulli beam. Lai [65], Zhai [123], Luo [74], Wu&Thompson [119], Lei [68,69], Kalker [51] and Hildebrand [38] modeled sleepers as rigid. Shamalta&Metrikine [94] used a Kirchhoff plate as by modelling the sleeper, where Karlström [53] assumed the Kirchhoff plate being anisotropic. Krylov [59,70] considered the sleepers as point sources in the low frequency domain. Hence the separation of sleepers becomes an important parameter.

When a continuous track model is used, the sleepers are modeled as a mass per unit length of track. This approach is used by the authors Picoux [86,87], Sheng [95,96,97,98,99], Verichev&Metrikine [117], Wu&Thompson [119], Gardien [27], Jones and Block. [48]

2.7. Ballast and substrate

The ballast is the part of the track, which deflects in a highly non-linear manner under load. These nonlinearities are caused by gaps between sleeper and ballast and by the ballast properties themselves. The stiffness of such a granular material depends on the void ratio, on the loading velocity and on the stress state [32,33]. Inside the ballast strip this stress state is inhomogeneous even on a small length scale.

Until about 1980 the lowest vertical natural frequency of a loaded track was reported to be at about 25-40 Hz. [57] However measurements made subsequently on BR track showed a first resonance peak for the track without wheelset to be 130 Hz. [29] This decreased under a vehicle to 50-80 Hz depending on the unsprung mass. As these measurements (and most of the subsequent measurements using an impulse hammer technique) are reliable only for frequencies greater than about 50 Hz, there may in fact be resonances both at 25-40 Hz and around 100 Hz: the former would arise from movement of both the ballast and the track above it on elasticity of the substrate, while the latter would arise from movement of the rail and sleepers on the ballast's own resilience. Most of the ballast models consist of springs and dashpots in parallel. There are only few models where the ballast mass is included.

Modeling of the substrate, where the vibrations are transmitted, is another important aspect of the whole problem. In an early paper by Gutowski and Dym [34], wave propagation through soil is investigated according to different source types and soil absorption characteristics. According to the authors, to properly predict excitation levels at a building due to an external source like surface or subsurface railway; one must be able to predict how much vibration, in terms of both levels and spectra, is

transmitted through the ground from the source. This problem has its complexities due to lack of enough understanding of soil behavior, the difficulty of determining accurate values of soil properties and the difficulty of modeling precisely the sources of vibration and the resulting near- and far-field behavior. The railway traffic on the surface produces ground waves on the surface as well as beneath the surface. The tunnel as a source will also produce surface and body (interior) waves in principle. But for a buried source the strength and behavior of the surface is not well understood. It is convenient to say that if buried deep enough the tunnel will excite body waves.

The basis of most of the work done on modeling the sources and the transmission paths can be found in the work of Lamb. [64] He investigated the response of isotropic, homogeneous elastic half-space to different kinds of sources like harmonic and impulsive point and line sources based on the laws of wave propagation in an unlimited medium developed by Green and Stokes and modified by the discoveries of Lord Rayleigh. Researchers developed solutions for different source characteristics. Lapwood [63] investigates the problem of the disturbance near the surface of a semi-infinite medium due to a buried line source emitting a pulse of the form of a Heaviside unit function by using double integral. Garvin [28] handles the same problem using Laplace transform techniques. Jette and Parker [47] reformulate Lapwood results for a buried line source of conical waves. Most of the models used to predict vibrations from surface and underground railway systems use this elastic half-space model. [1,2,35,50,67,72,94,100,101] According to Metrikine and Popp [78] the real subsoil possesses a viscosity and may be bounded. The visco-elastic model is developed to consider the effect of viscosity. [5,8,9,10,11,13,14,19,40,78,107,125] The main difference between the visco-elastic and the elastic halfspace model lies in the applied damping model. Hunt [42] uses in an early paper the frequency response function for a homogeneous, isotropic, damped half-space. In this work the elastic-viscoelastic analogy is used to apply damping to the model by writing the elastic moduli as complex quantities. Hao [35] applies hysteretic damping

theory due to its common use in practice to model soil energy loss and its easy application. Lefeuve-Mesgouez et.al [66] discussed a modified hysteretic damping model defined in the Fourier wavenumber domain and adapted for the problem of moving loads. The damping is added to the system by modifying Lamé constants μ and λ .

Theodorakopoulos [109] investigates the dynamic response of a poroelastic half-plane soil medium subjected to moving loads analytically/numerically under conditions of plane strain where hysteretic damping in the soil skeleton is also considered.

Forrest and Hunt model the soil surrounding the tunnel without a free surface, which would both reflect impinging body waves back towards the top of the tunnel and have surface waves excited upon it. [24,25] They claim that in the far field, it is likely that buildings would receive more energy from such surface (Rayleigh) waves than from body waves, since the former decay less rapidly. Nevertheless, the surface would have much less influence on responses near the tunnel, especially the deeper the tunnel is. Special attention will be paid to the works by these authors in the following chapters.

Knothe and Grassie [57] give in their literature survey a schematic representation of the models for the ballast and substrate. (Figure 9) The Type A is a simple 2-parameter model in the vertical direction. The model is applicable to the phenomena in high frequency range and for the cases when the axle is close to the sleeper of interest. There are many variations of this model in literature. Lai [65], Young [123], Kalker [51] and Wu&Thompson [119] use this model without making any change, where Hou [39] models the substrate as rigid. Ono and Yamada [85] assume that masses and elasticities of the ballast and the roadbed are uniformly distributed over their whole volume.

Another possible model is shown in Figure 9 as Type B, where the ballast and the substrate are considered together as elastic or visco-elastic half-space. [74] Karlström [53] uses this model with a layered viscoelastic halfspace, whereas Hildebrand [38] applies elastic halfspace.

To obtain better correlation between the calculated and measured response another sleeper support model is developed. (Type C) This model includes additional ballast masses below each sleeper, which are interconnected by springs and dashpots in shear. This model is used by Sun [104] and Zhai [124]. Sun uses in another paper [103] the ballast pyramid model based on the theory of elasticity, developed by Ahlbeck et al.

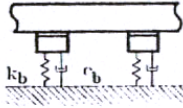
A general support model is shown as type D in Figure 9 with a layer of ballast on a three-dimensional half-space. Note that the theoretical investigation of such a model is extremely difficult. The ballast and substrate can be modelled in continuous track system by eliminating the discrete sleeper support. This condition necessitates modeling the ballast as vertical springs and dashpots in parallel per unit length of the track having consistent mass and a substrate model. This continuous model is used by authors Bitzenbauer [7], Takemiya [106], Wu and Thompson [119] and Ren. [91] Lei [68,69] and Picoux [86,87] only included the ballast in their model, whereas Sheng uses layered halfspace with rigid foundation in his researches [95-99] Jones and Block [48] use in their finite element model a similar layered model resting on a half-space. Gardien [27] extends the layered halfspace model to infinity in his finite element model by applying infinite boundary conditions.

2.8. Floating slab

A method for achieving substantial reductions in vibrations transmitted to tunnel structures is the use of resiliently supported track bed slabs (so-called "floating slabs")-either continuous cast-in-place slabs up to about 21 m (70ft) long, or a series of precast slabs 0.7 to 1.5 m long. [62] The concrete slab supporting the two rails is mounted on rubber bearings or steel springs to isolate it from the tunnel invert.

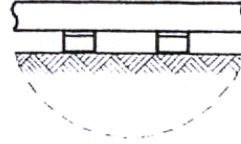
Type A

- discrete sleeper support
- ballast: spring and damper



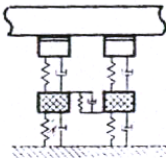
Type B

- discrete sleeper support
- halfspace modelling of ballast and substrate



Type C

- discrete sleeper support
- ballast: spring and damper
- interconnected ballast masses
- substrate: spring and damper



Type D

- discrete sleeper support
- continuous ballast layer
- halfspace substrate model

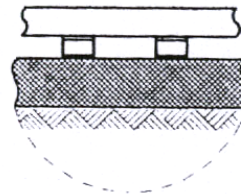


Figure 9. Ballast and substrate models [57]

To predict the effect of soft slab-bearings and the distribution of slab bearings by vibration isolation, Hussein and Hunt [44,45] use a comprehensive three-dimensional model of a deep underground railway tunnel with Euler-Bernoulli beams to account for the rails and the slab track.

In another paper by Forrest and Hunt, the slab is coupled to the tunnel system in a similar way. Their calculations show that floating the track slab may in fact cause increased transmission of vibration under certain conditions and the desired insertion loss may not be achieved in this way. [25]

2.9. The complete track model

All the mentioned track components form the complete track model. The main difference between track models occurs in the supporting type of the rails. According to the frequency range of interest, the rails can be modeled with continuous or discrete supports.

When the vehicle behavior in curves, the stability or the passenger comfort is of primary interest, which are phenomena with frequencies below 20 Hz, the track behaves essentially as a relatively stiff spring. Continuous support models, which are strictly valid only for calculation of the track's dynamic response at frequencies lower than about 500 Hz for vertical excitation and 400 Hz for lateral excitation, [57] are obtained by spreading the mass, stiffness and damping components of the discrete support along the track. Rails are resting on continuous viscoelastic foundation and a continuous layer representing the sleepers. The roots of the research on classical continuous models of infinite length can be found in Timoshenko's papers [112,113]. He studied an infinite Bernoulli-Euler beam on an elastic Winkler foundation under static and dynamic loads. This model has been analyzed mainly using Fourier transform techniques. The continuous model is preferred by many authors due to its simplicity. [7,15,59,60,78,86,87,94-99,106,117,119,125] Forrest and Hunt show the inadequateness of this model by giving a comparison between their track-tunnel-subsoil coupling model and the continuous model. [24,25]

A discrete support appears more representative of reality for the majority of track, which is laid on discrete sleepers. The masses and the elasticities of the ballast and the roadbed are taken into consideration. In this model every sleeper is supported by a separate foundation, which represents the ballast and the roadbed.

The inertias of different track components become important when dealing with higher frequencies. Thus, in the range up to 250 Hz the properties of ballast and subsoil have a strong effect on the track dynamics. For higher frequencies up to 700 Hz the properties of the pads are important and for frequencies above 700 Hz the geometry of the rails

has to be taken into account. An important distinction between discretely supported track models is that the track structure can be modeled as being either finite or infinite in length. The type of structure is closely connected to the solution technique. Track structures of infinite length are commonly used for frequency-domain solutions whereas finite track structures are more appropriate for time-domain solutions, particularly if there exists significant non-linearities. The main problem with a finite track model is that boundaries may introduce undesirable effects in studying the response to a moving load. [57] Discrete models of finite length are usually based on the finite element method.

2.10. Tunnel

Ground-borne vibration levels from underground railway systems are also affected by the type of tunnel structure, its mass and tunnel wall thickness. According to Kurzweil [62] a doubling of the average wall thickness, for the same material, can lead to reductions in the wall vibration levels of 5 to 18 dB.

Table 3. Effect of subway structure type on tunnel vibration levels [62]

Subway structure	Relative vibration level (dB)
Cast iron or steel single tunnel	+4
Concrete single tunnel or box	+2
Double box	0
Triple box	-2
Station	-4

The tunnel structure can be modeled as rigid or elastic, with or without wall thickness. In an early work by Krylov the tunnel diameter is assumed to be very small in comparison with characteristic wavelengths of generated ground vibration spectra. In another paper, [70] Lin and Krylov model generation and propagation of ground vibrations by considering the tunnel diameter. In this paper an approximate analytical approach is

developed to predict the effect of tunnel diameter on amplitudes and radiation patterns of generated vibrations, based on the use of the reciprocity principle.

Balendra [5] decomposes the total soil-structure interaction problem into a foundation radiation problem and a tunnel radiation problem. In this paper it is assumed that applied train loading is uniformly distributed and plane strain conditions would develop for reasonably uniform ground conditions. Also it is assumed that the foundation and the tunnel are both perfectly bounded with the soil.

Gardien uses a three dimensional finite element method to model the tunnel and the surrounding layers, where the characteristics of the tunnel are determined in terms of a Timoshenko beam. [27] The model is statically loaded in the vertical direction at the location of the track. As a result of this, the tunnel deflects vertically.

Another tunnel model is developed by Degrande. [20] In this paper the three-dimensional dynamic tunnel–soil interaction problem is solved with a subdomain formulation, using a finite element formulation for the tunnel and a boundary element method for the soil. The periodicity of the tunnel and the soil is exploited using the Floquet transform, limiting the discretization to a single bounded reference cell of the tunnel. The response of two tunnels in different sites, which are modeled using MATHLAB software, and the surrounding soil due to a harmonic load on the tunnel invert is considered. The obtained results are validated by means of in situ experiments.

Forrest and Hunt develop a three-dimensional model of the tunnel analytically as an infinitely long, thin cylindrical shell surrounded by soil of infinite radial extent. [24] In this paper interaction between spacing of train axles, the tunnel diameter and the distance from the tunnel to nearby building foundations is considered; since for typical soils, the wavelengths of ground vibration in the frequency range 20-100 Hz are comparable with these parameters.

The coupled problem is solved in the frequency domain by Fourier decomposition into ring modes circumferentially and a Fourier transform

into the wavenumber domain longitudinally. The advantage of this tunnel model is that the model is suitable for use in combination with different track models to calculate the ground vibration due to excitation by running trains. An accompanying paper to assess the effectiveness of floating-slab track uses the same model. [25]

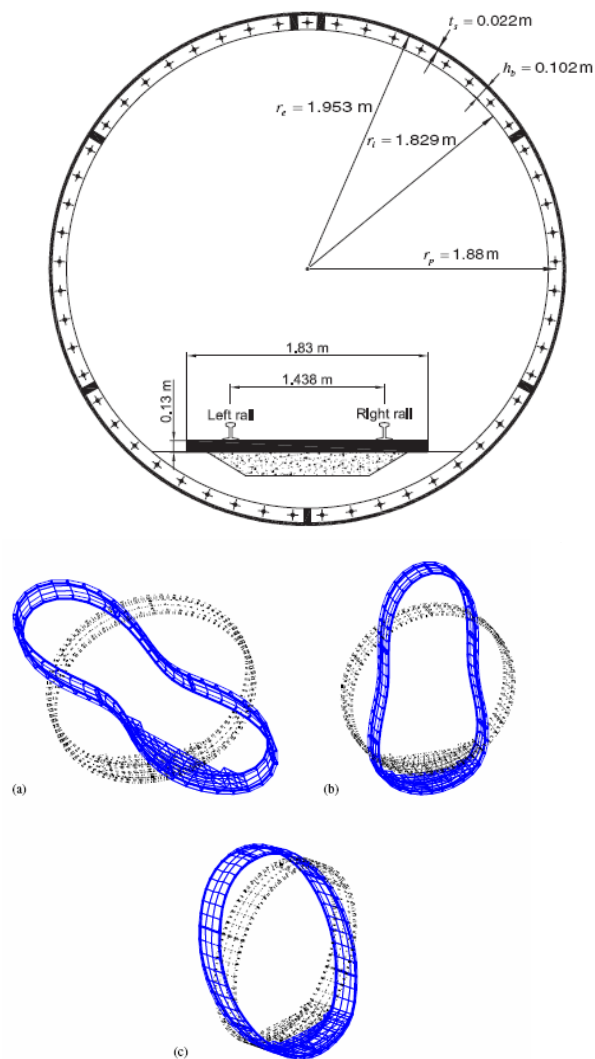


Figure 10. The first tunnel model developed by Degrande and the first (a,b) in-plane and (c) out-of-plane modes of the reference cell of the Bakerloo line tunnel.

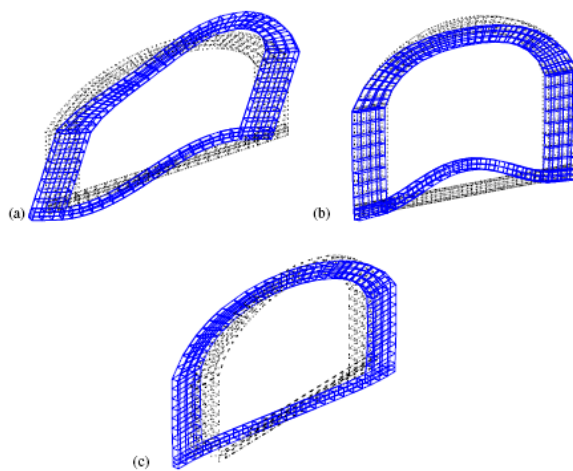
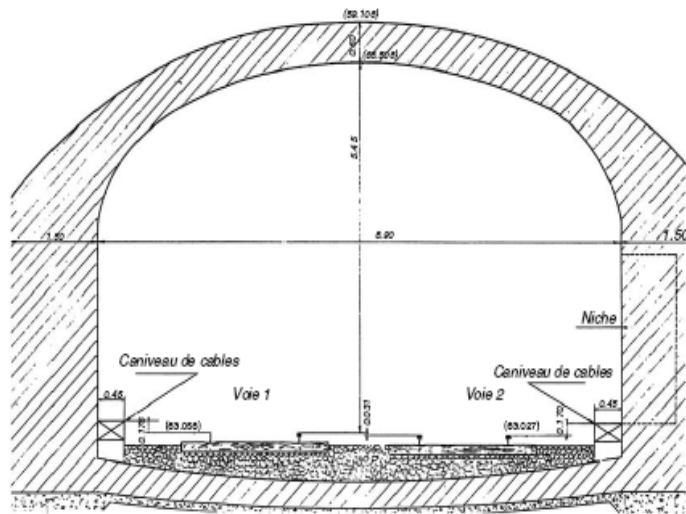


Figure 11. The second tunnel model developed by Degrande and the first (a,b) in-plane and (c) out-of-plane modes of the reference cell of the RER B tunnel.

2.11 Contact modeling

Another important component, which is necessary to model in the dynamic system of vehicle track, is the wheel/rail contact. Two main types

of model have been used to study wheel/rail interactions. One represents a wheel (or wheels/vehicle) rolling over roughness on the rail. This model was used by Nielson and Igeland [83]. The other is a moving irregularity model. This model can be regarded as one in which the wheel remains in a fixed position on the rail, and a strip combining the roughness on the wheel tread and railhead is effectively pulled at a steady speed between wheel and rail. The combined roughness forms a relative displacement input between the Wheel and rail, and thus the wheel/rail interaction force depends on the dynamic properties of the wheel and rail (including the contact zone) at the contact position. The moving irregularity model has been widely used to investigate problems of wheel/ rail interaction and rolling noise, for example by Remington [89] and Grassie et al. [29]. For high frequency vibration of railway track, for example above 50 Hz, the wave speed in the rail (hundreds of meters per second) is much higher than the train speed (tens of meters per second), and therefore assuming the wheel is stationary is an acceptable approximation which brings much convenience for studying wheel/rail interaction and vibration.

Figure 12 shows the form of the wheel/rail interaction using the moving irregularity model, in which a roughness is pulled between a stationary wheel and the rail. In this system there are three dynamic systems; the wheel and track are considered to be linear, while the contact stiffness is non-linear.

For a linear system, which is not time varying, the equation of motion can be expressed in the frequency-domain. In a simple case of vertical interaction between wheel and rail, the contact force F can be given as in [29]

$$F(\omega) = -\frac{R(\omega)}{\alpha^W(\omega) + \alpha^C(\omega) + \alpha^R(\omega)} \quad (2.8)$$

where

R is the relative displacement (roughness) between the wheel and rail; α^W , α^C and α^R are the point receptances (displacement divided by force) of the wheel, contact spring and rail respectively and ω is the circular frequency of the excitation (roughness).

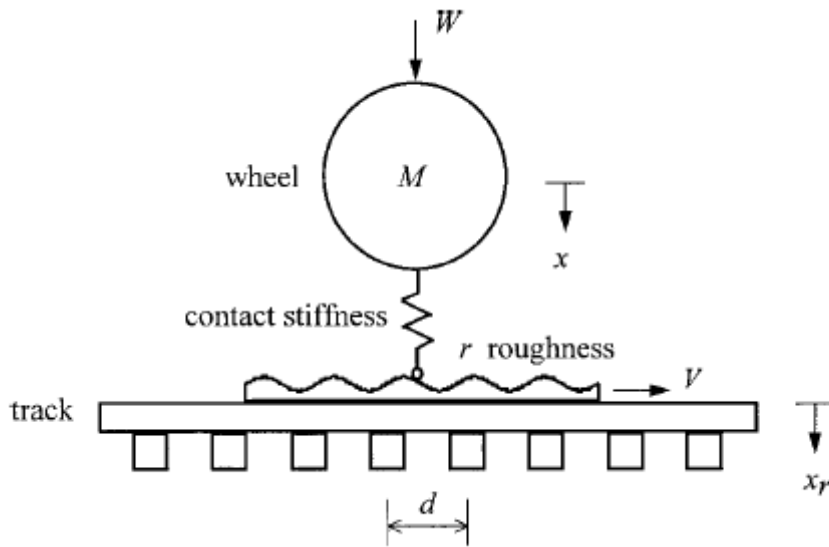


Figure 12. The moving irregularity wheel/rail interaction model, where V is the train speed

The contact receptance, α^C , represents the local elastic deformation of the wheel and rail in their contact zone. In general, however, the contact stiffness between the wheel and rail is non-linear and can be approximated by the Hertz law, whereas equation (2.8) is derived based on the assumption of a linear contact spring.

The representation of a non-linear wheel/rail contact force is not complex mathematically, it being proportional to the contact deflection to the power 3/2, which is given in the form

$$f = C_H (x_w - x_r - r)^{3/2} \quad (2.9)$$

where, f is the wheel/rail contact force, x_w and x_r are the wheel and rail displacement respectively, r is the roughness, C_H is the Hertzian constant.

This expression is exact for cylindrical surfaces, which meet at an elliptical contact patch, and provides an approximation for other contact geometry. However, the superposition principle does not hold for a system containing a non-linear element and thus calculations in the time-domain are essential rather than in the frequency-domain. The tangent stiffness,

$Kt = df/du$, with u the contact deflection, is used in the linear model and is chosen according to the static load applied.

According to Wu and Thompson [120,121] the effects of the non-linear contact on the wheel/rail interaction are affected by the static preload and the dynamic properties of the wheel and rail. Under a large static contact load the non-linear effects on the wheel/rail dynamic interaction and vibration are weak and can be ignored. This is because the difference between the non-linear stiffness and the equivalent linear (tangent) stiffness is very small for a large static preload. The non-linear effects on the wheel/rail interaction are also not noticeable at low frequencies up to 100 Hz because in this frequency region the wheel and rail dynamic stiffness is much less than the contact stiffness and thus the latter can be regarded as effectively rigid, so that the question of its linearity is unimportant here. From a practical point of view, the non-linear effects are also not noticeable at high frequencies (above 1 kHz) because the roughness level at short wavelengths is generally very low. In such a case the dynamic contact deflection is small and the non-linear contact force-deflection relation can be well approximated by a linear one. The non-linear effects are only noticeable when the roughness excitation is in the frequency region around 200 Hz and 900 Hz, where the dynamic stiffness of the wheel and rail is similar to the contact stiffness, but even so the difference between the non-linear and linear interactions is very limited.

The difference is also small when a typical broad band random roughness excitation is applied. In the examples considered, if the wheel and rail surfaces are in good condition (r.m.s. amplitudes of roughness below 15 μm), the linear model can be used without significant error for all static loads down to 25 kN (equivalent to an unloaded container wagon). When the track is corrugated with an r.m.s. amplitude of 25 μm , good agreement between linear and non-linear models is obtained for static loads of 50 kN and above, but agreement is less good for lower loads. Non-linear interactions modify the force spectrum by at most 2 dB for 50 kN; for 25 kN this increases to 4 dB.

All the above suggests that the non-linear wheel/rail dynamic interaction model can be well approximated using an equivalent linear model when the roughness level is not extremely severe and a moderate static preload is applied to keep the wheel and rail in contact. Since a linear model can be expressed in the frequency domain, use of such a model greatly simplifies calculations.

2.12 Excitation modeling

2.12.1 Vehicle Disturbances

For wheelsets, two kinds of disturbances are important: unround wheels and static and dynamic unbalances. With increasing vehicle velocity, the dynamic forces caused by these disturbances increase as well.

Unbalances occur due to imperfect shapes or mounting of the wheels or the brake discs. Their effects on the system behavior have been investigated by Szolc. [105] To obtain a realistic distribution of such unbalances measurements are desirable.

Since both, the wheel-rail contact stiffness and the mass of a wheelset are high, only small deviations from the ideal circular shape of a wheel can be tolerated. Otherwise harmful contact forces would occur.

2.12.2 Wheel and rail discontinuities

According to Sun [103] main cause of vibration excitation is discontinuities in wheel and the rail like gaps in the rail (e.g. at a switch) or partially flat parts of the wheel. Some discontinuities cause periodic excitation while others cause non-periodic or localized excitation defined as impulse excitation. The periodic irregularities include the rail corrugations, the out-of-round wheels or the rounded flat wheels and are represented by cosine functions. Table 4 shows some cases of the periodic excitation sources and the corresponding expression $W_d(t)$.

The non-periodic irregularities include the indentation on the railhead due to the spalling or the defect of welded joint and the dipped-joint. When the excitation source is non-periodic and $L_d \leq 2\sqrt{2ra - a^2}$;

where L_d is the wavelength of irregularity, r is the rolling radius of wheel, a is the wave depth of the irregularity and the wheel and the rail will not be in contact with the trough of the irregularity.

For small L_d , when the flat wheel runs on the perfect rail or the perfect wheel runs at the defective rail, the instantaneous rotating center of the wheel suddenly moves down or up, inducing a vertical impact velocity. These excitation sources are called impulse excitation sources. Table 5 shows various impact velocities caused by small wheel flats, the short length of rail shelling and spalling, and the defects from rail welded joints.

Table 4. Harmonic excitation sources [103]

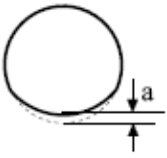
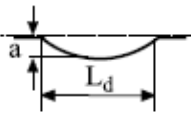
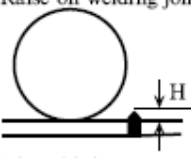
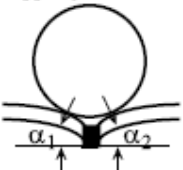
Name and geometry	Expression
Out-of-round wheel 	$W_d(t) = a(1 - \cos \Omega t)/2$ $\Omega = \frac{2\pi V}{L_d}$ $(0 \leq t \leq L_d/V)$
Indentation on rail surface 	a —wave length of irregularity L_d —wave depth of irregularity (for out-of-round wheel, L_d is the length of arc)

Table 5. Impulse excitation sources [103]

Name and geometry	Impulse velocity
Raise on welding joint 	$V_0 = V(\frac{2H}{r})^{1/2}$ r —wheel radius V —wagon speed
Dipped-joint 	$V_0 = (\alpha_1 + \alpha_2)V$ α_1, α_2 —dip angles of joint

2.12.3 Track irregularities

Small amplitude fluctuations on the surfaces of wheels and rails with a wide spectrum of wavelengths are always present. Such a roughness spectrum leads to a broadband relative displacement excitation of train and track, which generate high-frequency wheel-rail contact forces causing vibrations and rolling noise.

According to Nielsen [84] the increase in roughness amplitudes at different components in the system, i.e., between wheel and rail, or between wheel and brake block show a different characteristics due to different surface interaction mechanisms. A fundamental difference lies in assumptions regarding the coupling of the thermal and mechanical phenomena at surface interaction. A coupled thermo-mechanical analysis is needed to simulate the evolution of roughness during braking whereas at wheel-rail interaction the importance of the thermal phenomena is of second order. Thus the mechanical behavior is generally modeled as uncoupled from the thermal behavior.

Second difference is that the time scale of interaction between wheel and rail is of long-term nature, whereas the interaction between brake block and wheel is active only during the relatively short time that the train is braked.

Track irregularities are also caused by factors such as small imperfections in materials, imperfections in manufacturing of rails and rail joints, terrain irregularities, and errors in surveying during design and construction. In practice, the roughness excitation is composed of unevenness on the wheel and rail contact surfaces having a broadband spectrum over a range of wavelengths.

Since irregularities of different wavelengths are due to different independent factors, irregularity can be treated as a random function. Unevenness on the wheel and rail contact surface and the axle loads of the vehicles are often described as a stationary random process. [23] In literature different functions and power spectral density functions are applied to describe the irregularity phenomena. Lei [68] uses in his study

the power spectral density function $S(\omega)$ given by the American Railway Standards which is given as

$$S(\omega) = \frac{kA_v\omega_c^2}{(\omega^2 + \omega_c^2)\omega^2} \quad (2.10)$$

where A_v and ω_c are coefficients associated with line grade, which are given in Reference [68], k is a constant, normally taken as 0,25.

Lai [65] computes the effect of the dynamic forces caused by the unevenness of the rails on the loading spectra by using the following empirical relation:

$$G_D(\omega) = \frac{A \cdot a}{\left[\left(\frac{\omega}{v} \right)^2 + b^2 \right] \left(\frac{\omega}{v} + a \right)} \quad (2.11)$$

where G_D is the pressure power spectral density, ω is the angular frequency, v is the train speed, A is a coefficient of quality of the track ($A=1.558 \cdot 10^{-7}$ m rad for track in good conditions, $A=8.974 \cdot 10^{-7}$ m rad for track in poor conditions), a and b are empirical constants whose values are $a=0.8246$ rad/m and $b=0.0206$ rad/m

Hussein and Hunt [45] and Forrest and Hunt [25] use in their study Frederich's empirical power spectral density for the rail roughness is given by:

$$S_s(f) = \frac{a}{v(b + f/v)^3} \quad (2.12)$$

where a and b are constants computed by Frederich for different conditions of the rail, f is the frequency and v is the train speed. The important remark about this function is that it gives larger weights for lower frequencies. The coefficients for unevenness a and waviness b according to the rail condition are given in Table 6.

Table 6. Values of the unevenness a and waviness b of vertical railway track irregularity for three different conditions

	$a(\text{mm}^2 \cdot (1/\text{m})^2)$	$b(1/\text{m})$
Worst	9.39×10^{-1}	6.89×10^{-2}
Average	1.31×10^{-2}	2.94×10^{-2}
Best	1.90×10^{-4}	9.71×10^{-3}

CHAPTER 3

ORIGINAL MODEL

In this work the three-dimensional tunnel model, elastic continuum model and the vehicle model presented by Forrest and Hunt [24] will be extended to be applicable to different track and loading conditions.

In their work Forrest and Hunt conceptualize the tunnel as an infinitely long, thin cylindrical shell surrounded by soil of infinite radial extent. The advantage of the tunnel model is the applicability for use in combination with different track models to calculate the ground vibration due to irregularity excitation by running trains. The model also takes displacements in three dimensions into account.

The soil is modeled by wave equations for an elastic continuum without free surface. This three-dimensional soil model neglects reflected body waves and surface waves.

3.1. Cylindrical Shell Equations

The three-dimensional tunnel model is obtained by using Flügge equations of motion for a thin cylindrical shell made of linear elastic, homogeneous and isotropic material.

Equilibrium in the longitudinal direction x gives

$$a \frac{\partial^2 u}{\partial x^2} + \frac{(1-\nu)}{2a} \frac{\partial^2 u}{\partial \theta^2} + \frac{(1+\nu)}{2} \frac{\partial^2 v}{\partial x \partial \theta} - \nu \frac{\partial w}{\partial x} + \frac{h^2}{12} \left[\frac{(1-\nu)}{2a^3} \frac{\partial^2 u}{\partial \theta^2} + \frac{\partial^3 w}{\partial x^3} - \frac{(1-\nu)}{2a^2} \frac{\partial^3 w}{\partial x \partial \theta^2} \right] + a \frac{(1-\nu^2)}{Eh} q_x - \rho a \frac{(1-\nu^2)}{E} \frac{\partial^2 u}{\partial t^2} = 0 \quad (3.1)$$

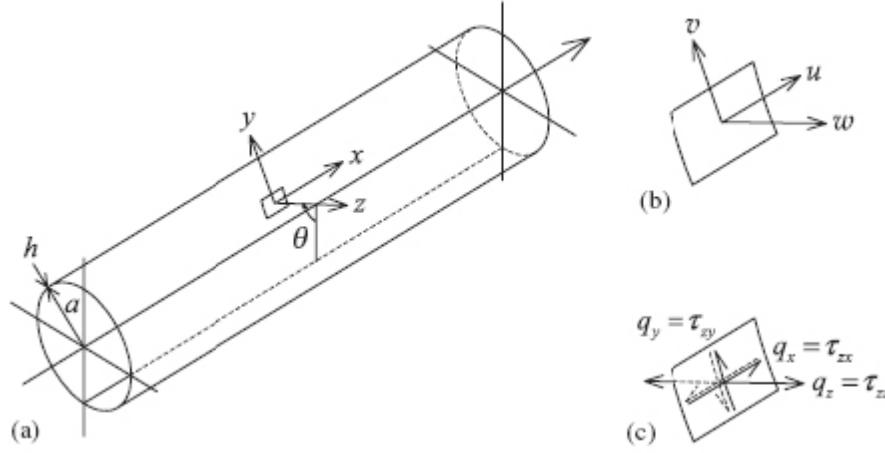


Figure 13. Coordinate system used for the thin-walled cylindrical-shell theory, (a) the principle directions for a typical element in the shell, (b) the corresponding displacement components and (c) the corresponding surface stress components.

Equilibrium in the tangential direction y gives

$$\begin{aligned} & \frac{(1+\nu)}{2} \frac{\partial^2 u}{\partial x \partial \theta} + a \frac{(1-\nu)}{2} \frac{\partial^2 v}{\partial x^2} + \frac{1}{a} \frac{\partial^2 v}{\partial \theta^2} - \frac{1}{a} \frac{\partial w}{\partial \theta} + \frac{h^2}{12} \left[\frac{3(1-\nu)}{2a} \frac{\partial^2 v}{\partial x^2} + \frac{(3-\nu)}{2a} \frac{\partial^3 w}{\partial x^2 \partial \theta} \right] + \\ & a \frac{(1-\nu^2)}{Eh} q_y - \rho a \frac{(1-\nu^2)}{E} \frac{\partial^2 v}{\partial t^2} = 0 \end{aligned} \quad (3.2)$$

Equilibrium in the radial direction z gives

$$\begin{aligned} & \nu \frac{\partial u}{\partial x} + \frac{1}{a} \frac{\partial v}{\partial \theta} - \frac{1}{a} w - \frac{h^2}{12} \left[a \frac{\partial^4 w}{\partial x^4} + \frac{2}{a} \frac{\partial^4 w}{\partial x^2 \partial \theta^2} + \frac{1}{a^3} \frac{\partial^4 w}{\partial \theta^4} \right] \\ & - \frac{h^2}{12} \left[\frac{\partial^3 u}{\partial x^3} - \frac{(1-\nu)}{2a^2} \frac{\partial^3 u}{\partial x \partial \theta^2} + \frac{(3-\nu)}{2a} \frac{\partial^3 v}{\partial x^2 \partial \theta} + \frac{1}{a^3} w + \frac{2}{a^3} \frac{\partial^2 w}{\partial \theta^2} \right] \\ & + a \frac{(1-\nu^2)}{Eh} q_z - \rho a \frac{(1-\nu^2)}{E} \frac{\partial^2 w}{\partial t^2} = 0 \end{aligned} \quad (3.3)$$

Effects of material damping can be included into the model by using complex material parameters in the frequency domain. Assuming the loading applied to an infinitely long cylindrical shell has stress components, which are harmonic in both space and time;

$$\begin{aligned}
q_x(x,t) &= \tilde{Q}_{xn} \cos(n\theta) e^{i(\omega t + \zeta x)} \\
q_y(x,t) &= \tilde{Q}_{yn} \sin(n\theta) e^{i(\omega t + \zeta x)} \\
q_z(x,t) &= \tilde{Q}_{zn} \cos(n\theta) e^{i(\omega t + \zeta x)}
\end{aligned} \tag{3.4}$$

then, the equations of motion are satisfied by the similarly harmonic displacement components.

$$\begin{aligned}
u(x,t) &= \tilde{U}_n \cos(n\theta) e^{i(\omega t + \zeta x)} \\
v(x,t) &= \tilde{V}_n \sin(n\theta) e^{i(\omega t + \zeta x)} \\
w(x,t) &= \tilde{W}_n \cos(n\theta) e^{i(\omega t + \zeta x)}
\end{aligned} \tag{3.5}$$

Note that the spatial exponential term $e^{i\zeta x}$ arises due to the infinitely long cylindrical shell assumption

In Figure 14, ring modes are shown as they relate to three displacement components u , v and w . The integer n indicates the number of waves developed around the circumference. Hence, for inplane flexural modes of Figure 14(a), which are associated with radial displacement w , $n = 0$ corresponds to an expansion or “breathing” mode, $n = 1$ corresponds to one full wave or translation of the cross-section, $n = 2$ corresponds to two full waves or a squashed cross-section. Substituting the harmonic stress (3.4) and displacement (3.5) elements into equations of motion putting all three equations into matrix form gives

$$[A] \begin{Bmatrix} \tilde{U}_n \\ \tilde{V}_n \\ \tilde{W}_n \end{Bmatrix} = \frac{-a(1-\nu^2)}{Eh} \begin{Bmatrix} \tilde{Q}_{xn} \\ \tilde{Q}_{yn} \\ \tilde{Q}_{zn} \end{Bmatrix} \tag{3.6}$$

If the stresses $\tilde{Q}_n = \{\tilde{Q}_{xn} \tilde{Q}_{yn} \tilde{Q}_{zn}\}^T$ are taken as unit loading functions, then the displacements $\tilde{U}_n = \{\tilde{U}_n \tilde{V}_n \tilde{W}_n\}^T$ represent the displacement frequency-response functions in the wavenumber domain for a particular circumferential mode n . To obtain actual stresses and displacements these modal quantities will be linearly combined.

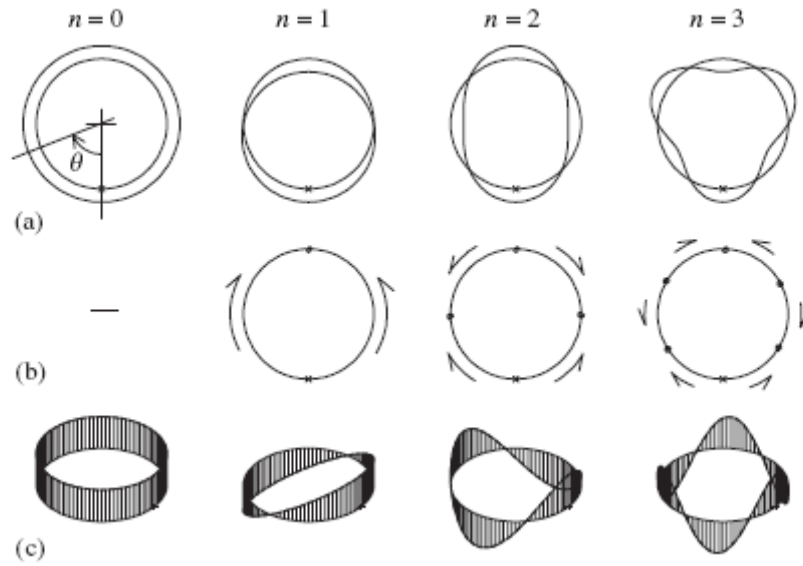


Figure 14. In plane ring modes varying according to n , the number of waves developed around the circumference (a) In-plane flexural ring modes, varying as $\cos(n\theta)$ and corresponding to radial displacement w ; (b) in-plane extensional ring modes, varying as $\sin(n\theta)$ and corresponding to tangential displacement v ; and (c) out-of-plane flexural ring modes, varying as $\cos(n\theta)$ and corresponding to longitudinal displacement u , for different values of circumferential modenumbers n .

3.2. Elastic Continuum Equations

In Forrest and Hunt's work, the soil surrounding the tunnel is modeled as a three dimensional, homogeneous, isotropic elastic solid in the form of a thick-walled cylinder with an inner diameter equal to the external diameter of the tunnel, and an outer diameter of infinite extent.

The wave equation describing motion within a 3D, homogeneous, isotropic, elastic, solid medium is given in equation (3.7).

$$(\lambda + \mu)\nabla\nabla \cdot u + \mu\nabla^2 u + \rho f = \rho \frac{\partial^2 u}{\partial t^2} \quad (3.7)$$

where $\lambda=2\nu G/(1-2\nu)$, $\mu=E/2(1+\nu)=G$ are Lamé's elastic constants.

Since a solution for vibration around equilibrium is searched, body forces due to gravity are ignored. Since the problem has cylindrical geometry, the cylindrical coordinate system will be used. The coordinate, displacement and stress directions are given in Figure 15. Note that a different notation from the cylindrical shell coordinates is used where z is denoting the longitudinal coordinate.

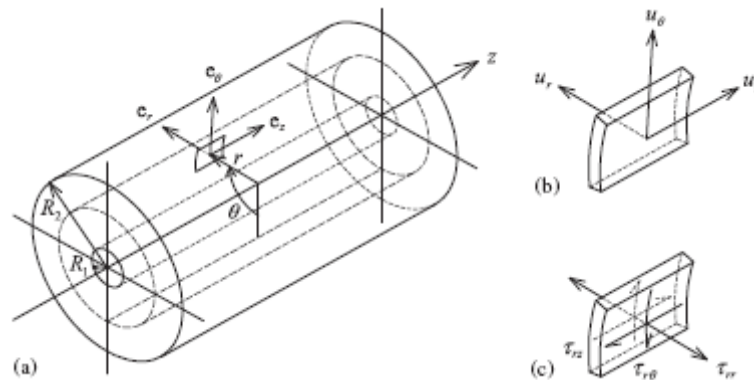


Figure 15. Coordinate system used for the theory of an elastic continuum with cylindrical geometry for (a) the principle directions with their unit vectors, (b) the corresponding displacement components and (c) the corresponding cylindrical-surface stress components.

The wave equation (3.7) can be solved by using the field transformation described by scalar and vector potentials, which are called as Lamé's potentials

$$u = \nabla \phi + \nabla \times H, \text{ with } \nabla \cdot H = F(r, t) \quad (3.8)$$

The scalar function $F(r, t)$ is arbitrary, due to the gauge invariance of the transformation. Usually H is defined by $\nabla \cdot H = 0$ for convenience, but Forrest and Hunt use arbitrary nature of $F(r, t)$ for the current problem. The wave equation (3.7) is satisfied if the potentials satisfy

$$\nabla^2 \phi = \frac{1}{c_1^2} \frac{\partial^2 \phi}{\partial t^2} \text{ and } \nabla^2 H = \frac{1}{c_2^2} \frac{\partial^2 H}{\partial t^2} \quad (3.9)$$

where $c_1 = \sqrt{(\lambda + 2\mu)/\rho}$ speed of pressure wave (compression)

and $c_2 = \sqrt{\mu/\rho}$ speed of shear wave

It should be noted that Rayleigh waves are not considered in this model due to the assumption that in the model no free surface is included.

For cylindrical coordinates, the Laplacian are

$$\nabla^2 \phi = \frac{1}{r} \frac{\partial \phi}{\partial r} + \frac{\partial^2 \phi}{\partial r^2} + \frac{1}{r^2} \frac{\partial^2 \phi}{\partial \theta^2} + \frac{\partial^2 \phi}{\partial z^2}$$

$$\nabla^2 H = \left(\nabla^2 H_r - \frac{H_r}{r^2} - \frac{2}{r^2} \frac{\partial H_\theta}{\partial \theta} \right) e_r + \left(\nabla^2 H_\theta - \frac{H_\theta}{r^2} - \frac{2}{r^2} \frac{\partial H_r}{\partial \theta} \right) e_\theta + \nabla^2 H_z e_z \quad (3.10)$$

Using the Laplacians together with the defined potentials give the displacement components as

$$u_r = \frac{\partial \phi}{\partial r} + \frac{1}{r} \frac{\partial H_z}{\partial \theta} - \frac{\partial H_\theta}{\partial z}$$

$$u_\theta = \frac{1}{r} \frac{\partial \phi}{\partial \theta} + \frac{\partial H_r}{\partial z} - \frac{\partial H_z}{\partial r} \quad (3.11)$$

$$u_z = \frac{\partial \phi}{\partial z} + \frac{1}{r} \frac{\partial(rH_\theta)}{\partial r} - \frac{1}{r} \frac{\partial H_r}{\partial \theta}$$

The components of stress τ_{jk} are given by the general stress–strain relation of Hooke's law, and are

$$\tau_{rr} = (\lambda + 2\mu)\varepsilon_{rr} + \lambda\varepsilon_{\theta\theta} + \lambda\varepsilon_{zz}$$

$$\tau_{\theta\theta} = \lambda\varepsilon_{rr} + (\lambda + 2\mu)\varepsilon_{\theta\theta} + \lambda\varepsilon_{zz}$$

$$\tau_{zz} = \lambda\varepsilon_{rr} + \lambda\varepsilon_{\theta\theta} + (\lambda + 2\mu)\varepsilon_{zz} \quad (3.12)$$

$$\tau_{r\theta} = 2\mu\varepsilon_{r\theta} = \tau_{\theta r}$$

$$\tau_{rz} = 2\mu\varepsilon_{rz} = \tau_{zr}$$

$$\tau_{\theta z} = 2\mu\varepsilon_{\theta z} = \tau_{z\theta}$$

It is noted that Hooke's law is defined for linear-elastic materials. Damping is introduced into the material due to the assumption that small magnitudes of vibration are considered. So, the material becomes viscoelastic and the stress–strain relations are still valid. The components of strain e_{jk} are defined in cylindrical coordinates by

$$\begin{aligned}
\varepsilon_{rr} &= \frac{\partial u_r}{\partial r}, \varepsilon_{\theta\theta} = \frac{1}{r} \frac{\partial u_\theta}{\partial \theta} + \frac{u_r}{r}, \varepsilon_{zz} = \frac{\partial u_z}{\partial z} \\
\varepsilon_{r\theta} &= \frac{1}{2} \left(\frac{1}{r} \frac{\partial u_r}{\partial \theta} + \frac{\partial u_\theta}{\partial r} - \frac{u_\theta}{r} \right), \varepsilon_{\theta z} = \frac{1}{2} \left(\frac{\partial u_\theta}{\partial z} + \frac{1}{r} \frac{\partial u_z}{\partial \theta} \right) \\
\varepsilon_{rz} &= \frac{1}{2} \left(\frac{\partial u_r}{\partial z} + \frac{\partial u_z}{\partial r} \right)
\end{aligned} \tag{3.13}$$

To obtain solutions separable in the three space variables r , θ and z , and the time variable t ; the following forms are assumed for the potentials in equation (3.9).

$$\begin{aligned}
\phi &= f(r) \cos(n\theta) e^{i(\omega t + \zeta x)} \\
H_r &= g_r(r) \sin(n\theta) e^{i(\omega t + \zeta x)} \\
H_\theta &= g_\theta(r) \cos(n\theta) e^{i(\omega t + \zeta x)} \\
H_z &= g_z(r) \sin(n\theta) e^{i(\omega t + \zeta x)}
\end{aligned} \tag{3.14}$$

It is noted that in these harmonic solution forms, variation with r is also included in the functions f , g_r , g_θ and g_z (which also vary with ω , ζ and n). Substituting the assumed solutions (3.14) into equation (3.9) making use of definitions (3.10) and considering each component of the equation in H in turn results in four differential equations

$$\begin{aligned}
r^2 f'' + r f' - \left[\left(\zeta^2 - \frac{\omega^2}{c_1^2} \right) r^2 + n^2 \right] f &= 0 \\
r^2 g_r'' + r g_r' - \left[\left(\zeta^2 - \frac{\omega^2}{c_2^2} \right) r^2 + n^2 + 1 \right] g_r + 2n g_\theta &= 0 \\
r^2 g_\theta'' + r g_\theta' - \left[\left(\zeta^2 - \frac{\omega^2}{c_2^2} \right) r^2 + n^2 + 1 \right] g_\theta + 2n g_r &= 0 \\
r^2 g_z'' + r g_z' - \left[\left(\zeta^2 - \frac{\omega^2}{c_2^2} \right) r^2 + n^2 \right] g_z &= 0
\end{aligned} \tag{3.15}$$

where prime denotes differentiation with respect to r .

It should be noted that the first and fourth functions of equation (3.15) are modified Bessel equations of order n and thus have solutions based on modified Bessel functions of order n .

To define the second and third equations in a known form Forrest and Hunt use property of gauge invariance. One of the functions g_r , g_θ or g_z

can be set arbitrarily without any loss of generality. Choosing $g_r = -g_\theta$ and substituting into the second equation of (3.15) gives

$$r^2 g_r'' + r g_r' - \left[\left(\zeta^2 - \frac{\omega^2}{c_2^2} \right) r^2 + (n+1)^2 \right] g_r = 0 \quad (3.16)$$

which is a modified Bessel equation of order $(n+1)$. Hence solutions for the functions f , g_r , g_θ and g_z can be deduced from equations (3.15) and (3.16) in the form of linear combinations of modified Bessel functions as

$$\begin{aligned} f &= A I_n(\alpha r) + B K_n(\alpha r) \\ g_r = -g_\theta &= A_r I_{n+1}(\beta r) + B_r K_{n+1}(\beta r) \\ g_z &= A_z I_n(\beta r) + B_z K_n(\beta r) \end{aligned} \quad (3.17)$$

where $\alpha^2 = \zeta^2 - \omega^2/c_1^2$, $\beta^2 = \zeta^2 - \omega^2/c_2^2$

I_n and K_n are modified Bessel functions of the first and second kinds, of order n , respectively. The coefficients A , B , A_r , B_r , A_z and B_z are arbitrary constants, which will be determined from boundary conditions. The displacements and stresses can be found in terms of the functions given by equation (3.17). Substituting expressions for potentials (3.14) into equation (3.11), recalling that $g_r = -g_\theta$ gives the displacements as

$$\begin{aligned} u_r &= \left[f' + \frac{n}{r} g_z + i \zeta g_r \right] \cos(n\theta) e^{i(\omega t + \zeta x)} \\ u_\theta &= \left[-\frac{n}{r} f + i \zeta g_r - g_z' \right] \sin(n\theta) e^{i(\omega t + \zeta x)} \\ u_z &= \left[i \zeta f - \frac{(n+1)}{r} g_r - g_r' \right] \cos(n\theta) e^{i(\omega t + \zeta x)} \end{aligned} \quad (3.18)$$

For stress elements the authors use the equation (3.12) by using the strain definitions (3.13) with the displacements (3.18). The most important stress elements are those acting on the cylindrical surface (τ_{rr} , $\tau_{r\theta}$ and τ_{rz}), since they are involved with the boundary conditions. These surface stresses are given by

$$\begin{aligned}
\tau_{rr} &= \left[\begin{array}{l} (\lambda + 2\mu)f'' + \frac{\lambda}{r}f' - \lambda\left(\frac{n^2}{r^2} + \zeta^2\right)f \\ + 2\mu i \zeta g'_r + 2\mu \frac{n}{r}g'_z - 2\mu \frac{n}{r^2}g_z \end{array} \right] \cos(n\theta)e^{i(\omega t + \zeta x)} \\
\tau_{r\theta} &= \left[\begin{array}{l} -2\mu \frac{n}{r}f' - 2\mu \frac{n}{r^2}f + \mu i \zeta g'_r - \mu i \zeta \frac{(n+1)}{r}g_r \\ -\mu g''_z + \frac{\mu}{r}g'_z - \mu \frac{n^2}{r^2}g_z \end{array} \right] \sin(n\theta)e^{i(\omega t + \zeta x)} \\
\tau_{rz} &= \left[\begin{array}{l} 2\mu i \zeta f' - \mu g''_r - \mu \frac{(n+1)}{r}g'_r + \mu \left(\frac{n+1}{r^2} - \zeta^2\right)g_r \\ + \mu i \zeta \frac{n}{r}g_z \end{array} \right] \cos(n\theta)e^{i(\omega t + \zeta x)}
\end{aligned} \tag{3.19}$$

The final expressions are determined by using recurrence relations containing the derivatives of Bessel functions. Bringing the harmonic solutions in matrix form

$$\begin{aligned}
u &= \begin{Bmatrix} u_r \\ u_\theta \\ u_z \end{Bmatrix} = [S] \cdot [U] \cdot Ce^{i(\omega t + \zeta x)} \\
\tau &= \begin{Bmatrix} \tau_{rr} \\ \tau_{r\theta} \\ \tau_{rz} \\ \tau_{\theta\theta} \\ \tau_{\theta z} \\ \tau_{zz} \end{Bmatrix} = \begin{bmatrix} S & 0 \\ 0 & S \end{bmatrix} \cdot [T] \cdot Ce^{i(\omega t + \zeta x)}
\end{aligned} \tag{3.20}$$

$$\text{with } [S] = \begin{bmatrix} \cos n\theta & 0 & 0 \\ 0 & \sin n\theta & 0 \\ 0 & 0 & \cos n\theta \end{bmatrix}$$

where $C = [A \ B \ A_r \ B_r \ A_z \ B_z]^T$ is the vector of coefficients, determined from boundary conditions.

The elements of 3X6 matrix [U] defining displacements, and the 6X6 matrix [T] defining stresses, are given in full, in Appendix A which are functions varying with wavenumber ζ , frequency ω and circumferential mode number n , as well as radius r and the material properties.

Finally, the solutions are written in a similar form with cylindrical shell equations as follows:

$$\begin{Bmatrix} \tilde{U}_m \\ \tilde{U}_{\theta n} \\ \tilde{U}_{zn} \end{Bmatrix} = [U] \cdot C \quad \text{and} \quad \begin{Bmatrix} \tilde{T}_{rm} \\ \tilde{T}_{r\theta n} \\ \tilde{T}_{rzn} \end{Bmatrix} = [T_r] \cdot C \quad (3.21)$$

where the 3X6 matrix [Tr] is the top half of the 6X6 matrix [T] in equation (3.20).

3.3. Applied load

Generally, the external loading applied to the tunnel will not be harmonic in space and time. Since steady state harmonic variation in time is of interest, the loading is also assumed to be harmonic. This assumption enables that each applied stress to be a linear combination of the spatially harmonic components given in equation (3.4) for the shell or equation (3.21) for the continuum.

In order to obtain results in wide areas of application, authors investigated the case of a point load. Hence, it is possible to determine the response to a more complicated loading condition by superposition of individual point-load responses with suitable translations and rotations.

Forrest and Hunt give the resolution of a point load in their work by defining the load as an appropriately scaled uniform normal stress acting over a small rectangular area centered on $x = 0$ and $y = 0$. The point force is achieved in the limit, as the area tends to zero. After defining the point load through Dirac Delta functions and taking the Fourier transform, harmonic stresses for a particular circumferential mode number n can be written as

$$\tilde{P}_{xn} = 0, \quad \tilde{P}_{yn} = 0, \quad \tilde{P}_{zn} = \begin{cases} 1/2\pi a, n = 0 \\ 1/\pi a, n \geq 0 \end{cases}, \quad (3.22)$$

for all ζ . Note that the longitudinal and tangential applied forces are set to zero.

If there are no loads applied on the outside surface of the shell, the loads P_x , P_y and P_z applied to the inside surface of the shell correspond to q_x , q_y and q_z in equation (3.4).

Using these harmonic stresses, harmonic displacements $\tilde{U}_n, \tilde{V}_n, \tilde{W}_n$ are calculated for each value of n from equation (3.6). Total displacements resulting from a time-harmonic unit point load are given by the linear combination of these spatially harmonic components as

$$\begin{Bmatrix} u \\ v \\ w \end{Bmatrix} = \begin{Bmatrix} U \\ V \\ W \end{Bmatrix} e^{i\omega t} = \frac{1}{2\pi} \int_{-\infty}^{\infty} \left(\begin{Bmatrix} \tilde{U}_0 \\ 0 \\ \tilde{W}_0 \end{Bmatrix} + \sum_{n=1}^{\infty} \begin{Bmatrix} \tilde{U}_n \cos(n\theta) \\ \tilde{V}_n \cos(n\theta) \\ \tilde{W}_n \cos(n\theta) \end{Bmatrix} \right) e^{i\zeta x} d\zeta e^{i\omega t} \quad (3.23)$$

The general, time-harmonic displacement response is the inverse Fourier transform of a sum of the circumferential modes in the wavenumber domain. The result in equation (3.23) holds for any type of time-harmonic loading condition. Loads that are not harmonic in time could be treated by introducing a second inverse Fourier transform from the frequency to time domain.

3.4. Modeling a thin-walled cylinder with elastic continuum theory

For an infinitely long, free cylindrical shell loaded on the inside surface only, the modal loading components \tilde{Q}_n of equation (3.4) will simply be the applied loading \tilde{P}_n . Thus, the modal displacement components can be calculated from equation (3.6) as

$$\begin{Bmatrix} \tilde{U}_n \\ \tilde{V}_n \\ \tilde{W}_n \end{Bmatrix} = \frac{-a(1-\nu^2)}{Eh} [A]^{-1} \begin{Bmatrix} \tilde{P}_{xn} \\ \tilde{P}_{yn} \\ \tilde{P}_{zn} \end{Bmatrix} \quad (3.24)$$

Note that the conventional notations used in shell theory and continuum theory do not correspond exactly to one another. In equations (3.25) the relationships between such notations for these theories are given

$$\begin{aligned}
u &\equiv u_z, & \tau_{zx} &\equiv -\tau_{rz}, \\
v &\equiv u_\theta, & \tau_{zy} &\equiv -\tau_{r\theta}, \\
w &\equiv -u_r, & \tau_{zz} &\equiv \tau_{rr},
\end{aligned} \tag{3.25}$$

Writing the inside and outside stress components in equation (3.21) as

$$[T_r]_{r=a-h/2} \cdot C = \begin{Bmatrix} \tilde{P}_{zn} \\ -\tilde{P}_{yn} \\ -\tilde{P}_{xn} \end{Bmatrix} \text{ and } [T_r]_{r=a+h/2} \cdot C = \begin{Bmatrix} 0 \\ 0 \\ 0 \end{Bmatrix} \tag{3.26}$$

and solving for C terms and substituting in the displacement components in equation (3.21) brings the modal displacement components into the following form:

$$\begin{Bmatrix} \tilde{U}_{rn} \\ \tilde{U}_{\theta n} \\ \tilde{U}_{zn} \end{Bmatrix} = [U]_{r=a} \cdot \begin{bmatrix} [T_r]_{r=a-h/2} \\ [T_r]_{r=a+h/2} \end{bmatrix}^{-1} \cdot \begin{Bmatrix} \tilde{P}_{zn} \\ -\tilde{P}_{yn} \\ -\tilde{P}_{xn} \\ 0 \\ 0 \\ 0 \end{Bmatrix} \tag{3.27}$$

3.5. Modeling a tunnel buried in soil

Until now general solutions for cylindrical shell and elastic continuum models have been presented. To model a complete tunnel-in-soil system, the tunnel is modeled by a cylindrical shell and the soil by an elastic continuum of infinite extent surrounding the tunnel. To solve this particular problem three sets of boundary conditions are applied:

1. Equality of loading and stresses;
2. Radiation condition;
3. Compatibility of displacements and equilibrium of stresses.

According to the first boundary condition, the stresses on the inside of the tunnel shell are equal to the applied loading. The stresses on the outside of the shell are not zero, so that the first condition can be used with the shell results (3.6) to write

$$[A_E] \cdot \tilde{U}_n = \frac{-Eh}{a(1-\nu^2)} [A] \begin{Bmatrix} \tilde{U}_n \\ \tilde{V}_n \\ \tilde{W}_n \end{Bmatrix} = \begin{Bmatrix} \tilde{Q}_{xn} \\ \tilde{Q}_{yn} \\ \tilde{Q}_{zn} \end{Bmatrix} = \begin{Bmatrix} \tilde{P}_{xn} \\ \tilde{P}_{yn} \\ \tilde{P}_{zn} \end{Bmatrix} - \begin{Bmatrix} \tilde{T}_{zxn} \\ \tilde{T}_{zyn} \\ \tilde{T}_{zzn} \end{Bmatrix}_{outside} \quad (3.28)$$

The second boundary condition, the radiation condition, means that the displacements of the soil continuum must decay to zero as the radius from the center of the tunnel increases towards infinity. The radiation condition is used to reduce the dimensions of the equations describing the response of the continuum by setting the appropriate coefficients of the boundary condition vector C to zero. The displacements u and stresses τ for the continuum are expressed as linear combinations of modified Bessel functions $I_n(\alpha r)$, $K_n(\alpha r)$, $I_n(\beta r)$, $K_n(\beta r)$, $I_{n+1}(\beta r)$ and $K_{n+1}(\beta r)$. It can be shown that, with small loss-factor damping associated with the wave speeds c_1 and c_2 , the principal values of the parameters α and β fall into the first quadrant of the complex plane. For z in this quadrant, as $|z| \rightarrow \infty$

- i. $K_n(z)$ tends to zero
- ii. $I_n(z)$ increases in magnitude.

Thus only the modified Bessel functions of the second kind K_n and K_{n+1} satisfy the radiation condition as $r \rightarrow \infty$ and the coefficients of the modified Bessel functions of the first kind I_n and I_{n+1} in equation (3.20) must be set to zero, so that

$$A = A_r = A_z = 0 \\ \Rightarrow C = \{0 \quad B \quad 0 \quad B_r \quad 0 \quad B_z\}^T \quad (3.29)$$

Thus, the application of the second boundary condition results in dropping out the terms containing Bessel functions I_n and I_{n+1} in matrices $[U]$ and $[T]$, that is, the first, third and fifth elements of each row of the equation.

The condition of compatibility can be used with the radiation condition expressed by equation (3.29), considering the differences between the shell and continuum coordinate systems given by equation (3.25). So, the displacements at the tunnel-soil interface can be written as

$$\begin{Bmatrix} \tilde{U}_n \\ \tilde{V}_n \\ \tilde{W}_n \end{Bmatrix} = \begin{Bmatrix} \tilde{U}_{zn} \\ \tilde{U}_{\theta n} \\ -\tilde{U}_{rn} \end{Bmatrix}_{r=a} = \begin{bmatrix} u_{32} & u_{34} & u_{36} \\ u_{22} & u_{24} & u_{26} \\ -u_{12} & -u_{14} & -u_{16} \end{bmatrix}_{r=a} \begin{Bmatrix} B \\ B_r \\ B_z \end{Bmatrix} = [U_\infty]_{r=a} \cdot B \quad (3.30)$$

while equilibrium means that the stresses at the interface are given by

$$\begin{Bmatrix} \tilde{T}_{zxn} \\ \tilde{T}_{zyn} \\ \tilde{T}_{zzn} \end{Bmatrix}_{outside} = \begin{Bmatrix} -\tilde{T}_{rzn} \\ -\tilde{T}_{r\theta n} \\ \tilde{T}_{rm} \end{Bmatrix}_{r=a} = \begin{bmatrix} -t_{32} & -t_{34} & -t_{36} \\ -t_{22} & -t_{24} & -t_{26} \\ t_{12} & t_{14} & t_{16} \end{bmatrix}_{r=a} \begin{Bmatrix} B \\ B_r \\ B_z \end{Bmatrix} = [T_\infty]_{r=a} \cdot B \quad (3.31)$$

Eliminating the stresses acting on the outside of the shell tunnel by substituting equation (3.31) into equation (3.28) and using equation (3.30), the unknown displacements and coefficients can be found. The solution takes after some rearrangement the following form:

$$\begin{Bmatrix} \tilde{U}_n \\ B \end{Bmatrix} = \begin{bmatrix} [A_E] & [T_\infty]_{r=a} \\ [I] & -[U_\infty]_{r=a} \end{bmatrix}^{-1} \begin{Bmatrix} \tilde{P}_n \\ 0 \end{Bmatrix} \quad (3.32)$$

where [I] is a 3x3 identity matrix. The displacements $\tilde{U}_n = \{\tilde{U}_n \tilde{V}_n \tilde{W}_n\}^T$ at the interface can directly be found from equation (3.32), whereas the displacements at some radius R elsewhere in the soil have to be calculated using the coefficients B from equation (3.32) as

$$\tilde{U}_n|_{r=R} = [U_\infty]_{r=R} \cdot B \quad (3.33)$$

3.6. Addition of slab beam to the track model

In an accompanying paper [25] Forrest and Hunt add a track model to the previously developed three-dimensional tunnel model to obtain the effectiveness of floating-slab track. All the couplings are achieved through interaction forces between the layers. The slab beam coupled to the tunnel as an infinitely long, continuous slab beam, in the wavenumber domain, with the slab bearings represented by an elastic layer.

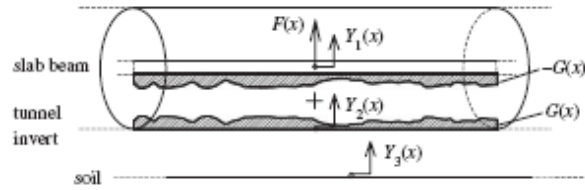


Figure 16. Joining an infinitely long slab beam to the tunnel and the interaction forces [25]

As shown in Figure 16, the slab beam and tunnel are joined along a single continuous line running longitudinally along the bottom of the tunnel invert. $G(x)$ and $-G(x)$ represent the interaction forces acting on the tunnel and its equal and opposite counterpart. External loading applied to the slab beam $F(x)$ is shown here as a point force.

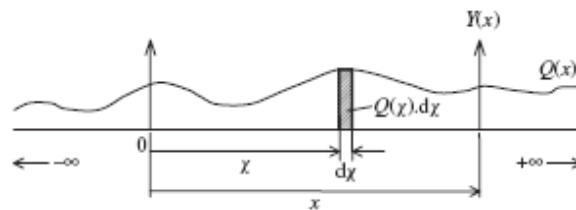


Figure 17. General force distribution per unit length $Q(x)$ acting along the line of joining [25]

Figure 17 shows a general continuous distribution of time-harmonic force per unit length $Q(x)$. Defining the train of point loads represented by pulses of infinitesimal width $d(\chi)$ and magnitude $Q(\chi)$, the increment of the time-harmonic displacement response $Y(x)$ to one of these point loads is $dY(x) = H(x-\chi)Q(\chi) d\chi$, where $H(x)$ is the frequency-response function (FRF) for $Y(x)$ to a point load acting at $x = 0$. Integrating $Y(x)$ over the

whole length of the infinite joining line gives the total displacement response as:

$$Y(x) = \int_{-\infty}^{\infty} H(x-\chi)Q(\chi)d\chi \quad (3.34)$$

Equation (3.34) is a convolution integral in space, which is equivalent to a Green's function formulation for the response, where $H(x-\chi)$ is Green's function. Taking the Fourier transform of both sides using the transform pair given in equation (3.35),

$$\tilde{Y}(\xi) = \int_{-\infty}^{\infty} Y(x)e^{-i\xi x} dx, \quad \tilde{Y}(x) = \frac{1}{2\pi} \int_{-\infty}^{\infty} \tilde{Y}(\xi)e^{i\xi x} d\xi, \quad (3.35)$$

where ξ is angular wavenumber and the tilde indicates wavenumber-domain quantities, equation (3.34) is written as:

$$\tilde{Y}(\xi) = \tilde{H}(\xi)\tilde{Q}(\xi), \quad (3.36)$$

Applying equation (3.36) to the coupled slab beam and tunnel invert to write the displacements yield

$$\tilde{Y}_1 = \tilde{H}_{11}(-\tilde{G} + 1), \quad \tilde{Y}_2 = \tilde{H}_{22}\tilde{G} \quad (3.37)$$

where the index denotes the lines along the slab as (1), the tunnel invert as (2) the soil as (3) and the line along the rail beam by 0 (zero). The displacements \tilde{Y}_1 along the beam and \tilde{Y}_2 along the invert are responses due to a unit point load acting on the slab at $x = 0$. The functions \tilde{H}_{11} and \tilde{H}_{22} are the frequency response functions for the response of the free beam to a point load at $x = 0$ and for the response of the uncoupled tunnel invert to a point load at $x = 0$ respectively in the wavenumber domain.

The joining of the slab beam can be achieved by either joining the beam directly to the tunnel invert, or by supporting it to the invert with resilient slab bearings. For direct joining, the equality of the displacements of the slab and invert yield in the wavenumber domain

$$\tilde{Y}_1 = \tilde{Y}_2 \quad (3.38)$$

Using equation (3.38) with equation (3.37) to eliminate \tilde{G} gives

$$\tilde{Y}_1 = \tilde{Y}_2 = \frac{\tilde{H}_{11}\tilde{H}_{22}}{\tilde{H}_{11} + \tilde{H}_{22}} \quad (3.39)$$

Joining the slab to the invert with resilient slab bearings, adds extra terms to the definition of the interaction force. The interaction force \tilde{G} is determined by the difference of displacements and the stiffness of the bearings. Modeling the bearings as a continuous resilient layer of stiffness k per unit length gives

$$\tilde{G} = k(\tilde{Y}_1 - \tilde{Y}_2) \quad (3.40)$$

Using equation (3.40) with equation (3.37) to eliminate \tilde{G} gives

$$\tilde{Y}_1 = \frac{\tilde{H}_{11}(1 + k\tilde{H}_{22})}{1 + k\tilde{H}_{11} + k\tilde{H}_{22}}, \quad \tilde{Y}_2 = \frac{k\tilde{H}_{11}\tilde{H}_{22}}{1 + k\tilde{H}_{11} + k\tilde{H}_{22}} \quad (3.41)$$

Applying the equation (3.36) and using the displacement \tilde{Y}_2 , the displacement along a line in the soil parallel to the joining line can be found as

$$\tilde{Y}_3 = \tilde{H}_{32}\tilde{G} = \tilde{H}_{32}\frac{\tilde{Y}_2}{\tilde{H}_{22}} \quad (3.42)$$

for either joining method, where H_{32} is the FRF of a particular soil-displacement component Y_3 to a point force acting on the uncoupled tunnel invert at $x = 0$.

The frequency response functions in equations (3.37)-(3.42) are associated with the displacements calculated from the tunnel in soil model for unit point load condition.

$$\tilde{H}_{22} = \tilde{W}\Big|_{r=a, \theta=0}, \quad \tilde{H}_{32} = \tilde{U}, \quad \tilde{V} \quad \text{or} \quad \tilde{W}\Big|_{r=a, \theta=0} \quad (3.43)$$

The FRF of the slab beam is determined through the equation of motion of an Euler beam as

$$m\frac{\partial^2 y}{\partial t^2} + EI\frac{\partial^4 y}{\partial x^4} = f(x, t), \quad (3.44)$$

where m is the beam's mass per unit length, EI is the bending stiffness, and $f(x, t)$ is the applied force per unit length. Assuming a harmonic solution in the form $y = \tilde{Y}e^{i(\omega t + \xi x)}$ with a force $f = \tilde{F}e^{i(\omega t + \xi x)}$ yields for unit spatial forcing at $x=0$

$$\tilde{H}_{YF} = \tilde{Y}\Big|_{\tilde{F}=1} = \frac{1}{EI\xi^4 - m\omega^2} \quad (3.45)$$

The solution of this form is treated as the free slab beam FRF. Thus

$$\tilde{H}_{11} = \tilde{H}_{YF} \quad (3.46)$$

3.7. Adding the rail beam

The rail beam is added to the track model by using the principle of convolution in space. Using the previously defined notation,

$$\tilde{Y}_{0a} = \frac{\tilde{H}_{00}(1 + k_r \tilde{H}_{11a})}{1 + k_r \tilde{H}_{00a} + k_r \tilde{H}_{11a}}, \quad \tilde{Y}_{1a} = \frac{k_r \tilde{H}_{00a} \tilde{H}_{11a}}{1 + k_r \tilde{H}_{00a} + k_r \tilde{H}_{11a}} \quad (3.47)$$

where \tilde{H}_{00a} is the FRF for the unjoined rail beam, \tilde{H}_{11a} is the FRF of the slab beam to the load on the slab before the rail is added in wavenumber domain, and k_r is the stiffness per unit length of the resilient layer between the rail and slab beams. To achieve joining of the rail beam to the slab and tunnel model again the concept of interaction force is used. In this case the coupling interaction force is defined by the response of the slab in the new combined model divided by its pre-rail-beam FRF, \tilde{H}_{11a} as $\tilde{Y}_{1a} / \tilde{H}_{11a}$. Using the coupling interaction force, the responses \tilde{Y}_{2a} along the tunnel invert and \tilde{Y}_{3a} in the soil can be determined as:

$$\tilde{Y}_{2a} = \tilde{H}_{21a} \frac{\tilde{Y}_{1a}}{\tilde{H}_{11a}}, \quad \tilde{Y}_{3a} = \tilde{H}_{31a} \frac{\tilde{Y}_{1a}}{\tilde{H}_{11a}}, \quad (3.48)$$

where \tilde{H}_{21a} and \tilde{H}_{31a} are the FRF's of the tunnel invert and the soil to a load on the pre-rail-beam slab in wavenumber domain. The FRF's in equations (3.47)-(3.48) are associated with the displacements calculated from the tunnel in soil model for unit point load condition. The FRF for the rail beam is again found from the equation of motion of an Euler beam and is given in equation (3.45) with the properties of the two rails instead of the slab. Thus,

$$\tilde{H}_{00a} = \tilde{H}_{YF}, \quad \tilde{H}_{11a} = \tilde{Y}_1, \quad \tilde{H}_{21a} = \tilde{Y}_2, \quad \tilde{H}_{31a} = \tilde{Y}_3 \quad (3.49)$$

3.8. Addition of axle masses to the complete track model

The vehicle dynamics are taken into account by adding axle masses to the track model at regular spacing[25]. The complete track model developed is shown in Figure 18. The tunnel, the simple slab beam supporting the rail beam with masses placed at intervals to represent the axle–wheel assemblies of a train are presented in this figure clearly.

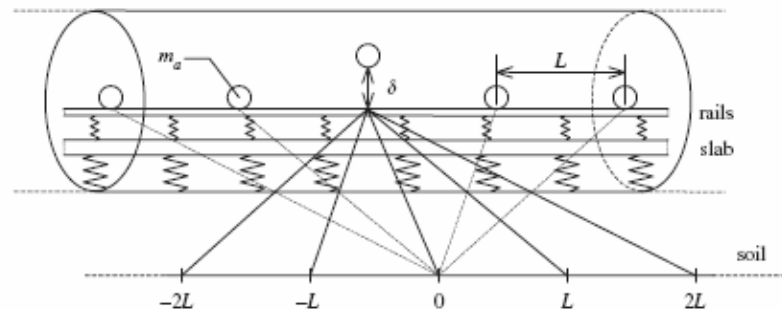


Figure 18. Complete track model with masses added at regular spacing [25]

The axle masses are the simplest model of a railway vehicle where only the unsprung mass of the train is considered by assuming that the primary suspension isolates the rest of each vehicle in the train.

The problem of finding the response at a single point in the soil due to a series of input loads along the rails is handled using shifting principle. Using the infinite structure assumption, it is concluded that the load and the observation point can be shifted longitudinally while maintaining their separation. The response at the observation point will not change. Thus, finding the set of FRF's for the soil response at $x = 0$ to a set of loads at various positions on the rail is equal to find the FRF's for the soil at those various longitudinal positions to a single load at $x = 0$. After scaling and

phasing properly, the total soil response due to all axle loads acting simultaneously can be calculated by linearly combining all the FRF's for an input at $x = 0$. Also note that the problem is reduced to a two-dimensional geometry due to infinitely long train and random inputs assumption. The linear combination of FRF's represents the response anywhere along the soil line and thus the three dimensional problem represented by the individual FRF's reduces to a two-dimensional problem of determining the vibration level at a particular point in the cross-section of the tunnel and soil.

Adding axle masses to the complete model is done in the space domain. This can be obtained by inverse Fourier transform of the ξ -domain responses along the rail from equation (3.47) and along a line in the soil parallel to the joining line from equation (3.48) to x-domain as

$$H_0(x) = \frac{1}{2\pi} \int_{-\infty}^{\infty} \tilde{Y}_{0a}(\xi) e^{i\xi x} d\xi, \quad H_3(x) = \frac{1}{2\pi} \int_{-\infty}^{\infty} \tilde{Y}_{3a}(\xi) e^{i\xi x} d\xi, \quad (3.50)$$

which represent the FRF of the rail and the soil to a point load acting at $x = 0$ at a particular frequency ω , respectively. It should be noted that $\tilde{Y}_{3a}(\xi)$ can be defined according to the desired component u, v, or w of soil displacement.

The rail responses at the positions of the masses are to formed into an FRF matrix as

$$Y_0 = [H_0]F_0 \quad (3.51)$$

where Y_0 is the vector of rail displacements at the positions where masses are added, and F_0 is the vector of interaction forces between the masses and the rail acting at those positions. The elements of H_0 matrix are derived from rail response FRF in x-domain in equation (3.50) for a regular axle spacing L as

$$[H_0] = \begin{bmatrix} H_0(0) & H_0(L) & H_0(2L) & H_0(3L) & H_0(4L) \\ H_0(L) & H_0(0) & H_0(L) & H_0(2L) & H_0(3L) \\ H_0(2L) & H_0(L) & H_0(0) & H_0(L) & H_0(2L) \\ H_0(3L) & H_0(2L) & H_0(L) & H_0(0) & H_0(L) \\ H_0(4L) & H_0(3L) & H_0(2L) & H_0(L) & H_0(0) \end{bmatrix} \quad (3.52)$$

It is noted that the authors presented the case of adding five masses as an example to the general approach[25]. The number of axle masses can be extended to give the convergence necessary to model an infinitely long train.

To add the axle masses the FRF matrix in equation (3.51) is inverted to obtain a dynamic stiffness matrix as

$$F_0 = [H_0]^{-1} Y_0 = [K_0] Y_0 \quad (3.53)$$

Axles are added to the model in the form of concentrated masses m_a by adding inertia terms of the form $-m_a \omega^2 Y$, where Y is the displacement at the axle's station, to the appropriate diagonal elements of the dynamic-stiffness matrix $[K_0]$. An axle mass is added to the free center station assuming a roughness displacement $d = \Delta e^{i\omega t}$. Then, matrix equation (3.52) becomes

$$\begin{bmatrix} k_{11} - m_a \omega^2 & k_{12} & k_{13} & k_{14} & k_{15} & 0 \\ k_{21} & k_{22} - m_a \omega^2 & k_{23} & k_{24} & k_{25} & 0 \\ k_{31} & k_{32} & k_{33} & k_{34} & k_{35} & -m_a \omega^2 \\ k_{41} & k_{42} & k_{43} & k_{44} - m_a \omega^2 & k_{45} & 0 \\ k_{51} & k_{52} & k_{53} & k_{54} & k_{55} - m_a \omega^2 & 0 \\ 0 & 0 & -1 & 0 & 0 & 1 \end{bmatrix} \begin{Bmatrix} Y_1 \\ Y_2 \\ Y_3 \\ Y_4 \\ Y_5 \\ Y_a \end{Bmatrix} = \begin{Bmatrix} 0 \\ 0 \\ 0 \\ 0 \\ 0 \\ \Delta \end{Bmatrix} \quad (3.54)$$

After calculating the vector of displacements of the rail at the axle masses from equation (3.53), the corresponding interaction forces F_0 acting on the rail at the mass stations is determined by substituting the vector of displacements back into equation (3.25). The interaction forces acting on the rail are used to find the soil displacements Y_3 from equation (3.50). Writing these FRF's in matrix form

$$Y_3 = [H_3] F_0 \quad (3.55)$$

3.9. Random Process Theory Applied to the Full-Track Model

Physical phenomena like roughness and other irregularities of rail and wheel surface profiles show a random distribution in reality. The response of the wheels to this randomly distributed surface irregularity will

also be considered as a random process. The soil responses will be calculated using the theory of random vibration described by Newland [82].

A random process is considered as stationary if the probability distributions obtained for the ensemble do not depend on absolute time. In the current system the inputs x_j , axle inputs provided by a train, are considered as stationary random inputs. According to the random process theory, the output y , the displacement response of a particular point in the soil is also stationary and random. The power spectral density (PSD), $S_y(\omega)$ of the output process y is then given by

$$S_y(\omega) = \sum_{p=1}^N \sum_{q=1}^N H_p^*(\omega) H_q(\omega) S_{x_p x_q}(\omega) \quad (3.56)$$

where $H_p(\omega)$ and $H_q(\omega)$ are the FRF's of y to the inputs x_p and x_q , respectively, $S_{x_p x_q}(\omega)$ is the cross-spectral density function between two inputs. It should be noted that the asterix above $H_p(\omega)$ denotes the complex conjugate of the FRF. This expression is the most general form of power spectral density. For special cases some simplifications will be made according to the statistical properties of inputs, especially in cross-spectral density term. Two input processes have the same statistical properties, that is, have the same spectrum $S_0(\omega)$, since the axles are running on the same rail profile. Considering that one lags the other such that $x_2(t) = x_1(t-T)$, the cross-spectral density is given by

$$S_{x_1 x_2}(\omega) = S_0(\omega) e^{-i\omega T}, \quad S_{x_2 x_1}(\omega) = S_0(\omega) e^{i\omega T}, \quad (3.57)$$

To apply equation (3.57) Forrest and Hunt [25] assume that the wheels of the trains are perfectly smooth. This assumption consequents that all irregularities are contained in the rail surface, so that the axle inputs differ by a time delay only. This assumption ignores the effect of wheel irregularities that are existent on trains in reality. Applying the time delay between two adjacent axles as $T = L/V$, where L is the axle spacing and V is the speed of the train, to equation (3.57) and substituting into equation (3.56) yields

$$S_y(\omega) = \sum_{p=1}^N \sum_{q=1}^N H_p^*(\omega) H_q(\omega) S_0(\omega) e^{-i\omega(q-p)L/V} \quad (3.58)$$

The use of equation (3.58) requires another assumption regarding to the constant axle spacing. The FRF's $H_p(\omega)$ and $H_q(\omega)$ in equation (3.58) are obtained from the appropriate elements of the soil-response vector Y_3 in equation (3.55), which are due to an input at the center axle mass only. Note that N indicates the number of axle masses. Also, Doppler effects are ignored due to very low train speeds when compared to the speeds of pressure and shear waves in the soil.

Another assumption to consider the process as stationary is that the observer is at a distance from the tunnel longer than the axle spacing. At this distance a hypothetical observer will not realize individual axles as they pass. The observer will hear a continuous noise instead.

Under these assumptions, equation (3.58) gives a reasonable estimate of the vibration spectrum at a stationary observation point in the soil. The PSD given in equation (3.58) shows a symmetric distribution for frequencies from $-\infty$ to $+\infty$. Since practically spectra are defined for positive frequencies, the PSD in equation (3.58) is converted to single-sided spectra for frequencies in cycles using the following equation:

$$S_y(f) = 4\pi S_y(\omega = 2\pi f) \quad (3.59)$$

Forrest and Hunt [25] use in their study Frederich's empirical power spectral density for irregularity based on many measurements of the track geometry of different surface roughness which is given by equation (2.12). The important remark about this function is that it gives higher weights for lower frequencies as it can be seen in Figure 19. The coefficients for unevenness a and waviness b according to the rail condition are given in Table 6. The empirical power spectral density for irregularity will be used in equation (3.58) as input spectrum $S_0(\omega)$.

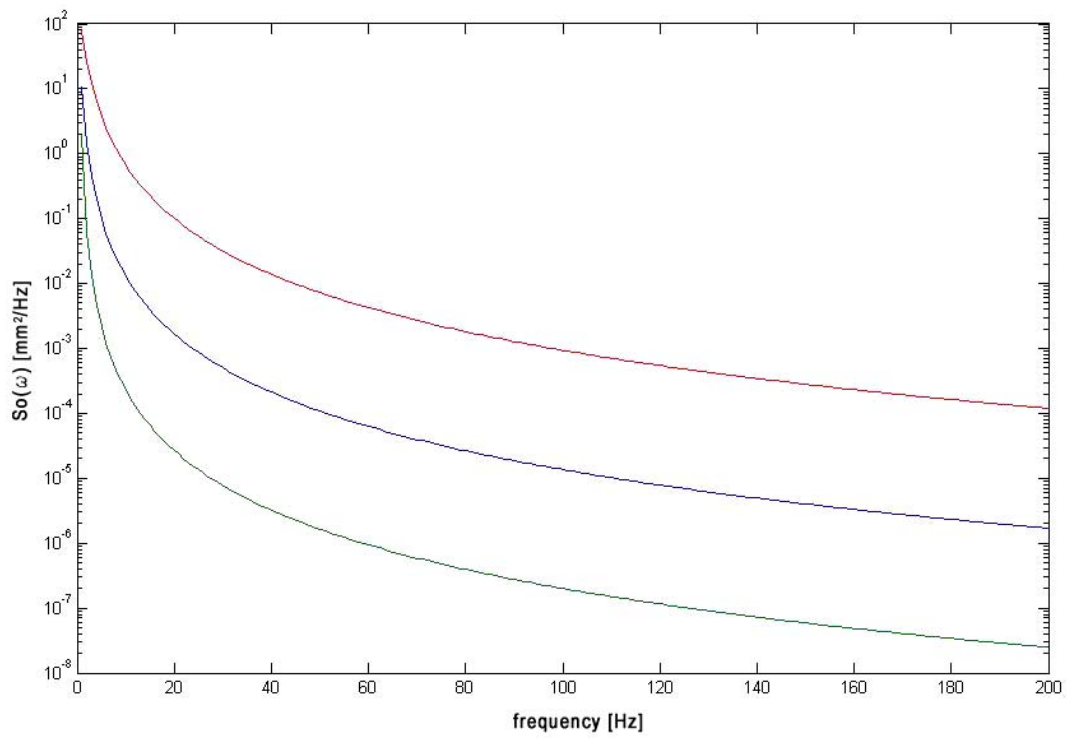


Figure 19. The power spectrum of irregularity for the worst (red), average (blue) and best (green) rail conditions, given by equation (2.12).

CHAPTER 4

MODIFIED MODEL

In this chapter, a new model based on Forrest and Hunt's work will be explained in detail. Differences between these two models will be described for each aspect by introducing theoretical background on the subject. Changes in track, vehicle and damping models are made due to applicability of Forrest and Hunt's tunnel and soil model to different track structures and loading conditions. In Table 7, these differences are summed up in four subjects.

Table 7. Differences between the models

Subject	Forrest & Hunt[24,25]	Modification
Track	Rail+Railpad+Floating Slab	Rail+Railpad+Sleepers
Vehicle Model	Axle masses	3 degrees of freedom
Damping Model	Hysteretic	New model described by L'Mesquez [66,67] for moving loads .
Hertz Contact	No	Yes

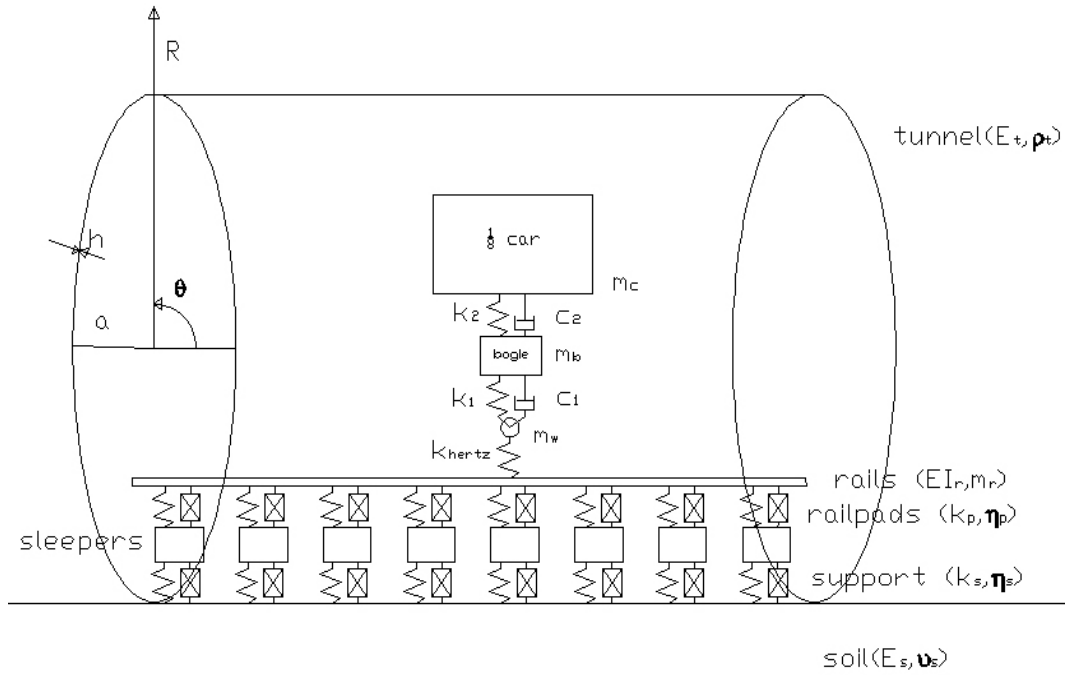


Figure 20. New track model including rigid sleepers, rails, railpads and bearings represented as complex stiffness elements.

4.1. Track Model

In previously developed model, the track model consists of two infinite Euler beams for floating slab and for rails with railpads between these beams. This model is mainly developed to evaluate the effectiveness of floating slab system by calculating the power spectral density of vibration at a specific point in the soil. Forrest and Hunt claim that it is possible to apply the tunnel and infinite soil model to different track models [25].

In this work the floating slab system will be replaced by rigid sleepers. The reason behind the sleeper adjustment is that in many existing subway systems like Istanbul and Ankara subways, sleepers are constructed under rails. The sleepers are modeled as concrete monoblock type sleepers. This model assumes that the sleepers are rigid. Each sleeper is supported by bearings of complex stiffness elements to include damping on the tunnel invert. (Figure 20) The rigid sleeper assumption is

verified by authors Lai [65], Luo [74], Kalker [51], Krylov [59, 70] and Hildebrand [38], for the frequency range of interest sought in this work, i.e. 1-200 Hz.

In this sleeper model; the sleepers are considered to provide discrete loads to the ground with a time, and therefore phase difference corresponding to the sleeper spacing and the train speed. Each sleeper acts as a vertical force applied to the underneath foundation during the time necessary for the deflection curve to pass through the sleeper. Thus, an individual sleeper can be regarded as a point source, which can radiate elastic waves. Also shifting principle is applied by using the infinite structure assumption to reduce the size of calculations. As in the original model, the load and the observation point can be shifted longitudinally while maintaining their separation. The response at the observation point will not change. Thus, finding the set of FRF's for the soil response at $x = 0$ to a set of loads at various positions on the rail is equal to find the FRF's for the soil at those various longitudinal positions to a single load at $x = 0$. The power spectral density function of ground vibration displacement at a designated observation point in soil is a superposition of the contributions from all sleepers.

The equations derived to obtain FRF's of the slab beam are modified according to the new model to include sleepers by setting $\tilde{H}_{11} = 1$. Thus, the pre-rail-beam FRF of the slab beam \tilde{H}_{11a} will be expressed as:

$$\tilde{H}_{11a} = \tilde{Y}_1 = \frac{1 + k\tilde{H}_{22}}{1 + k(1 + \tilde{H}_{22})} \quad (4.1)$$

where k represents the bearings of complex stiffness elements.

Also, the power spectral density equation (3.58) will be modified by defining the parameter L as the sleeper spacing. Hence, the time delay between two adjacent sleepers is given as $T = L/V$, where L is the sleeper spacing. The results of sleeper modification will be discussed in the next chapter in detail.

4.2. Modified hysteretic damping model

Forrest and Hunt use in their work [24,25] two different damping models. The Rayleigh (proportional) material damping governed by the two parameters α_R and β_R is used to compare results with the chosen finite element model. Later in these works material damping based on loss-factor concept is used by modeling the material damping and the track elements. In this damping model, the effects of material damping are included by using complex material parameters in the frequency domain.

It is assumed that all energy dissipation due to material damping in the soil occurs through shear motion. Thus, material damping in soil is mainly characterized by the shear modulus G , with no losses in volumetric expansion, which is defined by the bulk modulus $K=E/3(1-2\nu)$. In original model, the soil damping is included in the model by using the complex material parameters $G^*=G(1+i\eta_G)$ and $K^*=K(1+i\eta_K)$ in the frequency domain, where η_G is the constant hysteretic loss factor and η_K is the factor for non-zero volumetric damping. The constant hysteretic factor is derived based on Hunt's previous works for 100 Hz. This model also enables the contribution of volumetric deformations for saturated soil types through the parameter η_K .

The authors achieve their material damping model in soil by introducing a complex Poisson's ratio ν^* to obtain the damped Lamé's constant λ^* [24,25]. Thus, the complex damping relations become:

$$\nu^* = \frac{1}{2}(3K^* - 2G^*)/(3K^* + G^*) \quad (4.2)$$

$$\mu^* = G^* \quad (4.3)$$

$$\lambda^* = 2G^* \nu^* / (1 - 2\nu^*) \quad (4.4)$$

For the material damping in the tunnel invert, it is assumed that no damping occurs in the tunnel invert, since the material damping of the concrete is negligible compared to that of the soil[24,25].

Damping in the springs is taken as hysteretic, described by a constant loss factor. Therefore, complex stiffness $k(1+i\eta)$ is used in railpads and bearings [24,25].

4.2.1. Modified hysteretic damping

For stationary load and for a hysteretic damping model where the material exhibits damping characterized by a loss factor η , the complex Lamé constants are given by [66].

$$\lambda = \frac{\nu E(1+i\eta)}{(1+\nu)(1+2\nu)}, \quad \mu = \frac{E(1+i\eta)}{2(1+\nu)} \quad (4.5)$$

It is necessary to consider a suitable damping model for vibration problems in unbounded domains due to moving loads. In this thesis, a modified hysteretic damping model in the Fourier wavenumber domain will be used for moving harmonic loads derived by L'Mesgoues.[66] The modification is achieved by modifying Lamé constants by tracking the location of poles and branch points of the Rayleigh function for a stationary harmonic force, given in equation (4.6), for various load speeds, in the complex plane.

$$F_R(k_R) = \left(2 - \frac{k_2^2}{k_R^2}\right)^2 - 4 \left(1 - \frac{k_1^2}{k_R^2}\right)^{1/2} \left(1 - \frac{k_2^2}{k_R^2}\right)^{1/2} \quad (4.6)$$

The Lamé constants are modified with a factor $(1+i\eta f(k, \beta_m))$ where $f(k, \beta_m) = \text{sign}(k - \beta_m)$, $m=1,2$ denoting the number of the pole in wavenumber domain, and $k = \omega/V$ is the wavenumber corresponding to the moving load, with ω the excitation frequency and V the speed of the train. Thus, the expressions for Lamé constants (4.5), become

$$\lambda = \frac{\nu E(1+i\eta)}{(1+\nu)(1+2\nu)} (1+i\eta \text{sign}(1 - \beta/k)), \quad \mu = \frac{E(1+i\eta)}{2(1+\nu)} (1+i\eta \text{sign}(1 - \beta/k)) \quad (4.7)$$

The choice of this damping model is evident through examination of the propagating Rayleigh waves.

4.3 Vehicle model and Hertz contact

In Forrest and Hunt's work, the contribution of vehicle dynamics is added to the system by adding masses in dynamic stiffness matrix (3.54) as inertia terms. This model considers the vehicle as single degree-of-freedom masses to stand for axles [24,25]. Real train vehicles have pairs of axles attached to bogies, which also contribute to the low-frequency interaction with the rail (below and around the primary natural frequency of suspensions, that is, below about 10 Hz). Thus, the vehicle model will be modified by including the contribution of primary and secondary suspensions together with the bogie. It is aimed to investigate the behavior of the system in the low frequency range in more detail with a three degree-of-freedom vehicle model by lumping the whole car body in 1/8 vehicle mass and considering one contact point as seen in Figure 21.

For undamped single degree-of-freedom systems, with the characteristic frequency ω_n , the frequency-response function due to road displacement input $y(t)$ and vehicle-displacement response $x(t)$ is derived as

$$H_{xy}(\omega) = X(\omega)/Y(\omega) = 1/[1 - (\omega/\omega_n)^2] \quad (4.8)$$

The frequency-response function for the force applied to the roadway, $f(t) = m\ddot{x}$, is derived assuming that a harmonic road profile input $y(t) = Ye^{i\omega t}$ results in a harmonic output displacement $x(t) = Xe^{i\omega t}$

$$H_{fy}(\omega) = F(\omega)/Y(\omega) = -m\omega^2/[1 - (\omega/\omega_n)^2] \quad (4.9)$$

which describes the corresponding harmonic output force $Fe^{i\omega t}$ to the road profile. It is noted that in Forrest and Hunt's work, the upper part of the division in equation (4.9) is added as inertia terms to the dynamic stiffness matrix.

For a three-degree-of-freedom vehicle such as that shown in Figure 21, an equation similar to equation (4.9) can be derived in frequency domain using the relation between vertical wheel displacement and normal force as:

$$F(\omega) = k_w(\omega)Y(\omega) \quad (4.10)$$

where $k_w(\omega)$ can be gained using the impedance relations given in (4.11).

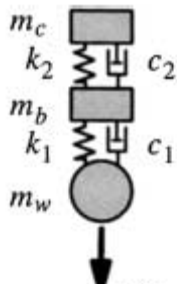


Figure 21. Three-degree-of-freedom model with one contact point [7]

$$k_c(\omega) = -\omega^2 m_c$$

$$k_s(\omega) = \frac{1}{\frac{1}{k_c(\omega)} + \frac{1}{i\omega c_2 + k_2}} - \omega^2 m_b \quad (4.11)$$

$$k_w(\omega) = \frac{1}{\frac{1}{k_s(\omega)} + \frac{1}{i\omega c_1 + k_1}} - \omega^2 m_w$$

For a single-axle vehicle model with any degrees of freedom, the expression $H_{f_y}(\omega) = mZ(\omega)/Y(\omega)$ applies generally, and that the acceleration term $Z(\omega)$ is fixed, when the ratio of masses and the characteristic frequencies within the vehicle are fixed. Wheel forces generated by vehicles with identical mass ratios and characteristic frequencies traveling at a given speed along a particular roadway will therefore be in direct proportion to the vehicles' mass alone. The impedance relations given in equation (4.11) are rearranged to the basic form to be applicable into the dynamic stiffness expression in terms of inertia. In practice, suspensions in the vehicle may have nonlinear behavior. However, to enable analysis in the frequency domain, each non-linear suspension is modeled as linear spring.

Also, Hertz contact is handled together with vehicle model. Forrest and Hunt neglected Hertz contact spring between each wheel and the rail,

due to the claim that Hertz contact does not have a significant effect on rail response below 750 Hz [17], which is above the frequency range of interest. In this thesis the effect of Hertz contact will be investigated by choosing comparable values for stiffness of the contact spring and the bearings.

Assuming that the roughness level in wheel and rails is not extremely severe and that moderate static preload is applied to keep the wheel and rail in contact; the nonlinear wheel/rail dynamic interaction model is approximated using an equivalent linear model. (Figure 12, 20) The use of a linear contact model also simplifies calculations, since a linear model can be expressed in the frequency domain.

Hertz contact is added to the model by considering its energy storing character i.e. subtracting linear Hertz contact spring elements from inertia terms in the dynamic-stiffness expression (3.54).

CHAPTER 5

RESULTS AND DISCUSSION

5.1 Parametric Study

In this chapter the results obtained using software prepared in MATLAB will be presented according to each change done in the model. To allow comparison with the original model developed by Forrest and Hunt, the parameters used in their work will be adapted to the modified model. For the parameters of modified vehicle and track model, realistic values are chosen from the literature. In Tables 8,9 and 10, these parameters are illustrated:

Table 8. Parameters to model the tunnel surrounded by soil [25]

Tunnel (cylindrical shell)	Soil (elastic continuum)
$E=50 \times 10^9$ Pa	$E=550 \times 10^6$ Pa
$\nu=0.3$	$\nu=0.44$
$\rho=2500$ kg/m ³	$\rho=2000$ kg/m ³
$a=3.0$ m	$\lambda=1.400 \times 10^9$ Pa
$h=0.25$ m	$\mu=G=191 \times 10^6$ Pa
Zero damping	$K=1.528 \times 10^9$ Pa
	$c_1=944$ m/s
	$c_2=309$ m/s
	$\eta_G=0.06$
	$\eta_K=0$

Table 9. Parameters for rails, slab beam and sleepers [25]

Slab beam	Rail beam	Sleepers
$EI=1430 \times 10^6 \text{ Pa m}^4$	$EI_r=10 \times 10^6 \text{ Pa m}^4$	$L=0.6 \text{ m}$
$m=3500 \text{ kg/m}$	$m_r=100 \text{ kg/m}$	Rigid sleepers
$k_s=1262 \times 10^6 \text{ N/m}^2$ ($f_n=60 \text{ Hz}$)	$k_r=400 \times 10^6 \text{ N/m}^2$	
$\eta_s=0.5$	$\eta_r=0.3$	

Table 10. Parameters for the vehicle model [25,7]

Vehicle
$m_a=500 \text{ kg}$
$L=20 \text{ m}$
Mass of 1/8 vagon(m_c)=5075 kg
mass of bogie(m_b)=745 kg
mass of wheelset(m_w)=880 kg
primary vertical stiffness(k_1)= $9.72 \times 10^5 \text{ N/m}$
secondary vertical stiffness(k_2)= $3.52 \times 10^5 \text{ N/m}$
primary vertical damping(c_1)= $1.2 \times 10^4 \text{ Ns/m}$
secondary vertical damping(c_2)= $1 \times 10^4 \text{ Ns/m}$
Hertzian contact stiffness= $2,7 \times 10^9 \text{ N/m}$

It should be noted that for the chosen vehicle, these parameters satisfy the condition that the natural frequency of primary suspension

system ($f_n = \frac{1}{2\pi} \sqrt{\frac{k_1}{m_w}} = 5.3 \text{ Hz}$) lies below 10 Hz. Also, the primary

suspension system is much stiffer than the secondary suspension system.

All the calculations are carried for the vehicle speed of 40 km/h. The number of contributing axles and sleepers is important since the convenient forcing vector must be used to model the response in the soil correctly. In the original model, it is claimed that 25 axles are sufficient for convergence. When modeling the track with rigid sleepers, the number of axles is substituted with the number of sleepers. The choice of the number of sleepers is dependent on the length of wavenumber and consequently space domain.

The MATLAB code creates 5-dimensional matrix of equation (3.32) whose components are given in Appendix A. Note there is a span of 18 orders of magnitude in the values of the matrix, which means that the assembled matrix is so badly scaled that numerical solution of the problem can produce inaccurate results. Therefore, row and column normalisation is used to reduce magnitudes of the elements in the assembled matrix to between zero and unity before attempting numerical solution. Displacements in wavenumber and frequency domain are added for each value of n to calculate the displacement at the interface and at a specified point in the soil. Inverse discrete Fourier transform is taken to transform the wavenumber domain to space domain. The frequency response functions and dynamic stiffness matrix are formed and the power spectral density function of displacement at a desired point in the soil is calculated. The algorithm of the code is given in Figure 22.

Due to requirements of high computational power and memory capacity, calculations could not be performed by the same number of variables in the original work. Only five circumferential modes could be included and the discrete Fourier Transform (DFT) is calculated using 128 points which correspond to a length of 64 meters in longitudinal direction. It is expected that, the program is able to yield the general characteristics of vertical displacement spectrum with less detail due to limitations on computational power.

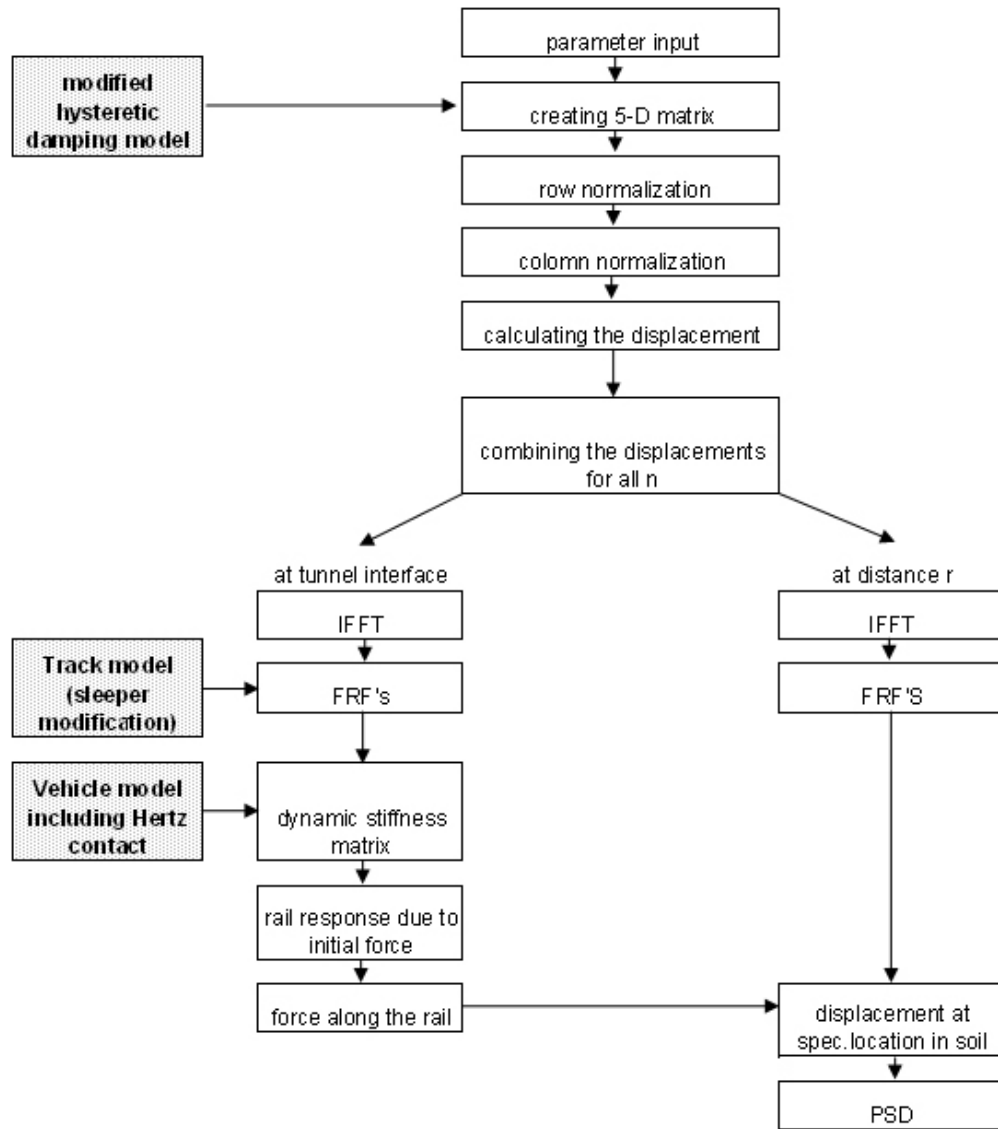


Figure 22. The MATLAB code algorithm and the lines where modifications are made

Each modification in the system will be compared with the original model where the track is modeled with slab beams on slab support stiffness defined for $f_n=60$ Hz according to the vertical displacement spectrum at $\theta=0$ and $r=20$ m, considering the best rail conditions at the vehicle speed of 40 km/h.

5.1.1 Track model

Modifications made in the track model affect the part where the definitions of frequency response functions are presented in the code. The rigid sleeper assumption changes H_{11} , originally the FRF of the slab beam as unity. Also L , axle spacing is redefined as the sleeper spacing. Note that the value of L and the length of wavenumber domain affect the number of contributing sleepers. Taking $L=0.6$ enables (length of x -domain)/ $L=2$ sleepers i.e.105 sleepers to be included in the length of space domain.

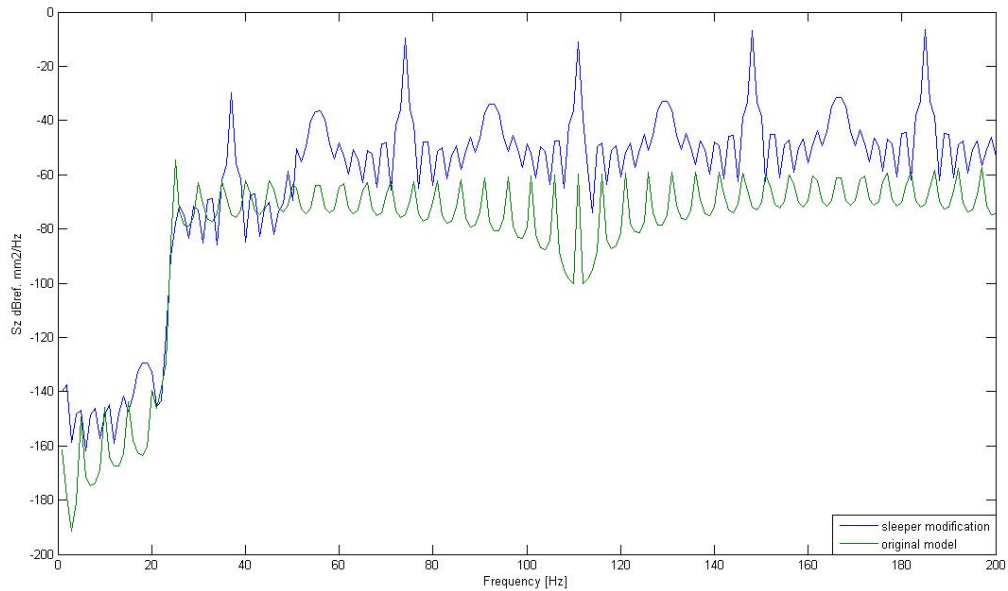


Figure 23. Result of sleeper modification (green: original system, blue: sleeper modification)

5.1.2 Modified damping model

The modified damping model changes the definition of Lamé constants in the code. In the modified model, λ and μ are variables changing in wavenumber domain with frequency and the vehicle speed. Accordingly Lamé constants are placed in the part where main matrices in equation (3.32) are created as seen in Figure 22.

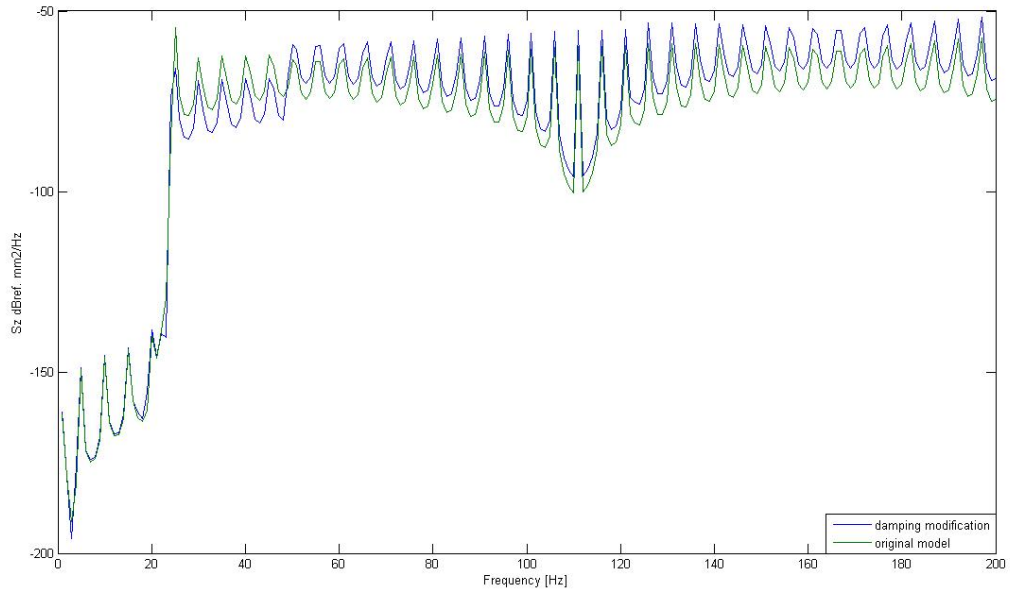


Figure 24. Effect of modified hysteretic damping for moving load (green: original system, blue: damping modification)

5.1.3. Modified vehicle model and Hertz contact

Modified vehicle model is added to the system by introducing inertia term of equation (4.10) instead of axle masses to the dynamic stiffness matrix (3.54). The vehicle parameters are chosen to reflect a realistic vehicle model. Damping is incorporated into the suspension by introducing viscous dampers. Also, Hertzian contact is included in the system by adding linear stiffness terms to dynamic stiffness expression considering the energy storing characteristic of spring elements.

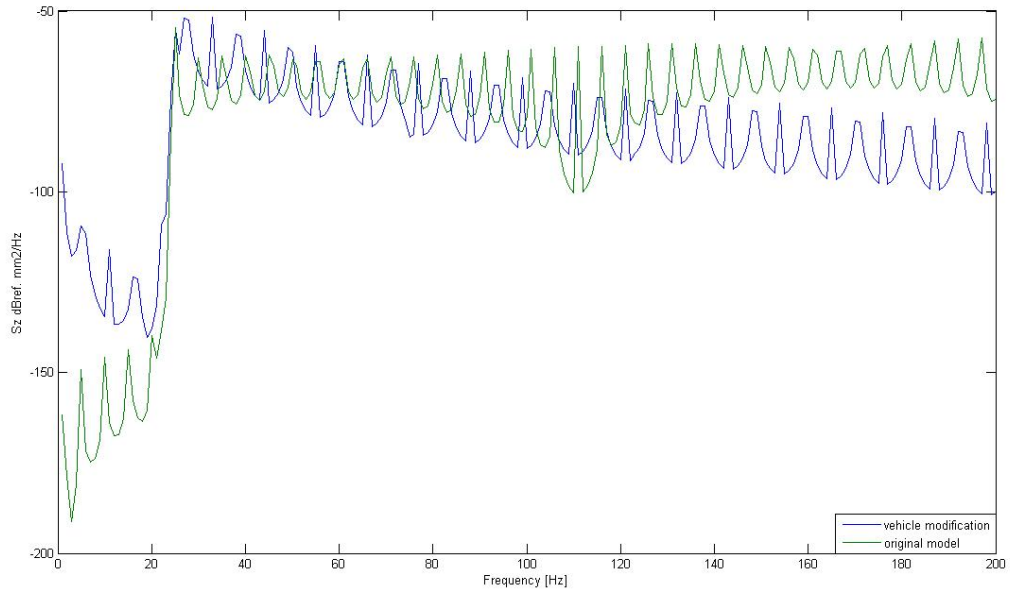


Figure 25. Effect of 3 degree-of-freedom vehicle model and Hertz contact on the model (green: original system, blue: vehicle modification)

5.1.4. The complete modified model

The complete model is obtained by including each modification to the original model developed by Forrest and Hunt. Thus the modified model takes new track, damping and vehicle model with Hertz contact spring into account to calculate the power spectral density function at a desired point in soil using Random Process Theory. The program is operated to give useful information about the ground borne vibration due to underground railway vehicles. In Figure 27 the isogram of spectral density function of vertical displacement for different positional angles is shown. In Figure 28, response in the soil at a distance of 20 meters from the tunnel centerline is evaluated for different vehicle speeds. In Figure 29, the change in root mean square value of vibration velocity with respect to distance from the tunnel centerline and frequency is shown. Calculations are performed in the frequency range of 1 to 80 Hz and the vibration velocity levels are compared with the limits specified in TS ISO 2631-2 standards.

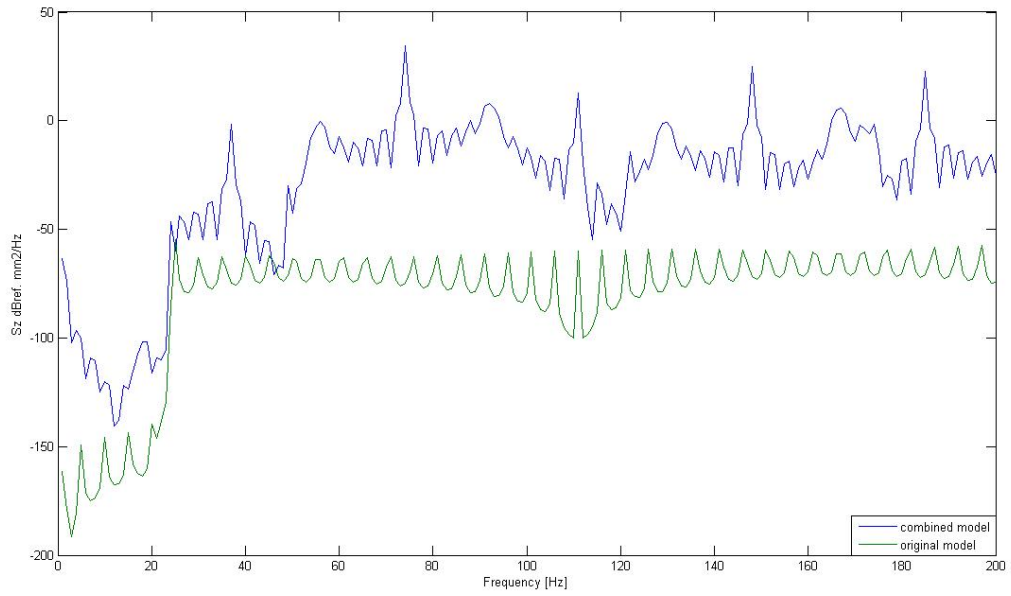


Figure 26. Comparison between two models on displacement vibration spectra at $\theta=0$ and $r=20\text{m}$ (green: original system, blue: combined modified system).

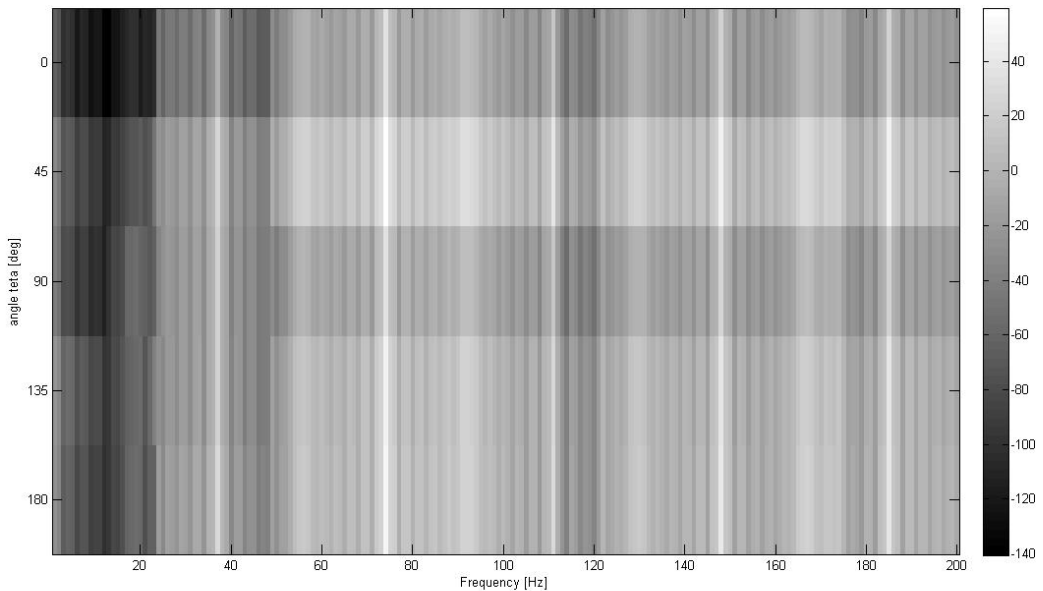


Figure 27. Vertical soil displacement spectrum for the modified model for different angles θ .

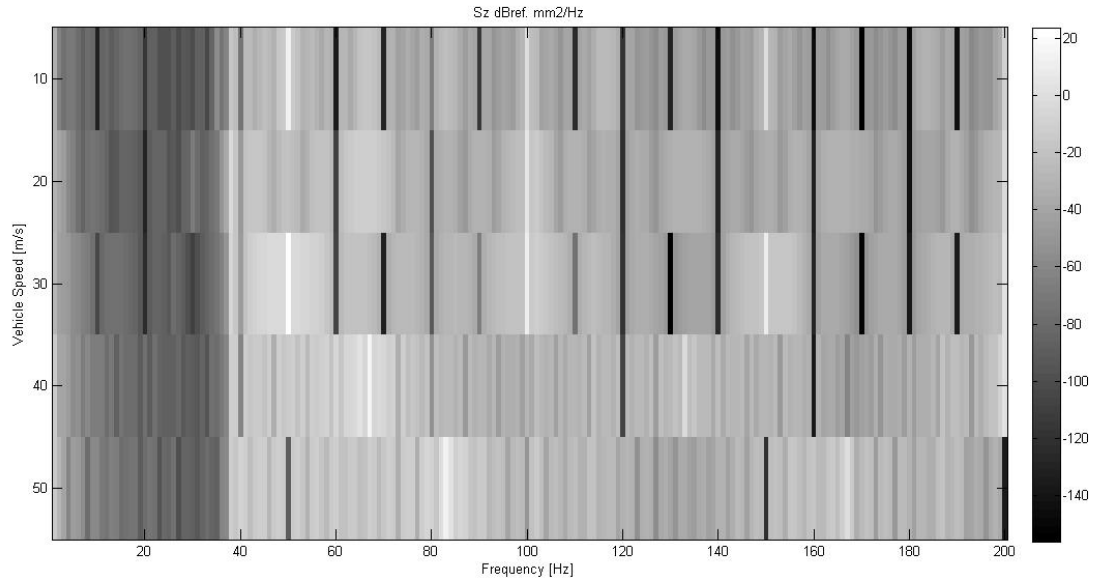


Figure 28. Change in vertical soil displacement spectrum at $\theta=0$ and $r=20\text{m}$ for different vehicle speeds.

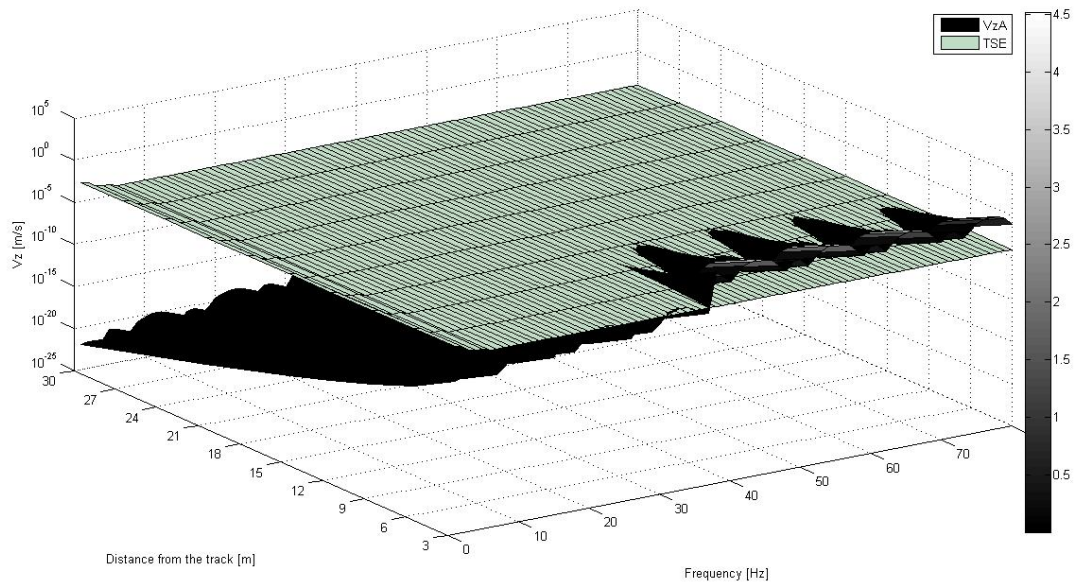


Figure 29. Root mean square value of vibration velocity compared with limit values specified in TS ISO 2631-2.

5.2 Discussion

For predictions of ground-borne vibration accurately it is necessary to represent both the discrete nature of the track support and characteristics of the vehicle as realistically as possible. The periodicity in the track model geometry gives rise to the transmission of vibration at characteristic frequencies into the ground. The aim of the modified model is to take the discrete nature of supports, and a more appropriate and/or sophisticated vehicle model with higher degrees of freedom into consideration. Modified damping model and Hertzian contact are included into the system model to study effects of these modifications. In Figures 23-26 results are presented for each modification in the system separately to enable comparison with those of the original model. In all the figures, it is observed that the original model underestimates vibration levels at low frequencies. This underlines the necessity and importance of a appropriate vehicle model.

In Figures 23 and 26, different effects of sleeper support and axle passing is detected in terms of sleeper passing frequency and axle spacing frequency. In the original model axle spacing plays an important role, which is defined as

$$f_A = \frac{U}{d} \quad (5.1)$$

where U is the vehicle speed in m/s and d is the axle spacing in meters.

The effect of axle spacing is reflected onto the spectrum as troughs of 5 Hz intervals conceptualized as wheelbase filtering due to coincidence of roughness wavelength with the axle spacing on the track. The same characteristics are also obtained in the original model. Forrest and Hunt explain this phenomenon with the motion of axle masses.[25]. It is claimed that, crests occur when all the axle masses move up and down in phase and troughs when they move out of phase. For the train speed of 40km/h (11.1 m/s) and axle spacing of 20 m, the expected frequency interval between peaks of in-phase force transmitted to the tunnel invert is 0.5 Hz, which is not clear in original model spectrum Figures 23-26. Main reason

for this is that the computations are performed for a frequency step of 1 Hz, this implies a resolution too coarse to show fluctuation at periods of 0.5 Hz. Thus, the fluctuation can only be observed at integer multiples of the fundamental frequency interval.

Generally, sleepers are considered to provide discrete loads to the ground with a time delay, and therefore associated phase difference corresponding to the sleeper spacing and the train speed. The sleeper passing frequency is defined as

$$f_s = \frac{U}{d} \quad (5.2)$$

where U is the vehicle speed in m/s and d is the sleeper spacing in meters.

In the current model the sleeper support modification is validated through sleeper passing frequency and wheel-track resonance frequency. As seen in Figure 30, the axle passing frequency has an effect in low frequency range, where sleeper passing frequency is more dominant at higher frequencies. The common peak at different vehicle speeds is designated by $f_{R/S}$, which is the range of wheel – track resonance.

To compare the results of the modified model, the power spectral density is calculated at tunnel walls and converted to root mean square of vertical vibration velocity. The results are evaluated in decibel scale where the reference is taken as 5×10^{-8} m/s and illustrated in Figure 30 in 1/3-octave bands together with experimentally measured values.

For a vehicle traveling at $U=11.1$ m/s on a track with sleeper support spacing of 0.6 meter, the first peak in the vertical vibration velocity spectrum is expected at the sleeper support frequency equal to 18 Hz. In Figure 23, representing the contribution of sleeper modification alone and in Figure 26 representing the combined modified model; the first jump in spectrum is detected around 18 Hz indeed. At higher frequencies, the figure takes a repeating shape with an interval of 18 Hz, the sleeper passing frequency. This characteristic form is consistent with the measured one-third octave vibration velocity level as shown in Figure 30. As seen in Figure 30 the wheel – track resonance of the modified model occurs at 63 Hz. A similar result has been observed in the measurements Heckl

conducted [36] on the tunnel walls. In Figure 27, the rise in power spectral density function around 60-80 Hz, obtained from the modified model at 20 meters distance from the track centerline can be explained with the same phenomenon.

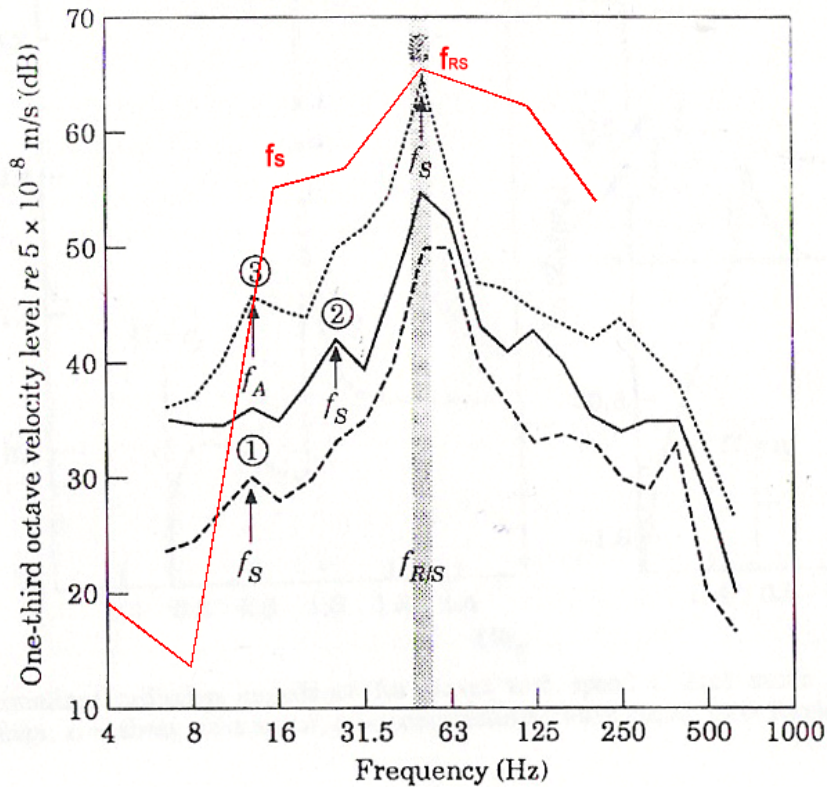


Figure 30. One-third octave band vibration levels measured on the tunnel walls for different vehicle speeds. and results computed by the modified model(in red) at U=40 km/h (1. U=30 km/h, $f_s=14$ Hz, 2. U=60 km/h $f_s=28$ Hz, 3. U=120 km/h $f_s=56$ Hz) [36].

A moving load on surface irregularity approach is used in the model. This necessitates a convenient damping model in the soil to be applied. With the modified damping model, where the soil damping parameters depend on the wavenumber, vehicle speed and frequency, little difference

from the original model is observed. At higher frequencies than 50 Hz, modified damping model results in overestimated values due to dependence of damping on frequency.

The vehicle is modeled as a three degree-of-freedom system taking primary and secondary suspension system, wheelset, bogie and 1/8 lumped vehicle mass and Hertzian contact into account. It is assumed that at low frequency region the vehicle's primary and secondary suspension isolate the bogie and body from the wheelset. Consequently the vehicle's "unsprung mass" is the only component which significantly affects vertical dynamic loads between wheelset and track, which is lumped in 1/8 vehicle mass. Thus unsprung mass can be represented satisfactorily for vertical excitations as a rigid body. As seen In Figure 25, vehicle modification with Hertzian contact results with a reasonable characteristic in the low frequency region where dynamic behavior of the vehicle with regard to stability, steering and passenger comfort is significant. Around the resonance of primary suspension system, i.e. 5.3 Hz, the peaks can be detected. With increasing frequency the values of power spectrum decrease retaining the repeating form due to axle spacing.

In general, the excitation of railway vehicles is distinguished in three completely different parts: the regular static part, the irregular static part (due to the scattering of the axle impulses) and the regular dynamic part (due to the sleeper passage). It is known that to model the tracks behavior at very low frequencies and at the near-field of the track, the regular static part, which is also called the quasi-static part, must be added to the system. In this thesis the ground vibration near railway lines is considered to be caused by dynamic loads due to irregularities of the vehicle and track or due to the regular track variation with sleeper passing frequency.

Track structures of infinite length are commonly used for frequency domain solutions. Practically, it is not possible to obtain a solution where infinite number of data is involved and generally a satisfactory convergence is aimed. In this work, due to limitations on computational power it is assumed that convergence is reached with less number of variables than in the original work. In Forrest and Hunt's work, the number

of contributing circumferential modes is taken as ten where in this thesis only five modes are considered. Also calculations are performed on a shorter wavenumber domain due to limitations in computer memory. However, by comparing the results with measurements, it is concluded that the modified model gives quite a realistic characteristic for vibration spectrum due to underground rail vehicles. It should be noted that, the modified model gives underestimated results in 1-18 Hz range, where it gives overestimated results in 18-200 Hz range.

The modified model has been operated for different angles θ to give vertical displacement spectrum, which is shown in Figure 27. The spectrum of vertical displacement has minima at $\theta=0^0$ and $\theta=90^0$. Note that for all the positional angles, the same general characteristics like sleeper passing frequency or wheel – track resonance are apparent.

In Figure 28, the variation of power spectral density function of vibration displacement in terms of different vehicle speeds is given. With the increase in train speed, vibration amplitudes of the vehicle excited by the random irregularity of the track do not change significantly. Depending on the change of sleeper passage frequency, the number of generated peaks changes. With increasing vehicle speed, less number of peaks is observed in the spectrum and peak frequencies shift up to higher frequencies.

In Figure 29, a real situation is modeled and the calculated vibration velocity levels are compared with the limit values specified in TS ISO 2631-2. Considering that the soil type surrounding the tunnel is clay stone and the vehicle speed is 80 km/h, calculations are performed to estimate the change in velocity level due to distance from the track and frequency. As seen in Figure 29, the peak around 37 Hz is attenuated under the limit values at 9 meters whereas the peak around 74 Hz is attenuated at 7 meters. The reason for that is that the soil damping is more efficient at higher frequencies.

CHAPTER 6

CONCLUSIONS

In this thesis, ground-borne vibration from underground rail vehicles is modeled, by modifying a previously developed model by Forrest and Hunt. In the same frequency range with the original work, modifications are made in four areas: track model, vehicle model, damping and contact model. The track is modeled with rigid sleepers together with railpads, the vehicle as a moving three-degree-of-freedom 1/8 vehicle. Modified hysteretic damping for moving loads in soil and Hertzian contact are included into the model for compliance with the real situation. In the frequency range of interest, effect of sleeper modification with modified hysteretic damping is found to be more essential. The characteristic component in the vibration spectrum, sleeper passing frequency is represented satisfactorily through the modifications made. Also comparison with the measurements from literature gives quite good agreement with the computed results by the modified model. All the calculations are performed and presented graphically for each modification separately to represent each effect in detail. Also, graphical results for vertical vibration displacement spectra of the system for different vehicle speeds and positional angles are included; a realistic case is studied by comparing vibration velocity levels with limit values specified in TS ISO 2631-2.

Throughout the modeling process, assumptions are made to simplify calculations without losing integrity with the real problem. The whole structure, which is surrounded by viscoelastic soil without free surface, is assumed to be infinite in extent. All calculations are performed

in frequency domain using random process theory by assuming that the model is completely linear. However, it is already known that there are several nonlinearities present in the system. The most significant of these is unloading of the wheel/rail contact. The contact stiffness itself is nonlinear, and other phenomena such as periodic rolling and slipping are inherently nonlinear. In practice, there are many irregularities in the structure of railway track, such as poorly supported sleepers, missing or defective railpads and fastenings, non-uniform sleeper spacing. A further study can cover all these defects by modifying the current track and vehicle model by representing these irregularities with the help of random process theory.

Frequency range of interest can be extended, since phenomena like noise, corrugation formation and other types of damage to the vehicle occur in high frequency range up to 5 kHz. Extension of the frequency range requires the vehicle and track model to be modeled more detailed. The vehicle model has to include dynamics of the complete vehicle. In higher frequency range it is more appropriate to model the rails as Timoshenko beams and the sleepers with finite stiffness need to be taken into account.

In conclusion, by entering correct parameters for wave speed in soil and stiffness elements to the prepared MATLAB code, real situation can be modeled with sufficient accuracy for prediction and mapping of vibration from underground rail vehicles in urban areas. It is also possible to design specific track elements like pads, mats and other types of support to meet the specified standards for ground –borne vibration like ISO 2631-2 or TS ISO 2631-2 or other possible vibration limits specified by authorities and/or legal documents.

REFERENCES

- [1] Alabi B.; A model for the problem of ground vibration induced by the wheels of a moving train; *Applied Mathematical Modeling* 13 (1989) 710-715
- [2] Alabi B.; A parametric study on some aspects of ground-borne vibrations due to rail traffic; *Journal of Sound and Vibration* 153(1) (1992) 77-87
- [3] Arnst M., Clouteau D., Chebli H., Othman R., Degrande G.; A non-parametric probabilistic model for ground-borne vibrations in buildings; *Probabilistic Engineering Mechanics* 21 (2006) 18–34
- [4] Auersch L.; Ground vibration due to railway traffic—The calculation of the effects of moving static loads and their experimental verification; *Journal of Sound and Vibration* 293 (2006) 599–610
- [5] Balendra T., Koh C.G., Ho Y.C.; Dynamic response of buildings due to trains in underground tunnels; *Earthquake Engineering and Structural Dynamics* 20 (1991) 275-291
- [6] Belotserkovskiy P.M.; On the Oscillations of Infinite Periodic Beams Subjected to a Moving Concentrated Force; *Journal of Sound and Vibration* 193 (1996) 705– 712.
- [7] Bitzenbauer J, Dinkel J; Dynamic interaction between a moving vehicle and an infinite structure excited by irregularities – Fourier Transform solutions; *Archive of Applied Mechanics* 72 (2002) 199-211
- [8] Borchardt R.D.; Rayleigh-type surface wave on a linear viscoelastic half space; *The Journal of the Acoustical Society of America* 1972 1651-1653
- [9] Borchardt R.D.; Energy and plane waves in linear viscoelastic media; *Journal of Geophysical Research* 78(14) 1973 2442-2453
- [10] Carcione J.M.; Wave propagation in anisotropic linear viscoelastic media: theory and simulated wavefields; *Geophysical Journal International* 101 (1990) 739-750
- [11] Carcione J.M.; Rayleigh Waves in isotropic viscoelastic media; *Geophysical Journal International* 108 (1992) 453-464

- [12] Cardona S., Fernandez-Diaz E., De Los Santos M. A., Tejado J. L.; Simple Model For The Time History Of The Ground Vibrations Generated by Underground Trains as the Means of Monitoring the Riding Quality of the Wheels of a Bogie, *Vehicle System Dynamics*, 33 (2000) 421–434
- [13] Cerveny V., Psencik I.; Plane waves in viscoelastic anisotropic media I. Theory; *Geophysical Journal International* 161 (2005) 197-212
- [14] Cerveny V., Psencik I.; Plane waves in viscoelastic anisotropic media II. Numerical examples; *Geophysical Journal International* 161 (2005) 213-229
- [15] Chen Y.H., Huang Y.H., Shih C.T.; Response Of An Infinite Timoshenko Beam on a Viscoelastic Foundation to a Harmonic Moving Load, *Journal of Sound and Vibration* 241(5), (2001) 809-824
- [16] Chua K.H., Lo K.W., Balendra T.; Building response due to subway train traffic; *Journal of Geotechnical Engineering*, November 1995, 747-754
- [17] Clark R.A., Dean P.A., Elkins J.A., Newton S.G.; An investigation into the dynamic effects of railway vehicles running on corrugated rails; *Journal of Mechanical Engineering Science* 24 (1982) 65-76
- [18] Clouteau D., Arnst M., Al-Hussaini T.M., Degrande G.; Freefield vibrations due to dynamic loading on a tunnel embedded in a stratified medium; *Journal of Sound and Vibration* 283 (2005) 173–199
- [19] de Barros F.C.P., Luco J.E.; Response of a layered viscoelastic half-space to a moving point load; *Wave Motion* 19 (1994) 189-210
- [20] Degrande G., Clouteau D., Othman R., Arnst M., Chebli H., Klein R., Chatterjee P., Janssens B.; A numerical model for ground-borne vibrations from underground railway traffic based on a periodic finite element–boundary element formulation, *Journal of Sound and Vibration* 293 (2006) 645–666
- [21] Degrande G., Schevenels M., Chatterjee P., Van de Velde W., Hölscher P., Hopman V., Wang A., Dadkash N.; Vibrations due to a test train at variable speeds in a deep bored tunnel embedded in London clay, *Journal of Sound and Vibration* 293 (2006) 626–644
- [22] Dings P.C., Dittrich M.G.; Roughness on Dutch railway wheels and rails; *Journal of Sound and Vibration* 193 (1996) 103–112.
- [23] Dodds C.J., Robson J.D.; The description of road surface roughness; *Journal of Sound and Vibration* 31(2) (1973) 175–183.

- [24] Forrest J.A., Hunt H.E.M.; A three-dimensional tunnel model for calculation of train-induced ground vibration; *Journal of Sound and Vibration* 294 (4-5) July 2006 678-705
- [25] Forrest J.A., Hunt H.E.M.; Ground vibration generated by trains in underground tunnels *Journal of Sound and Vibration*, 294 (4-5) July 2006 706-736
- [26] Fryba, L.; *Vibrations of Solids and Structures Under Moving Loads*; Noordhoff, Groningen, 1972.
- [27] Gardien W., Stuit H.G.; Modeling of soil vibrations from railway tunnels; *Journal of Sound and Vibration* 267 (2003) 605–619
- [28] Garvin W.W.; Exact transient solution of the buried line source problem; *Proceedings of the Royal Society of London, Series A*, 234 528-541
- [29] Grassie S.L., Gregory R.W., Harrison D., Johnson K.L.; The dynamic response of railway track to high frequency vertical excitation; *Journal of Mechanical Engineering Science* 24 (1982) 77-90.
- [30] Grassie S.L., Cox S.J.; The dynamic response of railway track with flexible sleepers to high frequency vertical excitation; *Proceedings of the Institution of Mechanical Engineers* 198D (1984) 117-124
- [31] Grassie S.L.; Dynamic Modelling of concrete railway sleepers; *Journal of Sound and Vibration* 187 (1995) 799–813
- [32] Gudehus G.; A Comprehensive Constitutive Equation for Granular Material; *Soils and Foundation* 36 (1996) 1– 12
- [33] Gudehus G.; Attractors, Percolation Tresholds and Phase Limits of Granular Soils; *Proc. Powders and Grain* (1997) 1– 15
- [34] Gutowski T.G., Dym C.L.; Propagation of ground vibration: a review; *Journal of Sound and Vibration* 49(2) (1976) 179-193
- [35] Hao H., Ang T.C.; Analytical modeling of traffic-induced ground vibrations; *Journal of engineering mechanics*, August 1998, 921-928
- [36] Heckl M., Hauck G., Wettschüreck R.; Structure-borne sound and vibration from rail traffic; *Journal of Sound and Vibration* 193(1) (1996) 175-184
- [37] Hiensch M., Nielsen J.C.O., Verheijen E.; Rail Corrugation in The Netherlands – Measurements and Simulations; *Wear* 253 (2002) 140–149.

- [38] Hildebrand R.; Effect of soil stabilization on audible band railway ground vibration; *Soil Dynamics and Earthquake Engineering* 24 (2004) 411–424
- [39] Hou K., Kalousek J., Dong R.; A dynamic model for an asymmetrical vehicle/track system *Journal of Sound and Vibration* 267 (2003) 591–604
- [40] Hung H.H., Yang Y.B.; Elastic waves in visco-elastic half-space generated by various vehicle loads; *Soil Dynamics and Earthquake Engineering* 21 (2001) 1-17
- [41] Hunt H.E.M.; Modeling of road vehicles for calculation of traffic-induced ground-vibration as a random process; *Journal of Sound and Vibration* 144(1) (1991) 41-51
- [42] Hunt H.E.M., Stochastic modeling of traffic-induced ground vibration; *Journal of Sound and Vibration* 144(1) (1991) 53-70
- [43] Hunt H.E.M.; Modeling of railway vehicles and track for calculation of ground-vibration transmission into buildings; *Journal of Sound and Vibration* 193(1) (1996) 185–194
- [44] Hussein M.F.M., Hunt H.E.M.; An Insertion Loss Model For Evaluating The Performance Of Floating-Slab Track For Underground Railway Tunnels; Tenth International Congress On Sound And Vibration, ICSV10
- [45] Hussein M.F.M., Hunt H.E.M.; A power flow method for evaluating vibration from Underground railways; *Journal of Sound and Vibration* 293 (2006) 667–679
- [46] Janssens M.H.A., Dittrich M.G., de Beer F.G., Jones C.J.C.; Railway noise measurement method for pass-by noise, total effective roughness, transfer functions and track spatial decay; *Journal of Sound and Vibration* 293 (2006) 1007–1028
- [47] Jette A.N., Parker J.G.; Excitation of an elastic half-space by a buried line source of conical waves; *Journal of Sound and Vibration* 67(4) (1979) 523-531
- [48] Jones C.J.C., Block J.R.; Prediction of ground vibrations from freight trains; *Journal of Sound and Vibration* 193(1) (1996) 205-213
- [49] Jones C.J.C., Sheng X., Petyt M.; Simulations Of Ground Vibration From A Moving Harmonic Load On A Railway Track; *Journal of Sound and Vibration* 231(3) (2000) 739-751

- [50] Jones D. V., Le Houédec D., Peplow A. T., Petyt M. ; Ground Vibration In The Vicinity Of A Moving harmonic rectangular load on a half-space; European Journal Of Mechanics A-Solids 17(1) 1998 153-166
- [51] Kalker J.J.; Discretely Supported Rails Subjected to Transient Loads; Vehicle System Dynamics 25 (1996) 71-88
- [52] Kanamori T.; A few experiments on elasticity of rubber pad; JNR, Railway Technical Review, Quarterly Reports 21(4) (1980)
- [53] Karlström A., Boström R.; An analytical model for train-induced ground vibrations from railways; Journal of Sound and Vibration 292 (2006) 221–241
- [54] Kenney, J.T.; Steady-State Vibrations of Beams on Elastic Foundation for Moving Load; Journal of Applied. Mechanics 21 (1954) 359 – 364.
- [55] Kim D.S., Lee J.S.; Propagation and attenuation characteristics of various ground vibrations; Soil Dynamics and Earthquake Engineering 19 (2000) 115–126
- [56] Kirzhner F., Rosenhouse G., Zimmels Y.; Attenuation of noise and vibration caused by underground trains, using soil replacement; Tunnelling and Underground Space Technology 21(5) SEP 2006 561-567
- [57] Knothe K.L., Grassie S.L.; Modeling of Railway track and vehicle/track interaction at high frequencies; Vehicle System Dynamics 22 (1993) 209-262
- [58] Knothe K., Willner K., Styzakowski Z.; Rail vibrations in the high frequency range; Journal of Sound and Vibration 169(1) 1994 111-123
- [59] Krylov V.V., Ferguson C.; Calculation of Low-Frequency Ground Vibrations from Railway Trains; Applied Acoustics 42 (1994) 199-213
- [60] Krylov V.V; Generation of ground vibrations from superfast trains; Applied Acoustics 44 (1995) 149-164
- [61] Krzyzynski T., Popp K.; A Mathematical Treatise on Periodic Structures under Travelling Loads with an Application to Railway Tracks; Proc. 9th Conf. Mathematics in Industry, Teubner, 1997 93 – 100.
- [62] Kurzweil L. G.; Ground-Borne Noise And Vibration From Underground Rail Systems
Journal of Sound and Vibration 66(3) (1979) 363-370

- [63] Lapwood E.R.; The disturbance due to a line source in a semi-infinite elastic medium; Philosophical Transactions of the Royal Society of London, Series A, Mathematical and Physical Sciences, 242 No.841 Jul. 4.1949 63-100
- [64] Lamb H.; On the Propagation of tremors over the Surface of an Elastic Solid; Philosophical Transactions of the Royal Society of London, Series A, Containing Papers of a Mathematical or Physical Character 203 (1904) 1-42
- [65] Lai C.G., Callerio A., Faccioli E., Morelli V., Romani P.; Prediction of Railway-Induced Ground Vibrations in Tunnels; Journal of Vibration and Acoustics 127 October 2005 503-514
- [66] Lefeuvre-Mesgouez G., Peplow A.T., Le Houédec D.; Ground vibration in the vicinity of a high-speed moving harmonic strip load. Journal of Sound and Vibration 231(5) 2000 1289–1309
- [67] Lefeuvre-Mesgouez G., Peplow A.T., Le Houédec D.; Surface vibration due to a sequence of high speed moving harmonic rectangular loads; Soil Dynamics and Earthquake Engineering 22 (2002) 459–473
- [68] Lei X., Noda N.A.; Analyses Of Dynamic Response Of Vehicle And Track Coupling System with Random Irregularity of Track Vertical Profile; Journal of Sound and Vibration 258(1), (2002) 147–165
- [69] Lei X., Mao L.; Dynamic response analyses of vehicle and track coupled system on track transition of conventional high speed railway; Journal of Sound and Vibration 271 (2004) 1133–1146
- [70] Lin Q.; Krylov V.V; Effect of Tunnel Diameter on Ground Vibrations Generated by Underground Trains; Journal of Low Frequency Noise, Vibration and Active Control; 19 (1) 2000 17-25
- [71] Lombaert G., Degrande G., Clouteau D.; The non-stationary free field response for a moving load with a random amplitude; Journal of Sound and Vibration 278 (2004) 611–635
- [72] Los H. S., Herman G. C., Hölscher P.; Dynamic Interaction Between Train Wheels And The Subsurface; Journal of Sound and Vibration 247(5) (2001) 917-926
- [73] Ludwig K.; Deformation of a Rail Elastically Supported and of Infinite Length by Loads Moving at a Constant Horizontal Velocity; Proc. 5th. Int. Congr. Appl. Mech. 1938 650 – 655.
- [74] Luo Y., Yin H., Hua C.; The dynamic response of railway balast to the action of trains moving at different speeds; Proceedings of the Institution of Mechanical Engineers, 210, 2 1996

- [75] Madshus C., Kaynia A. M.; High-Speed Railway Lines On Soft Ground: Dynamic Behaviour At Critical Train Speed; *Journal of Sound and Vibration* 231(3), (2000) 689-701
- [76] Meinders T.; Modeling of a Railway Wheelset as a Rotating Elastic Multibody System; *Machine Dynamics Problems* 20 (1998) 209 – 220
- [77] Melke J.; Noise and vibration from underground railway lines: proposals for a prediction procedure; *Journal of Sound and Vibration* 120(2) (1988) 391-406
- [78] Metrikine A.V., Popp K., Steady-state vibrations of an elastic beam on a visco-elastic layer under moving load; *Archive of Applied Mechanics* 70 (2000) 399-408
- [79] Metrikine A. V., Vrouwenvelder A. C. W. M.; Surface Ground Vibration Due To A Moving Train In A Tunnel: Two-Dimensional Model; *Journal Of Sound And Vibration* 234(1) (2000) 43-66
- [80] Müller S., Krzyzynski T., Ilias H.; Comparison of Semi-Analytical Methods of Analyzing Periodic Structures Under a Moving Load', In: Knothe, K., Grassie, S.L. and Elkins, J.A. (Eds.), *Interaction of Railway Vehicles with the Track and its Substructure. Proceedings of the 3rd Herbertoř Workshop held at Herbertoř, Czech Republic, September 1994. Supplement to Vehicle System Dynamics* 24(1995) 325– 339.
- [81] Nagy A.B., Fiala P., Marki F., Augusztinovicza F., Degrande G., Jacobs S., Brassens D.; Prediction of interior noise in buildings generated by underground rail traffic; *Journal of Sound and Vibration* 293 (2006) 680–690
- [82] Newland D.E.; *An Introduction to Random Vibrations, Spectral & Wavelet Analysis*, third ed., Longman, Harlow, Essex, England, 1993.
- [83] Nielsen J.C.O., Igeland A.; Vertical dynamic interaction between train and track influence of wheel and track imperfections; *Journal of Sound and Vibration* 187 (1995) 825-839.
- [84] Nielsen J. C.O., Lundén R., Johansson A., Verneršson T.; Train–Track Interaction and Mechanisms of Irregular Wear on Wheel and Rail Surfaces, *Vehicle System Dynamics* 40 (1-3) (2003) 3–54
- [85] Ono K., Yamada M.; Analysis of railway track vibration; *Journal of Sound and Vibration* 130(2) (1989) 269-297
- [86] Picoux B., Rotinat R, Regoina J.P., Le Houédec D., Prediction and measurements of vibrations from a railway track lying on a peaty ground; *Journal of Sound and Vibration* 267 (2003) 575–589

- [87] Picoux B., Le Houédec D.; Diagnosis and prediction of vibration from railway trains; *Soil Dynamics and Earthquake Engineering* 25 (2005) 905–921
- [88] Popp K., Kruse H., Kaiser I., *Vehicle-Track Dynamics in the Mid-Frequency Range*, *Vehicle System Dynamics*, (31) 1999 423-464
- [89] Remington P.J.; Wheel/rail rolling noise, 1: Theoretical analysis; *Journal of Acoustical Society of America* 81(6) 1987 1805-1823
- [90] Remington P.J.; Wheel/rail rolling noise, 2: Validation of theory; *Journal of Acoustical Society of America* 81(6) 1987 1824-1832
- [91] Ren Z., Sun S., Zhai W.; Study on lateral dynamic characteristics of vehicle/turnout System; *Vehicle System Dynamics* 43 (4) April 2005 285-303
- [92] Sato Y.; Study on high frequency vibrations in track operated with high-speed trains; *JNR, Railway Technical Review, Quarterly Reports* 18 (1977) 109-114
- [93] Sato Y., Matsumoto A., Knothe K.; Review on rail corrugation studies; *Wear* 253 (2002) 130–139
- [94] Shamalta M., Metrikine A. V.; Analytical study of the dynamic response of an embedded railway track to a moving load; *Archive of Applied Mechanics* 73 (2003) 131-146
- [95] Sheng X., Jones C.J.C., Petyt M.; Ground Vibration Generated By A Load Moving Along A Railway Track; *Journal of Sound and Vibration* 228(1) (1999) 129-156
- [96] Sheng X., Jones C.J.C., Thompson D.J.; A comparison of a theoretical model for quasi-statically and dynamically induced environmental vibration from trains with measurements; *Journal of Sound and Vibration* 267 (2003) 621–635
- [97] Sheng X., Jones C.J.C., Thompson D.J.; A theoretical model for ground vibration from trains generated by vertical track irregularities; *Journal of Sound and Vibration* 272 (2004) 937–965
- [98] Sheng X., Jones C.J.C., Thompson D.J.; A theoretical study on the influence of the track on train-induced ground vibration, *Journal of Sound and Vibration* 272 (2004) 909–936
- [99] Sheng X., Jones C.J.C., Thompson D.J.; Responses of infinite periodic structures to moving or stationary harmonic loads; *Journal of Sound and Vibration* 282 (2005) 125–149

- [100] Sherwood J.W.C.; Elastic Wave Propagation in a semi-infinite solid Medium; Proceedings of the Physical Society. 71(2) 207-219
- [101] Silva W.; Body waves in a layered anelastic solid; Bulletin of seismological Society of America 66(5) 1976 1539-1554
- [102] Sun L., Greenberg B.S.; Dynamic response of linear systems to moving stochastic sources; Journal of Sound and Vibration 229(4) (2000) 957–972.
- [103] Sun Y.Q., Dhanasekar M.; A dynamic model for the vertical interaction of the rail track and wagon system International Journal of Solids and Structures 39 (2002) 1337–1359
- [104] Sun Y.Q., Dhanasekar M.D., Roach D.; A three-dimensional model for the lateral and vertical dynamics of wagon-track systems, Proceedings of the Institution of Mechanical Engineers; 217(1) 2003 31-45
- [105] Szolc, T.; Medium Frequency Dynamic Investigation of the Railway Wheelset-Track System using a Discrete-Continuous Model; Archive of Applied Mechanics 68 (1998) 30-45.
- [106] Takemiya H.; Simulation of track–ground vibrations due to a high-speed train: the case of X-2000 at Ledsgard; Journal of Sound and Vibration 261 (2003) 503–526
- [107] Tal-Ezer H., Carcione J. M., Kosloff D.; An accurate and efficient scheme for wave propagation in linear viscoelastic media Geophysics 55(10) October 1990 1366-1379
- [108] Tamboli J.A, Joshi S.G.; Optimum Design Of A Passive Suspension System Of A Vehicle Subjected To Actual Random Road Excitations, Journal of Sound and Vibration 219(2) 1999 193-205
- [109] Theodorakopoulos D.D.; Dynamic analysis of a poroelastic half-plane soil medium under moving loads; Soil Dynamics and Earthquake Engineering 23 (2003) 521–533
- [110] Thompson, D.J.; Theoretical Modelling of Wheel/Rail Noise Generation; Journal of Rail and Rapid Transit, Proc. Instn. Mech. Engrs. 205F (1991) 11– 19
- [111] Thompson D.J., Jones C. J. C.; A Review Of The Modeling Of Wheel/Rail Noise Generation; Journal of Sound and Vibration 231(3) (2000) 519-536
- [112] Timoshenko S.; Stresses in rails; Transaction of the Institute of Ways of Communication, 1915.

- [113] Timoshenko S.; Method of Analysis of Statical and Dynamical Stresses in Rail; Proc. 2nd Int. Congress for Appl. Mech., Zürich, 1926 407 – 418.
- [114] Trochides A.; Ground-borne Vibrations in Buildings Near Subways; Applied Acoustics 32(4) 1991 289-296
- [115] Vadillo E.G., Herreros J., Walker J.G; Subjective Reaction To Structurally Radiated Sound From Underground Railways: Field Results; Journal of Sound and Vibration 193(1) (1996) 65-74
- [116] Vai R., Castillo-Covarrubias J.M., Sanchez-Sesma F.J., Komatitsch D., Vilotte J.P; Elastic wave propagation in an irregularly layered medium; Soil Dynamics and Earthquake Engineering 18 (1999) 11–18
- [117] Verichev S.N., Metrikine A.V.; Instability Of A Bogie Moving On A Flexibly Supported Timoshenko Beam; Journal of Sound and Vibration 253(3) (2002) 653-668
- [118] Wolf S.; Potential low frequency ground vibration (o6.3 Hz) impacts from underground LRT operations; Journal of Sound and Vibration 267 (2003) 651–661
- [119] Wu T.X., Thompson D.J.; A Double Timoshenko Beam Model For Vertical Vibration Analysis Of Railway Track At High Frequencies; Journal of Sound and Vibration 224(2) (1999) 329-348
- [120] Wu T.X., Thompson D.J.; Theoretical Investigation Of Wheel/Rail Non-Linear Interaction Due To Roughness Excitation; Vehicle System Dynamics, 34 (2000) 261–282
- [121] Wu T.X., Thompson D.J.; Wheel/Rail Non-Linear Interactions With Coupling Between Vertical And Lateral Directions; Vehicle System Dynamics 41 (1), 2004 27–49
- [122] Yang Y.B., Hung H.H., Chang D.W.; Train-induced wave propagation in layered soils using finite/infinite element simulation; Soil Dynamics and Earthquake Engineering 23 (2003) 263–278
- [123] Young T.H., Li C.Y.; Vertical Vibration Analysis Of Vehicle/Imperfect Track Systems; Vehicle System Dynamics 40(5) 2003 329–349
- [124] Zhai W., Cai Z.; Dynamic Interaction Between A Lumped Mass Vehicle And A Discretely Supported Continuous Rail Track; Computers & Structures 63 (5) 1991 987-997
- [125] Zheng D. Y., Fan S. C.; Instability Of Vibration Of A Moving-Train-And-Rail Coupling System Journal Of Sound And Vibration 255(2) (2002) 243-259

APPENDIX A

SHELL AND CONTINUUM COEFFICIENTS

Below the coefficients for cylindrical shell form Flügge equations and elastic continuum equations are given. [24]

For the elements of [A] matrix:

$$a_{11} = \frac{\rho a(1-\nu^2)}{E} \omega^2 - a \zeta^2 - \frac{(1-\nu)}{2a} \left(1 + \frac{h^2}{12a^2} \right) n^2,$$

$$a_{12} = \frac{(1+\nu)}{2} i \zeta n,$$

$$a_{13} = -\nu i \zeta + \frac{h^2}{12} (i \zeta)^3 - \frac{h^2}{12a^2} \frac{(1-\nu)}{2} i \zeta n^2,$$

$$a_{21} = -\frac{(1+\nu)}{2} i \zeta n,$$

$$a_{22} = \frac{\rho a(1-\nu^2)}{E} \omega^2 - \frac{a(1-\nu)}{2} \left(1 + \frac{h^2}{4a^2} \right) \zeta^2 - \frac{1}{a} n^2,$$

$$a_{23} = \frac{1}{a} n - \frac{h^2}{12} \frac{(3-\nu)}{2a} \zeta^2 n,$$

$$a_{31} = \nu i \zeta - \frac{h^2}{12} (i \zeta)^3 - \frac{h^2}{12a^2} \frac{(1-\nu)}{2} i \zeta n^2,$$

$$a_{32} = \frac{1}{a} n + \frac{h^2}{12a} \frac{(3-\nu)}{2} \zeta^2 n,$$

$$a_{33} = \frac{\rho a(1-\nu^2)}{E} \omega^2 - \frac{h^2}{12} \left(a \zeta^4 + \frac{2}{a} \zeta^2 n^2 + \frac{1}{a^3} n^4 \right) - \frac{1}{a} + \frac{h^2}{12a^3} (2n^2 - 1),$$

For the elements of [U] matrix:

$$u_{11} = \frac{n}{r} I_n(\alpha r) + \alpha I_{n+1}(\alpha r),$$

$$u_{12} = \frac{n}{r} K_n(\alpha r) - \alpha K_{n+1}(\alpha r),$$

$$u_{13} = i\zeta I_{n+1}(\beta r),$$

$$u_{14} = i\zeta K_{n+1}(\beta r),$$

$$u_{15} = \frac{n}{r} I_n(\beta r),$$

$$u_{16} = \frac{n}{r} K_n(\beta r),$$

$$u_{21} = -\frac{n}{r} I_n(\alpha r),$$

$$u_{22} = -\frac{n}{r} K_n(\alpha r),$$

$$u_{23} = i\zeta I_{n+1}(\beta r),$$

$$u_{24} = i\zeta K_{n+1}(\beta r),$$

$$u_{25} = -\frac{n}{r} I_n(\beta r) - \beta I_{n+1}(\beta r),$$

$$u_{26} = -\frac{n}{r} K_n(\beta r) + \beta K_{n+1}(\beta r),$$

$$u_{31} = i\zeta I_n(\alpha r),$$

$$u_{32} = i\zeta K_n(\alpha r),$$

$$u_{33} = -\beta I_n(\beta r),$$

$$u_{34} = \beta K_n(\beta r),$$

$$u_{35} = 0,$$

$$u_{36} = 0,$$

For the elements of [T] matrix:

$$t_{11} = \left(2\mu \frac{(n^2 - n)}{r^2} - \lambda \zeta^2 + (\lambda + 2\mu) \alpha^2 \right) I_n(\alpha r) - 2\mu \frac{\alpha}{r} I_{n+1}(\alpha r),$$

$$t_{12} = \left(2\mu \frac{(n^2 - n)}{r^2} - \lambda \zeta^2 + (\lambda + 2\mu) \alpha^2 \right) K_n(\alpha r) - 2\mu \frac{\alpha}{r} K_{n+1}(\alpha r),$$

$$t_{13} = 2\mu i \zeta \beta I_n(\beta r) - 2\mu i \zeta \frac{(n+1)}{r} I_{n+1}(\beta r),$$

$$t_{14} = -2\mu i \zeta \beta K_n(\beta r) - 2\mu i \zeta \frac{(n+1)}{r} K_{n+1}(\beta r),$$

$$\begin{aligned}
t_{15} &= 2\mu \frac{(n^2 - n)}{r^2} I_n(\beta r) + 2\mu \frac{n}{r} \beta I_{n+1}(\beta r), \\
t_{16} &= 2\mu \frac{(n^2 - n)}{r^2} K_n(\beta r) - 2\mu \frac{n}{r} \beta K_{n+1}(\beta r), \\
t_{21} &= -2\mu \frac{(n^2 - n)}{r^2} I_n(\alpha r) - 2\mu \frac{n}{r} \alpha I_{n+1}(\alpha r), \\
t_{22} &= -2\mu \frac{(n^2 - n)}{r^2} K_n(\alpha r) + 2\mu \frac{n}{r} \alpha K_{n+1}(\alpha r), \\
t_{23} &= \mu i \zeta \beta I_n(\beta r) - 2\mu i \zeta \frac{(n+1)}{r} I_{n+1}(\beta r), \\
t_{24} &= -\mu i \zeta \beta K_n(\beta r) - 2\mu i \zeta \frac{(n+1)}{r} K_{n+1}(\beta r), \\
t_{25} &= \left(-2\mu \frac{(n^2 - n)}{r^2} - \mu \beta^2 \right) I_n(\beta r) + 2\mu \frac{\beta}{r} I_{n+1}(\beta r), \\
t_{26} &= \left(-2\mu \frac{(n^2 - n)}{r^2} - \mu \beta^2 \right) K_n(\beta r) - 2\mu \frac{\beta}{r} K_{n+1}(\beta r), \\
t_{31} &= 2\mu i \zeta \frac{n}{r} I_n(\alpha r) + 2\mu i \zeta \alpha I_{n+1}(\alpha r), \\
t_{32} &= 2\mu i \zeta \frac{n}{r} K_n(\alpha r) - 2\mu i \zeta \alpha K_{n+1}(\alpha r), \\
t_{33} &= -\mu \frac{n}{r} \beta I_n(\beta r) - \mu (\zeta^2 + \beta^2) I_{n+1}(\beta r), \\
t_{34} &= \mu \frac{n}{r} \beta K_n(\beta r) - \mu (\zeta^2 + \beta^2) K_{n+1}(\beta r), \\
t_{35} &= \mu i \zeta \frac{n}{r} I_n(\beta r), \\
t_{36} &= \mu i \zeta \frac{n}{r} K_n(\beta r), \\
t_{41} &= \left(-2\mu \frac{(n^2 - n)}{r^2} + \lambda (\alpha^2 - \zeta^2) \right) I_n(\alpha r) + 2\mu \frac{\alpha}{r} I_{n+1}(\alpha r), \\
t_{42} &= \left(-2\mu \frac{(n^2 - n)}{r^2} + \lambda (\alpha^2 - \zeta^2) \right) K_n(\alpha r) - 2\mu \frac{\alpha}{r} K_{n+1}(\alpha r), \\
t_{43} &= 2\mu i \zeta \frac{(n+1)}{r} I_{n+1}(\beta r),
\end{aligned}$$

$$t_{44} = 2\mu i \zeta \frac{(n+1)}{r} K_{n+1}(\beta r),$$

$$t_{45} = -2\mu \frac{(n^2 - n)}{r^2} I_n(\beta r) - 2\mu \frac{n}{r} \beta I_{n+1}(\beta r),$$

$$t_{46} = -2\mu \frac{(n^2 - n)}{r^2} K_n(\beta r) + 2\mu \frac{n}{r} \beta K_{n+1}(\beta r),$$

$$t_{51} = -2\mu i \zeta \frac{n}{r} I_n(\alpha r),$$

$$t_{52} = -2\mu i \zeta \frac{n}{r} K_n(\alpha r),$$

$$t_{53} = \mu \frac{n}{r} \beta I_n(\beta r) - \mu \zeta^2 I_{n+1}(\beta r),$$

$$t_{54} = -\mu \frac{n}{r} \beta K_n(\beta r) - \mu \zeta^2 K_{n+1}(\beta r),$$

$$t_{55} = -\mu i \zeta \frac{n}{r} I_n(\beta r) - \mu i \zeta \beta I_{n+1}(\beta r),$$

$$t_{56} = -\mu i \zeta \frac{n}{r} K_n(\beta r) + \mu i \zeta \beta K_{n+1}(\beta r),$$

$$t_{61} = (\lambda a^2 - (\lambda + 2\mu)\zeta^2) I_n(\alpha r),$$

$$t_{62} = (\lambda a^2 - (\lambda + 2\mu)\zeta^2) K_n(\alpha r),$$

$$t_{63} = -2\mu i \zeta \beta I_n(\beta r),$$

$$t_{64} = 2\mu i \zeta \beta K_n(\beta r),$$

$$t_{65} = 0,$$

$$t_{66} = 0,$$